Exploring the functions of a Kaposi´s sarcoma-associated herpesvirus-encoded microRNA *in vitro* and *in vivo*

Dissertation

Zur Erlangung der Würde des Doktors der Naturwissenschaften
des Fachbereichs Biologie, der Fakultät für Mathematik, Informatik und Naturwissenschaften,
der Universität Hamburg

vorgelegt von
Christine Dahlke,
geb. Henning
aus Lüneburg

Hamburg, Oktober 2012

Die vorliegende Arbeit wurde in der Zeit von Februar 2009 bis Oktober 2012 unter Anleitung von Dr. Adam Grundhoff in der Arbeitsgruppe Zelluläre Virusabwehr am Heinrich-Pette-Institut, Leibniz-Institut für Experimentelle Virologie angefertigt und von Prof. Dr. Thomas Dobner betreut.

1. Gutachter: Prof. Dr. Thomas Dobner
2. Gutachter: Dr. Adam Grundhoff

Tag der Disputation: 07.12.2012

Dedicated to my parents

Zusammenfassung

Das humanpathogene Kaposi Sarkom-assoziierte Herpesvirus (KSHV) ist das ätiologische Agens des Kaposi Sarkoms sowie des primären Effusionslymphoms und wird darüber hinaus mit der Pathogenese bestimmter Formen der multizentrischen Castleman Krankheit in Verbindung gebracht. Die genaue Rolle des KSHV während der Ätiogenese dieser Tumore ist noch ungewiss. Aufgrund der Tatsache, dass KSHV-positive Tumorzellen latent infiziert sind, scheinen jedoch Latenzgene eine bedeutende Rolle zu spielen. Während der Latenz werden neben einigen wenigen Proteinen insgesamt 12 virale microRNA (miRNA) Gene exprimiert. Besondere Aufmerksamkeit gilt in diesem Kontext der KSHV-kodierten miR-K12-11.

miRNAs sind kleine (~ 21 - 24 nt), nicht-kodierende RNA-Moleküle, die post-transkriptionell die Genexpression regulieren. Es wird vermutet, dass die kurze *seed*-Sequenz der miRNA (2 - 8 nt ausgehend von dem 5´-Ende) wichtig für die Bindung an die 3´-UTR der Ziel-mRNA ist. In diesem Sinne ist die miR-K12-11 interessant, da sie eine 100-%ige Übereinstimmung der zellulären miR-155 in der *seed*-Sequenz aufweist, was eine Mimikry vermuten lässt. Für das Virus erscheint diese funktionelle Analogie bedeutsam, da wichtige Funktionen der miR-155 in der B-Zell Antwort und der Aktivierung von Keimzentren liegen. Darüber hinaus ist die als oncomiR klassifizierte miR-155 in einer Vielzahl von Krebsarten überexprimiert. Es wird daher vermutet, dass die miR-K12-11 Expression auch in die KSHV-induzierte Tumorgenese involviert ist. Diese Annahme wird durch die Beobachtung der konstitutiven miR-K12-11 Expression in KSHV-assoziierten Tumorzelllinien gestützt.

Zur Untersuchung der Funktion der miR-K12-11 *in vivo* wurde ein retroviral-vermittelter Gen-Austausch mit anschließender Knochenmarkstransplantation in C57BL/6 Mäusen durchgeführt, so dass in Empfängermäusen die transplantierten hämatopoetischen Vorläuferzellen miR-K12-11 oder humane (hsa-) miR-155 konstitutiv exprimierten. Auf diese Weise konnte die Auswirkung der miR-K12-11 und hsa-miR-155 Expression direkt *in vivo* verglichen werden.

Mit dieser Arbeit konnte gezeigt werden, dass die Expression sowohl der humanen als auch der viralen miRNA in transplantierten hämatopoetischen Vorläuferzellen zum vermehrten Auftreten von B-Zellen in den lymphatischen Organen der Empfängermäuse führte. Darüber hinaus wurde die verstärkte Bildung von Keimzentren in der Milz beobachtet. Diese Beobachtung gleicher Phänotypen innerhalb beider miRNA Maus Kohorten deutet eine Mimikry an. Des Weiteren wurde Jarid2, eine Komponente des *Polycomb repressive complex 2*, als neues Ziel-Gen für miR-K12-11 mittels eines Luciferase Reporter Assays und einer Western Blot Analyse erfolgreich validiert. Zusätzlich wurden geringere Jarid2 Expressionslevel in isolierten miRNA-exprimierenden

Knochenmarkszellen im Vergleich zu Kontrollzellen detektiert. Erwähnenswert ist hierbei, dass eine reprimierte Jarid2 Expression in B-Zellen vermutlich das Überleben der Zelle fördert.

Insgesamt bestärken die erzielten Daten die Hypothese, dass miR-K12-11 die Funktion der zellulären miR-155 nachahmt. Die Expression der miR-K12-11 repräsentiert somit einen potentiellen Mechanismus, der zur Induktion der Differenzierung von infizierten naiven B-Zellen in B-Gedächtniszellen sowie zum Überleben der Zelle beitragen könnte. Dies würde zum einen dem Virus ermöglichen, lebenslang im Wirt zu persistieren, und könnte zum anderen die infizierte Zelle für eine maligne Transformation prädisponieren.

Abstract

Kaposi´s sarcoma-associated herpesvirus (KSHV), a human lymphotropic gamma-herpesvirus, is etiologically linked to Kaposi's sarcoma (KS) and to two B-cell lymphoproliferative diseases: primary effusion lymphoma (PEL) and multicentric Castleman's disease (MCD). Because the majority of tumor cells in these malignancies are latently infected, latent genes are thought to play an important role in virus-induced tumorigenesis. In this regard, the KSHV-encoded microRNA (miRNA) miR-K12-11 has garnered considerable interest.

miRNAs are ~ 21 - 24 - nucleotide long RNAs that post-transcriptionally repress gene expression. It is commonly accepted that a perfect binding of the so-called seed region of the miRNA (2 - 8 nt from the 5′ -end) to the 3'-UTR of the target mRNA is crucial for miRNA-mediated repression. miR-K12-11 is constitutively expressed in cell lines derived from KSHV-associated tumors and shares perfect seed homology to the human hsa-miR-155, an oncomiR which is overexpressed in numerous human cancers. Thus, it seems likely that mimicry of miR-155 by miR-K12-11 may contribute to cellular transformation in KSHV-associated disease. Since miR-155 functions in B-cell development and differentiation as well as germinal center formation, one advantage the virus might gain by this mimicry is the ability to modulate B-cell responses.

To explore miRNA functions and mimicry *in vivo*, retroviral-mediated gene transfer combined with bone marrow transplantation in C57BL/6 mice was performed such that mouse recipients constitutively expressed miR-K12-11 or human (hsa-) miR-155 in hematopoietic progenitor cells (HPCs). Phenotypic alterations associated with constitutive expression of either hsa-miR-155 or viral miR-K12-11 were investigated side-by-side.

We observed that retroviral-mediated gene transfer and subsequent bone marrow transplantation led to increased B-cell fractions in lymphoid organs, as well as enhanced germinal center formations in spleen in both miRNA mouse cohorts. Additionally, Jarid2, a component of Polycomb repressive complex 2, was validated as a novel target of miR-K12-11 using luciferase reporter assay and western blot analysis. The downregulation of this gene was furthermore confirmed in miR-K12-11 as well as hsa-miR-155 expressing bone marrow cells. Interestingly, previous studies have suggested that repression of Jarid2 might contribute to increased B-cell survival.

These findings underscore the notion that miR-K12-11 may have evolved to mimic hsa-miR-155 functions in KSHV-infected B-cells. The expression of miR-K12-11 may represent one mechanism by which KSHV reprograms naïve B-cells toward long-living memory B-cells, but which at the same time may pre-dispose infected lymphocytes to malignant transformation.

1 INTRODUCTION

This study focuses on a Kaposi's sarcoma-associated herpesvirus (KSHV)-encoded microRNA (miRNA) and its function during viral infection and virus-induced tumorigenesis.

1.1 FAMILY OF HERPESVIRIDAE

Herpesviruses belong to the double-stranded (ds) DNA viruses and are highly disseminated in nature. To date more than 170 members have been identified that mainly infect vertebrates. These pathogens have co-evolved with their hosts during the last 60-80 million years and as a result show a very high degree of host adaptation (McGeoch & Davison, 1999). Herpesviruses persist life-long in their host. The functional basis of this ability is their biphasic replication cycle, consisting of a lytic and a latent phase of infection. Latent infection is a hallmark of herpesviruses. Many herpesvirus infections are not clinically apparent, but if the host immune defenses are compromised, may have a severe outcome.

1.2 BIOLOGICAL PROPERTIES

The typical herpes virion is spherical and consists of an envelope in which viral and cellular glycoproteins are embedded. The glycoproteins are important for viral entry. The tegument, a matrix of densely-packed regulatory proteins, surrounds the capsid. The icosahedral capsid contains 162 capsomeres that encapsidate the linear ds DNA. The structural elements of a herpes virion are depicted in figure 1.

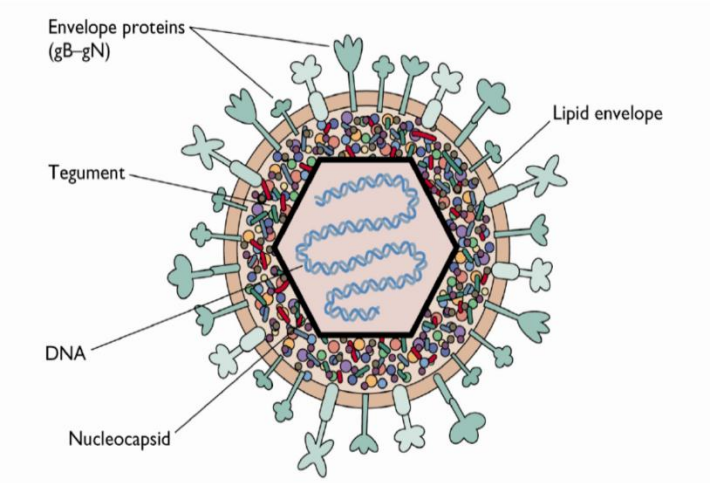

Figure 1: Structural elements of a herpes virion. The lipid envelope anchors viral glycoproteins that are essential for adsorption of the virus to the host cell and subsequent endocytosis. The tegument surrounds the nucleocapsid. The icosahedral nucleocapsid contains the ds viral genome. (Figure: (Flint et al., 2004)).

Although members of the herpesviridae share these structural elements, they show a large diversity in virion morphology and genome organization. The size of herpes virions ranges from 120 to nearly 300 nm. The viral genomes vary in length (120 - 250 kilobasepairs (kbp)), in the number of open reading frames (ORFs) (~ 70 ORFs to ~ 200 ORFs), in base composition (31 – 75 % GC content), and in the copy number of terminal as well as internal repeated sequences.

1.3 HUMAN HERPRESVIRUSES

Humans are the natural host of eight different herpesviruses that are classified into three subfamilies, named alpha-, beta- and gamma-herpesviruses (figure 2). Classification is based on sequence phylogeny, nucleotide sequences and biological properties such as pathogenicity, cell tropism and replication.

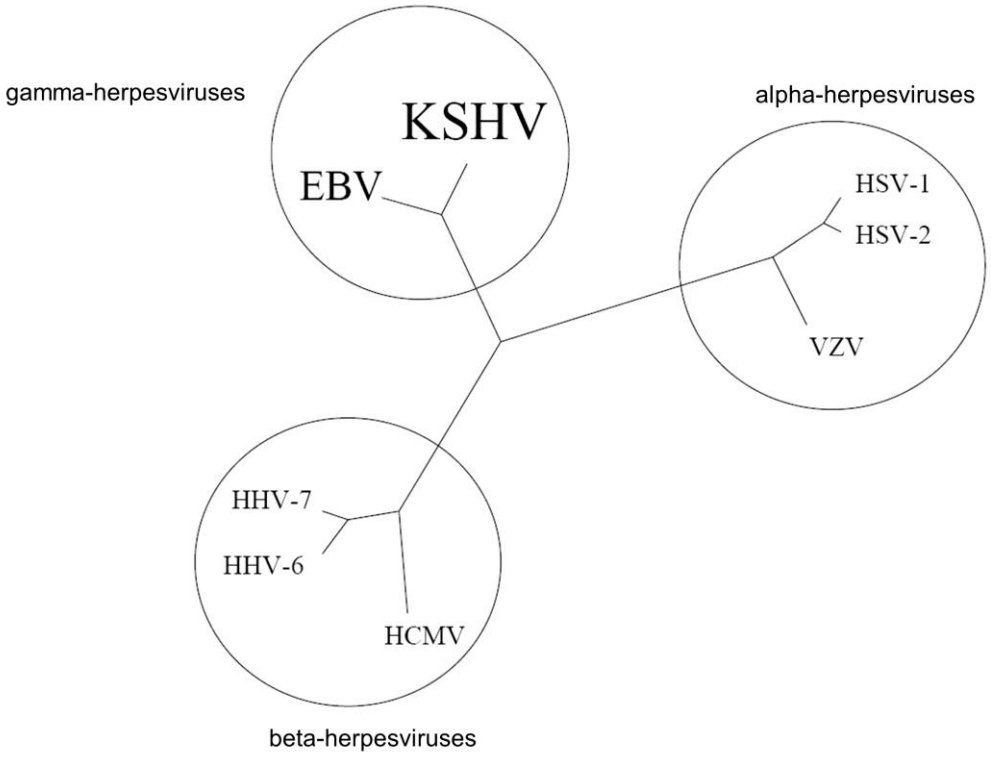

Figure 2: Family of human *herpesviridae*. Thus far, eight human herpesviruses are identified. Since this study focuses on the gamma-herpesviruses, particularly on KSHV, both are highlighted in bold letters. (Figure : (Moore et al., 1996b); modified).

The ***alpha-herpesviruses*** include the human members herpes simplex virus 1 (HSV1) and HSV2, as well as the Varicella Zoster virus (VZV; also known as human herpesvirus 3 (HHV3)). Their hallmarks are a broad host range, a relatively rapid reproductive cycle, and the capacity to establish a latent infection preferentially in sensory ganglia. The ***beta-herpesviruses*** are characterized by their restricted host range and their slow replication.

This subfamily comprises the human cytomegalovirus (HCMV, HHV5) as well as the roseoloviruses HHV6 and HHV7.

The subfamily of human ***gamma-herpesviruses*** includes the members Epstein-Barr virus (EBV, HHV4) and KSHV (HHV8). This subfamily contains two genera: the lymphocryptovirus (EBV) and the rhadinovirus (KSHV). EBV is highly disseminated with nearly 90 % of the worldwide population being EBV-positive. KSHV is grouped into the genus of rhadinovirus, owing to its sequence homology with a number of other rhadinoviruses, such as herpesvirus saimiri (HVS), rhesus monkey rhadinovirus (RRV) and murine gamma-herpesvirus 68 (MHV68) (Neipel et al., 1997; Li et al., 1999). Gamma-herpesviruses have a limited tissue tropism and a narrow host range *in vivo*. They are lymphotropic infecting mainly B- and T-cells. Furthermore, KSHV is detected in myeloid and endothelial cells. A striking feature of many gamma-herpesviruses is their association with neoplastic disease in their host. Worldwide, the human gamma-herpesviruses KSHV and EBV are thought to be implicated in the pathogenesis of nearly 2 % of all novel tumor cases (Parkin, 2006).

1.4 KAPOSI'S SARCOMA-ASSOCIATED HERPESVIRUS (KSHV)

In 1872, the Hungarian dermatologist Moritz Kaposi described idiopathic, multiple pigmented sarcomas of the skin. In the year 1994, Chang and Moore identified two herpesvirus-like DNA sequences in Kaposi´s sarcoma (KS) lesions obtained from acquired immunodeficiency syndrome (AIDS) patients by using representational difference analysis (RDA) (Chang et al., 1994). They succeeded in identifying the eighth human herpesvirus, termed KSHV (Chang et al., 1994).

1.5 KSHV GENOME

The linear ds KSHV-genome comprises approximately 170 kbp (figure 3). A long terminal repeat (TR) region of 801 base-pairs (bp) with high GC content (84.5 % GC content) flanks the long unique coding region (LUR), which consists of 140 kbp (54 % GC content) (Russo et al., 1996; Neipel et al., 1997).

The LUR shows homology to genes from HVS, the closest relative of KSHV. Homologous ORFs are named after their HVS counterparts, from ORF 1 to ORF 75. ORFs without homologies to HVS are named with a prefix “K” and are numbered ORF K1 to K15. To date, 87 viral proteins and 12 pre-miRNAs have been characterized, all of them encoded within the LUR (Russo et al., 1996; Neipel et al., 1997; Cai & Cullen, 2006).

The viral genes are categorized into lytic and latent genes, whereby the lytic genes are further classified into immediate early (IE), early (E) and late genes (L) (see figure 3), depending on their time-point of expression. During latency only a small region (nt 117436

to 127886 (NC_009333.1)), named the latency-associated region (LAR), is actively transcribed. Four proteins and all viral precursor-miRNAs (pre-miRNAs) are encoded in this region (see also 1.6.1).

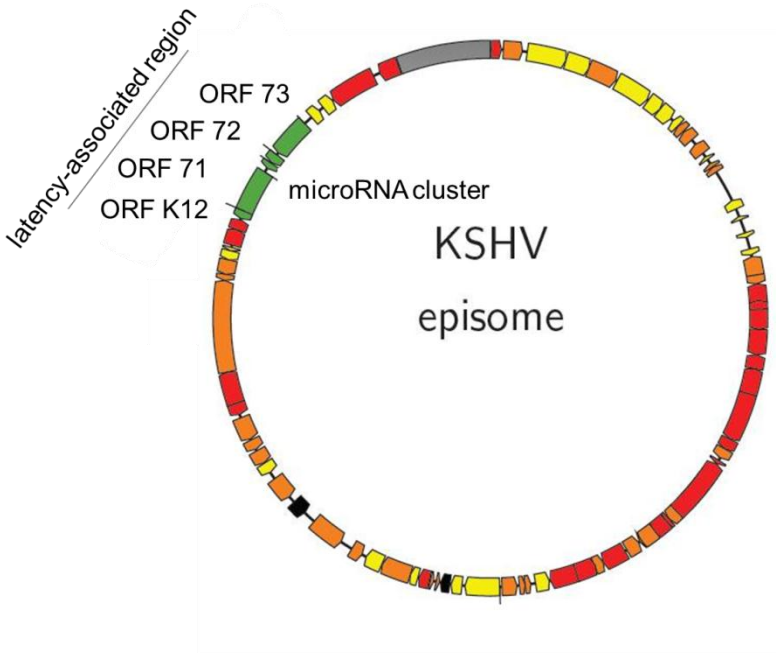

Figure 3: Schematic representation of the KSHV genome. The long unique region (LUR) consists of 140 kbp and is flanked by long terminal repeats (gray boxes). KSHV encodes at least 87 proteins. Most of them are highly restricted in their expression during latency. Only a small region is actively transcribed (green box) during latency, which is termed as latency-associated region (LAR). Four proteins and a miRNA cluster are encoded in this region. Depending on their timepoint of expression the lytic genes are classified into three subgroups: immediate early genes (IE, orange), early genes (E, yellow) and late genes (L, red). (Figure: Philipp Schult; modified).

1.6 KSHV LIFE-CYCLE

Like all herpesviruses KSHV exists in one of the two life-cycle programs, known as latency or lytic replication (Dourmishev et al., 2003). Both are essential for its long-term persistence in the host.

1.6.1 Latent infection

After KSHV infection the viral DNA circularizes and persists as an episome in the nuclei of infected cells, thereby establishing a latent infection. It has been shown that epigenetic modifications of histones and, at later time points, DNA methylation play an important role in the establishment of latency (Günther & Grundhoff, 2010); nevertheless a comprehensive understanding of this process has not yet been fully elucidated.

The early phase of KSHV infection is characterized by the expression of latent and a limited number of lytic genes. Following infection the lytic gene expression is highly

restricted and latent gene products become predominant, resulting in the establishment of latency. It has been postulated that the establishment of latency is a strategy which has evolved to allow the virus modulation of host signaling and avoidance of antiviral immune responses (Djerbi et al., 1999; Naranatt et al., 2004).

During latency the LAR is constitutively expressed, leading to the expression of at least four latent proteins, namely (a) latency associated nuclear antigen-1 (LANA, LANA-1, ORF 73), (b) a viral homologue of cyclin D, called vCyclin (ORF 72), (c) a viral Fas-associated death domain-like interferon converting enzyme (FLICE) inhibitory protein (vFLIP, ORF 71) and (d) the small membrane-associated proteins kaposin A, B and C, encoded by ORF K12 (ORF K12), as well as 12 pre-miRNAs. The proteins ORF 71 - ORF 73 belong to a multicistronic transcriptional unit named LT cluster (LT_C) (Dittmer et al., 1998). ORF K12 is separated from this cluster by a 4 kbp region that includes a set of pre-miRNAs (Cai et al., 2004, 2005; Pfeffer et al., 2005; Samols et al., 2005; Cai & Cullen, 2006; Grundhoff et al., 2006a) (figure 4).

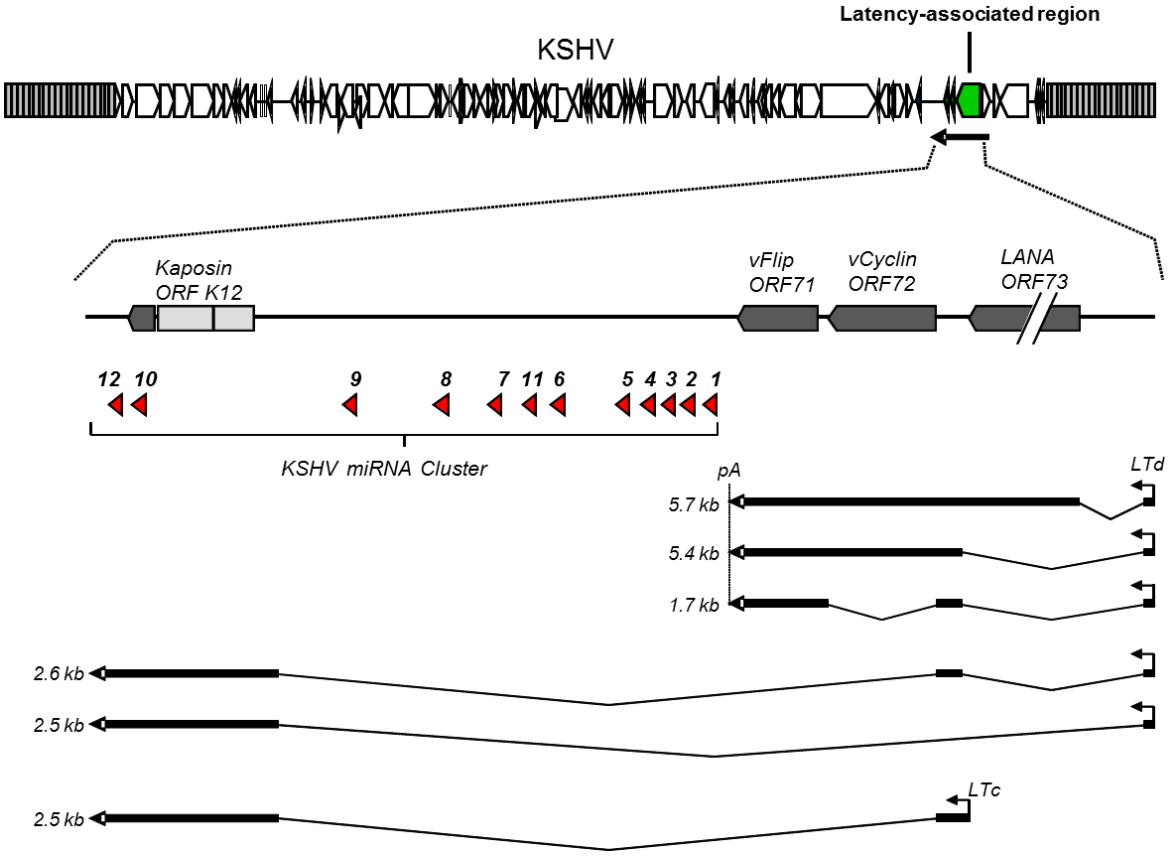

Figure 4: Four proteins and 12 pre-miRNAs of KSHV miRNAs are encoded in the LAR. Scheme of the KSHV genome, in particular the latency-associated region (LAR) including LANA (ORF 73), v-cyclin (ORF 72), v-FLIP (ORF 71), and Kaposin (ORF K12) (gray boxes). Pre-miRNA sequences are indicated by numbered red arrows. The schematic depicts exons (thick lines), introns (thin lines), transcription start sites (black arrows) and splice variants. (Figure: Adam Grundhoff).

The expression of these latent gene products is regulated by complex mechanisms, such as usage of different promoters, transcription of multicistronic mRNAs, splicing, translational control by internal ribosome entry sites (IRES), as well as the read-through of poly-A sites.

The latent proteins have been shown to modulate host gene expression. vCyclin can activate cyclin A and thereby induces the cell cycle machinery, hence affecting cell proliferation (Duro et al., 1999). The viral protein vFLIP is a homologue of the cellular FLICE inhibitor. It has been proposed that vFLIP activates nuclear factor kappa B (NFkB), thereby leading to increased proliferation and decreased apoptosis rates (Djerbi et al., 1999). ORF K12 is also transcribed during latency, and together with upstream sequences encodes for three small membrane-associated proteins termed Kaposin A, B and C. Kaposin B is predominantly detected in KSHV-infected cells and is associated with the activation of p38/Mk2 signaling pathway (McCormick & Ganem, 2005). Kaposin B increases the expression of cytokines by blocking the degradation of their mRNAs (McCormick & Ganem, 2005).

LANA, a multifunctional protein, is expressed in virtually all KSHV-infected cells and associated tumors. This protein is of fundamental importance for the persistence of viral episomes in infected cells. Like the EBV nuclear antigen 1 (EBNA-1), LANA is a DNA binding protein (Moore et al., 1996b; Ballestas et al., 1999). The C-terminal domain of LANA binds to the latent KSHV origin of replication, the TR region (Moore et al., 1996b), whereas the N-terminal domain interacts with human mitotic chromosomes, thereby tethering the episome to mitotic host chromosomes (Ballestas et al., 1999; Grundhoff & Ganem, 2003). LANA is essential for recruitment of origin recognition complex (ORC) proteins, which enables the recruitment of the minichromosome maintenance complex (MCM) to the origin of replication (here: TR region) (Lim et al., 2002; Grundhoff & Ganem, 2003; Stedman et al., 2004). The viral episome replicates in synchrony with the cellular genome, which ensures the segregation of KSHV episomes to daughter cells during mitosis (Ballestas et al., 1999; Grundhoff & Ganem, 2003). Additionally, LANA acts as a transcriptional modulator of its own and of cellular genes (Verma et al., 2007). It is capable of prolonging the cellular life-span, increases cellular proliferation, influences cytokine production and immune responses (Friborg et al., 1999; Watanabe et al., 2003). For example, LANA interacts with p53 and inhibits p53 transcriptional activity and p53 dependent apoptosis (Friborg et al., 1999). Another example for a protein that interacts with LANA is Glycogen synthase kinase-3β (GSK-3β). This interaction probably promotes S-phase entry (Fujimuro 2003). Furthermore, LANA can activate B-cells and induces numerous pathways in B-cells that lead to a survival advantage (Fakhari et al., 2006; Sin et al., 2010).

LANA-2 (also referred to as vIRF3 (interferon regulatory factor 3), ORF K10.5) is expressed in lymphoblastoid cells (Primary effusion lymphoma (PEL), Multicentric Castleman´s disease (MCD)). Although LANA-2 is not encoded in the LAR, the protein is also expressed during latency (Lubyova & Pitha, 2000). The viral interleukin 6 (vIL6 (ORF K2)) is designated as lytic protein, but also detected in latent infected cells (Cannon et al., 1999; Aoki et al., 2001). This protein is a homologue to the cellular IL6, and thus shares many of its features. It is postulated that vIL6 plays an important role during B-cell response. Both, LANA-2 and vIL6, are thought to have a critical impact on lymphomagenesis (Wies et al., 2009).

1.6.2 **Lytic replication**

Reactivation results in production of infectious virions, which is important for dissemination and maintenance of viral loads in the persistently infected host. Although the mechanisms leading to reactivation are not fully understood, one putative trigger in latently infected B-cells includes the induction of endoplasmic reticulum stress (ER stress). ER stress induces the expression of X-box-binding protein-1 (XBP-1), which then binds to the viral replication and transcription activator (RTA, ORF 50), leading to the induction of KSHV reactivation (Wilson et al., 2007; Yu et al., 2007).

The viral lytic program proceeds in a temporally regulated cascade of gene expression. The expression of the viral lytic transactivator RTA mediates the transcriptional activation of early as well as some late genes. During lytic replication the full repertoire of viral genes are expressed, which results in the assembly of new infectious viral particles and the lysis of the host cell (Renne et al., 1996; Jenner et al., 2001).

1.7 KSHV-ASSOCIATED MALIGNANCIES

KSHV is considered the etiologic agent of two cancers, the endothelial cell derived KS and the B-cell tumor PEL, and is furthermore strongly linked to certain forms of MCD, which is likewise of B-cell origin (Whitby et al., 1995; Schulz & Moore, 1999). All of these malignancies have a greatly increased incidence in immunosuppressed individuals.

1.7.1 **Kaposi´s sarcoma**

In the year 2000, molecular and sero-epidemiological studies confirmed KSHV as the etiologic agent of KS (Dupin et al., 2000; Schulz, 2000b, a). KS has been classified into four subtypes: classical, endemic, AIDS-associated, and iatrogenically acquired (Schulz, 2000a). The KSHV genome is detected in all KS forms. Before the outbreak of AIDS, KS was a rarely occurring tumor in elderly men that was detected most commonly in Mediterranean regions. Nowadays, KS is the most frequent AIDS-defining cancer

worldwide. Notably, although nearly all tumor cells are latently infected, a small subset of lytically infected cells (1 – 5 %) also co-exists in this tumor (Renne et al., 1996). Lytic replication as well as autocrine and paracrine effects induced directly by KSHV-encoded cytokines or indirectly through the induction of cellular cytokines may promote the propagation of infectious virus to new target cells (Grundhoff & Ganem, 2004; Schulz, 2006).

1.7.2 **Primary effusion lymphoma (PEL)**

PEL is a rare B-cell-non-Hodgkin lymphoma, commonly found in KSHV- and human immunodeficiency virus (HIV) -positive individuals (Cesarman et al., 1995). An effective therapy for PEL does currently not exist, and the majority of patients die within a few months after diagnosis (Boulanger et al., 2005). KSHV is detected in all primary tumors and PEL derived tumor cell lines and is therefore believed to play an important role during pathogenesis (Cesarman et al., 1995).

Most PEL cells exhibit a strictly latent expression profile, but nevertheless a handful of latent KSHV genes being expressed (Rivas et al., 2001). In addition to the latent proteins, all 12 KSHV-encoded pre-miRNAs, as well as the lytic protein vIL6, are detectable (Rainbow et al., 1997; Jones et al., 1999; Parravicini et al., 2000; Rivas et al., 2001; Pfeffer et al., 2005; Sakakibara & Tosato, 2011). vIL6 has been shown to play an important role in the control of proliferation and differentiation of B-cells *in vitro* and it has been postulated to play a role in development and progression of PEL (Moore et al., 1996a; Burger et al., 1998; Jones et al., 1999).

PEL cells are monoclonal cells of B-cell origin (Gaidano et al., 1997; Carbone et al., 1998). Studies examing the detailed cellular origin of PEL have revealed the expression of somatically mutated immunoglobulin (Ig) genes of B-cells, indicating that these cells originate from a germinal center/post-germinal center stage (Gaidano et al., 1997; Fais et al., 1999).

1.7.3 **Multicentric Castleman´s disease**

In 1956, the pathologist Benjamin Castleman described the rarely occuring lymphoproliferative MCD (Castleman et al., 1956). The two most important pathologic variants of MCD are the plasmablastic variant, which is highly associated with latent KSHV infection, and the hyaline variant, which is not (Soulier et al., 1995). The plasmablastic variant shows an aggressive clinical course. Contrary to PEL, KSHV-associated MCD occurs in patients with and without HIV infection and mainly involves lymph nodes and the spleen (Du et al., 2002). It has been proposed that HIV-infection can increase the severity of MCD by increasing KSHV viral load (Grandadam et al., 1997;

Oksenhendler et al., 2000). In contrast to PEL, in MCD the expression profile of KSHV is not restricted to the latent genes. Several lytic genes are expressed including the genes ORF K8, K9, K10 and ORF 59 as well as vIL6 (ORF K2) (Parravicini et al., 2000).

1.8 KSHV EXPLOITS NORMAL B-CELL BIOLOGY

The primary target cells of KSHV and its close relative EBV are lymphocytes, predominantly $CD19^+$ B-cells (Mesri et al., 1996; Rappocciolo et al., 2006). After primary infection, the viruses persist life-long in the host by establishing latency reservoirs in memory B-cells. This type of B-cell is a long-living cell and displays an optimal niche for latent viruses to persist. Unlike KSHV, EBV is a well characterized pathogen, and its virus-host interactions may therefore provide important insights into mechanisms that KSHV utilizes.

To understand how EBV and KSHV might use different aspects of B-cell biology to gain access to the pool of memory B-cells, a brief overview is given about hematopoiesis, B-cell development and differentiation.

Normal B-cell biology

B-cells originate from hematopoietic stem cells (HSCs), which reside in the bone marrow (BM) compartment and give rise to all blood cell lineages, including cells of the immune system, as it is depicted in figure 5. The process of hematopoiesis is highly regulated and controlled by complex molecular events that regulate commitment, differentiation and apoptosis. The starting point of hematopoiesis is the HSC, which can be classified into two cell types, long-term (LT) and short-term (ST) stem cells. While both LT-HSCs and ST-HSC can regenerate all the different types of blood cells, this capacity is limited for a time-period of 8 - 12 weeks for ST-HSC. In the hematopoietic system LT-HSCs differentiate into ST-HSCs and the latter into multi-potent progenitors (MPPs) which have only a highly limited ability of self-renewal (Spangrude et al., 1988; Snodgrass & Keller, 1990; Spangrude et al., 1991; Morrison et al., 1997). Every step of differentiation causes the restriction of multipotency (Miyamoto et al., 2002). The development toward B-cells proceeds through several stages: Starting from HSCs, cells commit to become MPPs and CLPs (common lymphoid progenitors), then proceed to pro-B-cell, pre-B-cells and mature B-cells.

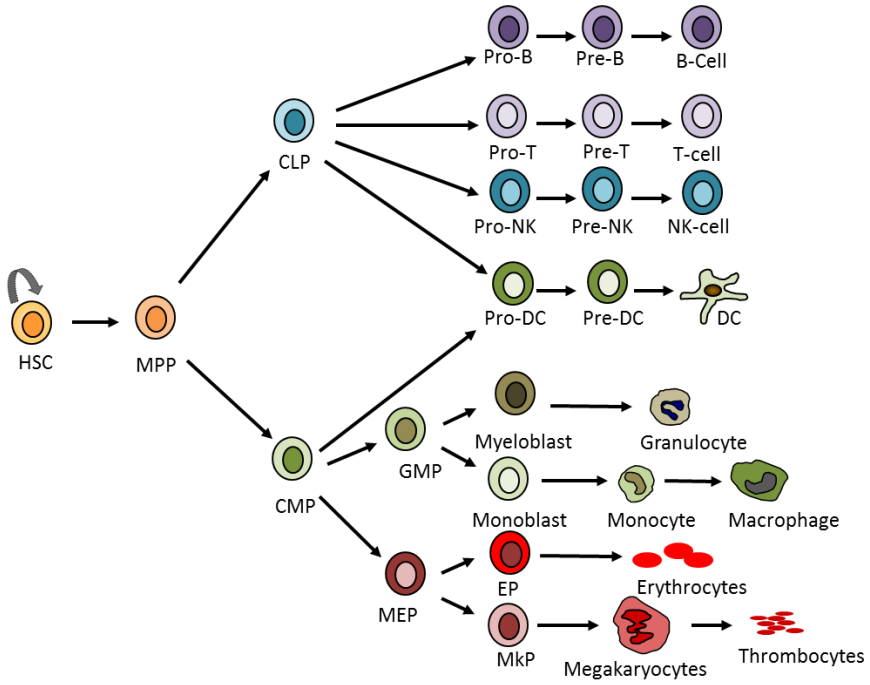

Figure 5: Schematic of hematopoiesis. The process of hematopoiesis is shown simplified. Formation of cellular blood components starts with hematopoietic stem cells (HSCs). Multipotent progenitors (MPPs) can give rise to common lymphoid progenitors (CLPs) or common myeloid progenitors (CMPs). CMPs can commit to megacaryotic/erythroid progenitors (MEPs) and granulo/monocytic progenitor (GMPs). MEPs can differentiate into megacaryocytes, which are responsible for the production of blood or into erythrocytes, which are responsible for oxygen transport. CLPs can differentiate into natural killer cells (NK), dendritic cells (DC), immature B- or T-cells. (Figure: Birte Niebuhr; modified).

A detailed schematic of B-cell development in the bone marrow is depicted in figure 6 Different cell-surface proteins are expressed during commitment, which enables the distinction between B-cell stages. When the B-cell reaches the IgM^+ state, the B-cell is termed as immature and emerges in the periphery.

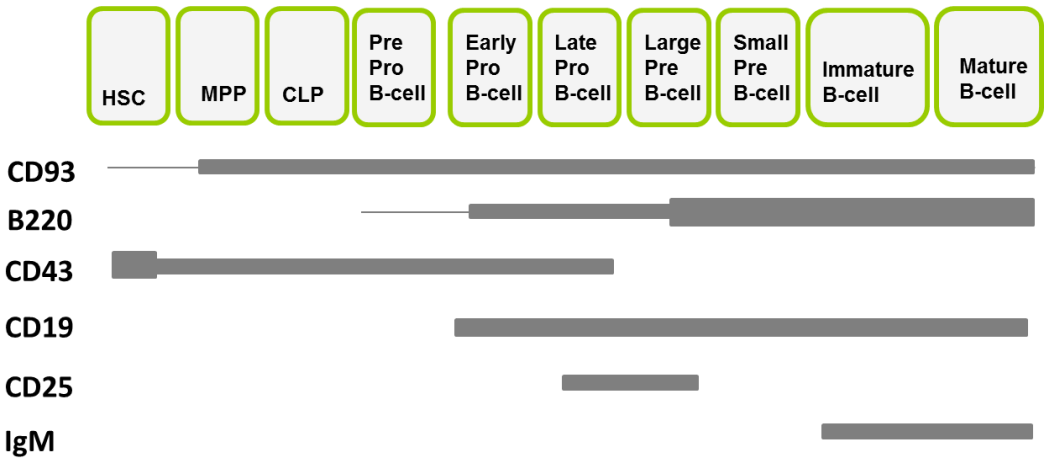

Figure 6: Expression of selected cell-surface proteins during B-cell development in mouse. Development of B-lineage cells in bone marrow. Shown is the ordered expression of surface-proteins during B-cell development. Mature B-cells origin from HSCs. (Schematic drawing of (Hardy et al., 2007); modified).

Immature B-cells can circulate through peripheral lymphoid tissues, such as spleen or lymph nodes. Each B-cell that expresses functional, non-self-reactive B-cell receptors (BCRs) are positively selected into the pool of mature B-cells, also termed as naïve B-cell, that circulate in the periphery.
When circulating mature B-cells encounter an antigen and receive signals from T-helper cells, they differentiate into activated B-cells. Such B-cells form or participate in the formation of germinal centers (GCs) in secondary lymphoid organs. During GC reaction B-cells undergo extensive and rapid proliferation, somatic hypermutation of variable gene segments and class switch recombination. A competitive selection is followed to positively select those cells that bind the antigen best. These surviving cells leave the GC as antibody producing plasma or long-living memory B-cells. The B-cell differentiation is depicted in figure 7 (upper figure).

B-cell biology and the parallel with human gamma-herpesviruses

EBV is the closest human relative of KSHV, and in contrast to KSHV, an *in vitro* B-cell system to study EBV biology can be established. *In vitro*, EBV-infected primary B-cells establish latency, followed by cellular transformation, and finally result in a lymphoproliferative cell line (LCL) (Alfieri et al., 1991; Thorley-Lawson, 2005; Boshoff, 2011). Although KSHV is lymphotrop *in vivo*, infection of established B-cell lines have been highly refractory (Myoung & Ganem, 2011). This hampers the understanding of how KSHV hijacks B-cell specific processes and how the virus facilitates the differentiation toward memory B-cells; and lastly which virus-host interactions contribute to tumor development. Therefore, the understanding of KSHV biology and tumorigenesis remains incomplete so far.

Studies on EBV revealed that EBV infects naïve B-cells and that tightly regulated transcription programs of latent proteins are used to activate these B-cells to become proliferating cells. They might either initiate or participate in GC reactions. During this process EBV infected cells transit through the GC without the necessity of either T-cell help or antigen binding, hence without any external signaling or stimulation. These infected B-cells further differentiate into plasma or memory B-cells. During later stages of infection, EBV infected memory B-cells might differentiate into plasma cells to produce infectious virus (Laichalk et al., 2002; Laichalk & Thorley-Lawson, 2005). The lower drawing in figure 7 depicts a model of how EBV likely uses B-cell biology to establish and maintain latency in the host. It is thought that deregulation of cellular genes by viral latent gene products promotes lymphomagenesis.

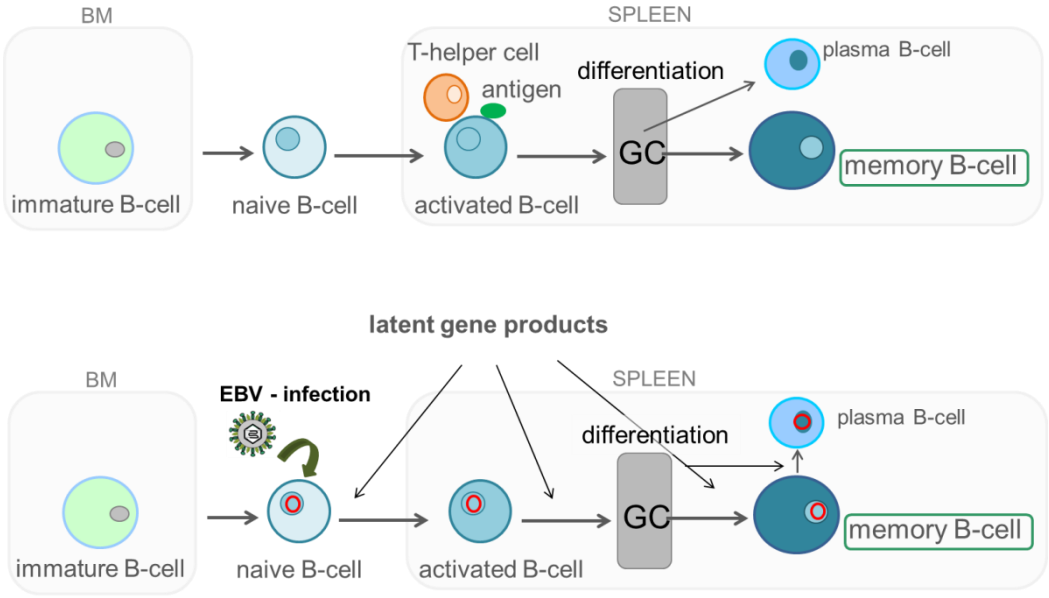

Figure 7: A simplified schematic drawing of how EBV uses normal B-cell biology to maintain and persist in memory B-cells. Upper figure: When a B-cell reaches the immature B-cell state in the BM compartment the cell emerges in the periphery, where it receives further survival signals to differentiate into a mature B-cell. When the B-cell binds an antigen plus a T-helper cell in a secondary lymphoid organ like spleen it may cause germinal center (GC) formation. B-cells within the GC can differentiate into plasma or long-living memory B-cells. Lower figure: EBV infects naïve B-cells that circulate in the periphery (red circle: EBV episome). EBV uses different transcription programs to activate these cells to become first proliferating cells and further on memory B-cells by undergoing GC response. Memory B-cells display an optimal reservoir for the virus to persist life-long in the host.

It is suggested that KSHV uses nearly every aspect of normal B-cell response, as EBV does. Importantly, latent proteins of EBV and KSHV are not conserved, but it seems very likely that the mechanisms they use to gain access to the memory B-cell pool are conserved. KSHV probably utilizes mechanisms similar as EBV, but so far it is not clear to what extent KSHV pushes the infected naïve B-cells into the memory state and if so, which KSHV gene products may orchestrate this process. Futhermore, it is unclear which molecular mechanisms are crucial for the development of KSHV-induced lymphoma.

1.9 MICRORNAS IN KSHV DISEASE

miRNAs comprise a large family of small (22 - 24 nt), non-coding, regulatory RNA molecules that mediate the post-transcriptional repression of protein-coding genes (Bartel, 2004; Hammond, 2005; Kim, 2005). Nowadays, it is well accepted that miRNAs are important regulators of diverse cellular processes such as cellular differentiation, proliferation, apoptosis and metabolism. To date more than 15000 miRNAs have been registered at miRBase (http://www.mirbase.org/cgi-bin/browse.pl), of which ~ 1500 primary miRNAs (pri-miRNAs) have a human and 240 a viral origin.

1.9.1 **miRNA biogenesis and their mode of action**

miRNAs are transcribed as part of much longer (typically several thousand nucleotides (nt) in length) precursor transcripts termed pri-miRNAs. While most pri-miRNAs are transcribed by RNA polymerase II (RNA pol II), a subset may be transcribed by RNA pol III, such as the MHV68 encoded miRNAs (Bogerd et al., 2010). Pri-miRNAs may be mono- or polycistronic and encode a single miRNA or a cluster of several miRNAs (Lee et al., 2004). RNA pol II-derived pri-miRNAs are capped and polyadenylated and contain at least one characteristic hairpin structure of typically 60 - 80 nt.

The processing of the pri-miRNA to a functional miRNA form involves several enzymatic steps (Figure 8). The RNAse III-like enzyme Drosha, a highly conserved protein among animals, recognizes the hairpin. Drosha forms together with its co-factor DGCR8 (DiGeorge syndrome critical region gene 8) the microprocessor complex. It is thought that DGCR8 assists Drosha in RNA recognition (Denli et al., 2004). The microprocessor cleaves the pri-miRNA approximately 22 nt from the stemloop junction, thereby liberating a 60 nt pre-miRNA with a 2 nt 3´overhang (Lee et al., 2002). Exportin 5 (Exp5) recognizes this specific overhang and transports the pre-miRNA to the cytoplasm in a Ran/GTP dependent manner (Yi et al., 2003; Zeng & Cullen, 2004). In the cytoplasm, the same overhang is then recognized by another RNAse III endonuclease, named Dicer. This enzyme is conserved among most eukaryotic organisms (Bernstein et al., 2001). Dicer cleaves the terminal loop, generating a siRNA-like molecule, the ~ 21 nt long miRNA/miRNA* duplex, which exhibits 2 nt 3´overhangs at both strands (Bernstein et al., 2001; Hutvágner et al., 2001; Chendrimada et al., 2005).

The next step is integration of the miRNA into the multiprotein complex RISC (RNA-induced silencing complex), which provides the enzymatic machinery to inhibit gene expression. Typically, one strand of the miRNA/miRNA* duplex enters the RISC complex, whereas the other strand (commonly termed as passenger strand or miRNA*) is degraded. Nowadays, the nomenclature miRNA-3p/miRNA-5p is commonly used instead miRNA/miRNA*.

The core protein components of the mammalian RISC are one of four Argonaute proteins (Ago1-4) and GW182. These proteins are important to anchor the miRNA in the complex and are furthermore crucial for translational inhibition.

Once the miRNA is loaded in the RISC, miRNAs guide the RISC to complementary sites predominantly in 3´UTRs (untranslated region) of target mRNAs. Generally, miRNAs can act by inhibiting translation or promoting cleavage of target transcripts (Bartel, 2004; Liu et al., 2004; Meister et al., 2004; Fabian et al., 2010; Guo et al., 2010). Cleavage or ‘slicing’ occurs whenever the miRNA is perfectly complementary to the mRNA. A single phosphodiester bond in the mRNA is cleaved between nt 10 and 11 away from miRNAs

5´-end (Elbashir et al., 2001). This mechanism is rarely observed in animals, but frequently found in plants (Elbashir et al., 2001; Behm-Ansmant et al., 2006). In animals, the complementarity of miRNA-mRNA binding is often restricted to the seed region (Lewis et al., 2003), which comprises the nucleotides 2 - 8 (minimally 2 - 7 nt), numbered from the 5´-end of the miRNA. This imperfect miRNA-mRNA interaction results in bulges in the central region, which prevents the so called “slice” activity of Ago2 (Bartel, 2009). Nevertheless this interaction is sufficient to suppress gene expression via translational inhibition

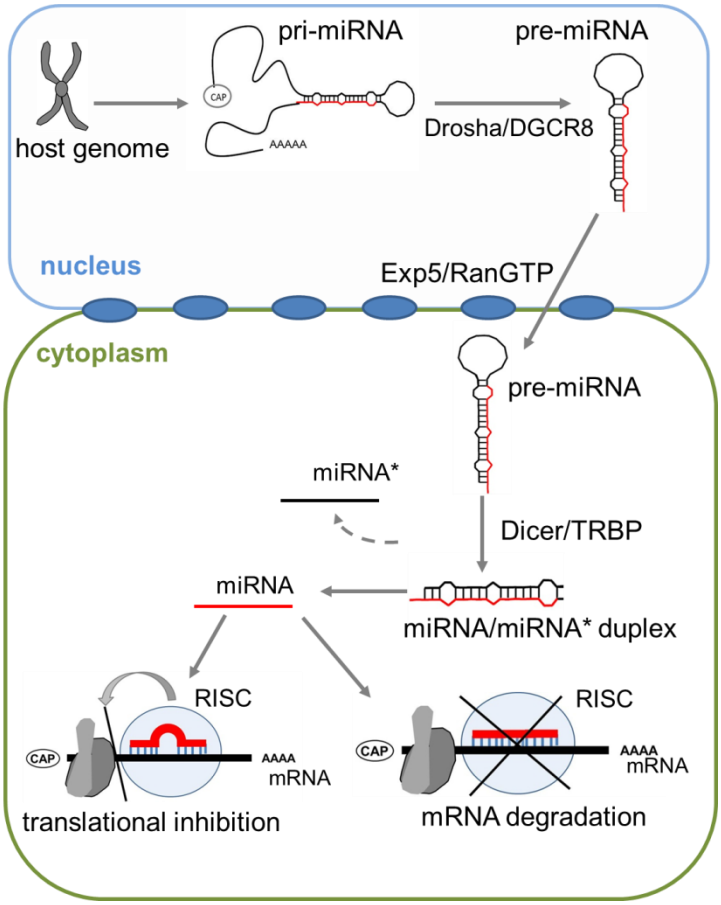

Figure 8: miRNA biogenesis. miRNA genes are transcribed by RNA pol II to generate pri-miRNAs. The hairpin is recognized by the microprocessor Drosha/DGCR8, which cleaves the pri-miRNA and liberates a 60 nt pre-miRNA. Exp5 transports the pre-miRNA in a Ran/GTP manner to the cytoplasm. Dicer recognizes and cleaves the hairpin, processing a siRNA like miRNA/miRNA* duplex. One strand is preferentially incorporated into RISC and mediates translational inhibiton (imperfect binding) or mRNA degradation (perfect binding). (Figure: Adam Grundhoff; modified).

1.9.2 **Target identification**

Bioinformatics and experimental approaches suggest that miRNAs regulate ~ 30 – 70 % of protein-coding genes (Friedman & Jones, 2009; Grundhoff & Sullivan, 2011). Although remarkable progress has been made in understanding the mechanisms that miRNAs use, their functions are still elusive.

To elucidate the functional role of miRNAs, it is indispensable to identify their targets. The seed-complementarity is the most important criteria for identifying targets and most computational algorithms search for seed matches in the 3´UTR to predict miRNA targets. Because of the limited complementarity required for miRNA regulation, individual miRNAs may potentially regulate hundreds of transcripts (Bartel, 2009). On the other hand, many sites that match the seed of given miRNA confer very little or no repression, making the target identification complex. Moreover, not all miRNAs bind via their seed. A lacking seed match can be compensated by base-pairing between mRNA target and the 3´-end or the central region of the miRNA (Bartel, 2009; Shin et al., 2010). miRNAs bind generally within the 3´UTR, but there are exceptions that target the 5´UTR or the coding region. Additionally, multiple miRNAs may act combinatorial by binding a single mRNA. miRNA-induced changes are often subtle and changes in the mRNA- and protein-level are hardly measurable, making the identification of functionally or biologically relevant targets a challenging task.

1.9.3 **KSHV-encoded miRNAs**

KSHV encodes 12 pre-miRNAs that give rise to 25 mature miRNAs, which were all expressed during latency (Cai et al., 2005; Pfeffer et al., 2005; Samols et al., 2005; Grundhoff et al., 2006a). Notably, the number of miRNAs (25 mature miRNAs) exceeds that of 12 pre-miRNAs. This is explainable with the abundant expression of 5p and 3p miRNAs and the seed editing of miR-K12-10; thus there is an unedited miR-K12-10a and an edited miR-K12-10b, in which adenosine was edited to inosine. All miRNAs are located in the LAR (see figure 4 in section 1.6.1) (Cai et al., 2005; Pfeffer et al., 2005; Cai & Cullen, 2006; Grundhoff et al., 2006b). They are called miR-K12-1 to miR-K12-12, due to their close position to the ORF K12. While ten of the twelve miRNAs are located in the intergenic region between ORF K12 and ORF 71, two of them, miR-K12-10 and 12, are encoded in the coding region and the 3´UTR of ORF K12, respectively (Cai & Cullen, 2006). Both stemloops might be cis-regulatory RNA elements that probably destabilize the *kaposin* mRNA (ORF K12), which consequently reduce protein expression from these transcripts (Lin & Sullivan, 2011).

Since KSHV miRNAs are constitutively expressed during latency, these molecules might be beneficial during establishment and maintenance of latent infections. However, the understanding of their role in KSHV life-cycle and pathogenesis is still elusive (Grundhoff & Sullivan, 2011; Gottwein, 2012). So far, a few targets were identified, generally by using miRNA overexpression experiments followed by gene expression profiling and validating

targets with luciferase reporter assays. Examples of KSHV-miRNA targets are described below.

Targets of KSHV miRNAs can be either host or cellular mRNAs. Because the KSHV genome is small in size compared to the host genome, the identification of viral mRNA targets is much easier than finding cellular targets. But so far, only one viral mRNA target has been validated as a target, namely RTA, the master regulator of the latent-lytic switch. miR-K12-9* (also named as miR-K12-9-5p) targets RTA, which consequently regulates the entry into lytic KSHV replication (Bellare & Ganem, 2009).
Viral miRNAs may also regulate host cell gene expression by targeting host mRNAs to benefit the virus for its persistence in the host. The few identified cellular targets are predicted to support processes like the viral escape from immune response, cell cycle progression and anti-apoptosis. For example, miR-K12-10a is considered to target *TWEAKR*, which is involved in the induction of apoptosis (Abend et al., 2010). miR-K12-7 targets the *MICB* mRNA (MHC class I polypeptide-related sequence B) leading to repression of the recognition by natural killer cells (NK cells). This represents an important mechanism to evade the immune system (Nachmani et al., 2009). miR-K12-1 has been shown to influence cell cycle arrest, which targets p21, an inhibitor of cyclin complexes. Repression of p21 probably leads to evasion of cell cycle arrest (Gottwein & Cullen, 2010). An important target in regard to tumorigenesis represents SMAD5, which is targeted by miR-K12-11. SMAD5 repression attenuates TGFβ (transforming-growth factor β) signaling and consequently might promote tumor formation (Liu et al., 2012). Furthermore, KSHV miRNAs may also regulate proliferation and cell survival by targeting *BACH-1* (miR-K12-11) and *BCLAF* (Bcl2-associated transcription factor) (miR-K12-5, K12-9-3p, K12-10a, K12-10b). The transcriptional reprogramming has also been postulated as a function influenced by miRNAs. Hansen et al. proposed that *MAF* (musculoaponeurotic fibrosarcoma oncogene homolog) is a target of miR-K12-1, miR-K12-6-5p and miR-K12-11. They revealed in KSHV-infected lymphatic endothelial cells that these miRNAs regulate transcriptional reprogramming and thereby having an influence in differentiation. Epigenetic processes are also thought to be regulated by KSHV miRNAs. Evidence provides a study, in which they demonstrated that miR-K12-4-5p targets Retinoblastoma-like protein 2 (RBL2), which likely results in the increase of DNA methyltransferases DNMT1, 3a and 3b. They assume that KSHV miRNAs regulate epigenetic reprogramming to modulate methylation pattern of the viral and host genome (Lu et al., 2010).

Given the above, there is strong evidence that KSHV miRNAs targets multiple pathways to maintain the latent state of the KSHV genome and regulate multiple cellular processes to evade cell cycle arrest, cell death and immune evasion. Functional experiments are now required to gain insight into how and to what extent the miRNAs are important for KSHV latency and tumorigenesis.

1.9.4 **miR-K12-11 shares seed sequence homology with miR-155**

Some viral-encoded miRNAs share sequences with host miRNAs and therefore possibly use the pre-existing network of cellular miRNAs, suggesting that they function as viral analogs of cellular miRNAs.

A few KSHV-encoded miRNAs share seed homologies to cellular miRNAs (Gottwein 2011). A well characterized analog represents miR-K12-11, which shares extensive sequence identity including a perfect seed match with the cellular miR-155. This cellular miRNA is encoded in the *BIC* (B-cell integration cluster) gene, which was originally identified as a frequent retroviral integration site for avian leucosis virus (Clurman & Hayward, 1989; Tam et al., 1997). *BIC* RNA is highly conserved among mammalian species, whereby the precursor hairpin is the most conserved characteristic. As depicted in figure 9 (page 18), the mature sequence of human (hsa) and mouse (mmu) miR-155 is almost identical. There is only one nucleotide exchange at position twelve.
The mimicry of hsa-miR-155 by miR-K12-11 garnered considerable interest since hsa-miR-155 functions in diverse processes like hematopoiesis, B-cell development and immune response (Costinean et al., 2006; Rodriguez et al., 2007; Thai et al., 2007; O'Connell et al., 2008). A moderate increase of hsa-miR-155 levels is observed in many types of malignancies of B-cell or myeloid origin. *BIC*/miR-155 is highly overexpressed in several cancers such as chronic lymphocytic leukemia (CLL), diffuse large B-cell lymphoma *(*DLBCL), acute myelogenous leukemia *(*AML) and Burkitt´s lymphoma (Eis et al., 2005; Volinia et al., 2006). The correlation between miR-155 and lymphomas was complemented by a study with transgenic miR-155 mice (Costinean et al., 2006). These mice express miR-155 in a B-cell dependent manner and developed pre-B-cell lymphoproliferative disorders which later progressed to full B-cell lymphomas. Furthermore, miR-155 was the first miRNA described as a so-called oncomiR; a miRNA with oncogenic activity. Nevertheless, precise mechanisms by which miR-155 modulate lymphocyte differentiation and transformation are not clear.

A role of miR-K12-11 in the viral life-cycle and in virus-induced lymphomagenesis has not been validated so far. It is postulated that KSHV evolved the seed of miR-K12-11 to mimic

hsa-miR-155 functions by tapping into the hsa-miR-155 target network. KSHV downregulates the expression of hsa-miR-155, which suggests that miR-K12-11 replace this miRNA and supplant important signals for KSHV. Since miR-155 plays a role in B-cell development and GC formation, the seed sharing might be one putative strategy for KSHV to drive infected naïve B-cells to the long-living memory B-cells to persist in the host.

Evidence that miR-K12-11 is a functional ortholog provide *in vitro* studies that revealed shared targets. They validated target genes that were involved in B-cell function (*SLA* gene) and mediating expression of transcription factors, such as FOS and BACH1 (Gottwein et al., 2007; Yin et al., 2008a; Bolisetty et al., 2009; Liu et al., 2012). The analogy between miR-K12-11 and hsa-miR-155 was confirmed using PAR-CLIP (Photoactivatable-Ribonucleoside-Enhanced Crosslinking and Immunoprecipitation) by the recovery of ~ 40 % of all known hsa-miR-155 targets as candidate targets of miR-K12-11 in PEL cell lines (Gottwein et al., 2011a).

It is worth to note that not only KSHV utilizes the mimicry with miR-155. The alpha-herpesvirus Marek´s disease virus (MDV) encodes miR-M4, which shares the seed sequence with miR-155, as miR-K12-11 (figure 9) (Zhao et al., 2011). Strikingly, although EBV does not encode a viral miRNA with an identical seed to hsa-miR-155, it utilizes mechanisms that strongly enhance the endogenous hsa-miR-155 expression level (Gatto et al., 2008; Yin et al., 2008a; Linnstaedt et al., 2010; Cameron et al., 2008). These examples emphasize the hypothesis that these herpesviruses require either the viral or cellular miRNA for their life-cycle. Importantly, all three viruses are associated with cancers, assuming that the cellular miRNA or the viral orthologs play a critical role in virus-induced tumorigenesis (Zhao et al., 2011).

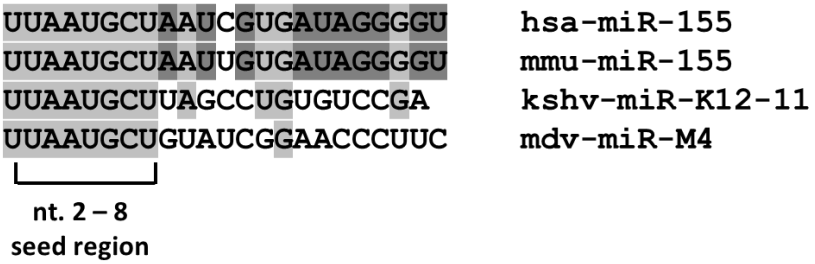

Figure 9: Seed sharing between viral and cellular miRNAs. Alignment of the human (hsa) and murine (mmu) miR-155 as well as the KSHV-encoded miR-K12-11 and the MDV-encoded miR-M4. Conserved nucleotides between hsa, mmu and the viral miR-K12-11 and/or miR-M4 are highlighted in light gray boxes. Nucleotides that are conserved between hsa- and mmu-miR-155 are shown in dark gray boxes. Non-conserved nucleotides are shown with white background. The seed region (nt 2 - 8) is considered to be the most critical region for base-pairing between miRNA and target 3`UTR. (Figure: Adam Grundhoff).

1.10 AIM OF THE STUDY

This study is based on the hypothesis that the KSHV-encoded miR-K12-11 has evolved to mimic the human miR-155. Because miR-155 plays a critical role in hematopoiesis and B-cell response, it is assumed that the virus utilizes the pre-existing target network of hsa-miR-155 to drive infected naïve B-cells toward the long-living memory B-cells, which enables the virus to reside life-long in the host. Furthermore, hsa-miR-155 is overexpressed in a number of human tumors and associated with their genesis, hence it is supposed that mimicry of hsa-miR-155 by miR-K12-11 contributes to cellular transformation in KSHV-associated malignanices.

This study aids to unravel if and to what extent the shared seed sequence of both miRNAs results in mimicking functions *in vivo* – and if miR-K12-11 influences B-cell response and lymphomagenesis. To address this issue, a side-by-side study was designed using a BM transplantation mouse model to force expression of hsa-miR-155 or miR-K12-11 in hematopoietic progenitor cells (HPCs). When seed sharing is sufficient, this should ensue in same phenotypic alterations. To gain further insight into cellular mechanisms and molecular processes that underlie these alterations, RNA from BM cells was isolated and expression levels of certain genes were analyzed to verify if they are downregulated *in vivo* in both miRNA mouse cohorts, assuming that these are shared targets.

Consequently, the study investigates the impact of miR-K12-11 in the context of hematopoiesis, lymphopoiesis and tumordevelopment and its mimicry to hsa-miR-155. Therefore this study aims to gain new insights into KSHV biology.

2 MATERIAL AND METHODS

2.1 CHEMICALS AND EXPENDABLE MATERIALS

If not specified elsewhere all chemicals and consumables were obtained from the following companies: Advanced Biotechnologies, Ambion, AMS Biotechnology, Applied Biosystems, Bayer Healthcare, BD Falcon, BD Bioscience, Beckmann, BioLegend, Bio-Rad, Biomol, Biozym, Boehringer Mannheim, Braun, Cambrex Cell Signaling, Covance, DAKO, Dianova, Diapath, Duxford, eBioscience, Eppendorf, GE Healthcare, Gibco, Gilson, GlassLine, Greiner, GRY-Pharma GmbH, Hartenstein, Heidolph, Heraeus, Invitrogen, Jackson Laboratory, Knick, Kodak, Lennox/Roth, Lonza, Medingen, Merck, Mettler, Millipore, mwg, NatuTec, New Brunswick, New England Biolabs, PAA, peqlab, Peprotech Pharmingen, Promega, Qiagen, Quantace, Roche, Rockomat Tecnomara, Roth, Santa Cruz, Sarstedt, Schleicher & Schuell, Schott, Seqlab, Sigma-Aldrich, Sorvall, StemCell Technologies, Stratagene, Southern Biotechnology, TaKaRa Bio INC., Thermo Electron, Vector Laboratories and Whatman.

2.2 COMMERCIAL SYSTEMS AND KITS

The following table summarizes the used commercial systems and kits.

Table 1: Commercial Systems and Kits that were used in this work.

Name	***Features***	***Company***
Superscript III	Reverse Transcriptase	Invitrogen
RNAse-Free DNase Set	Depletion of ds and ss DNA molecules	Qiagen
peqGOLD Plasmid Miniprep Kit	Isolation of plasmid DNA in small scale	peqlab
RNeasy FFPE Kit	Isolation of RNA from formalin-fixed, paraffin-embedded (FFPE) tissue sections	Qiagen
Maxi-Prep QIAGEN	Isolation of plasmid DNA in large scale	Qiagen
SensiMixPlus SYBR	SYBR Green for Real-Time PCR	peqlab
RNeasy Mini Kit	Purification of RNA	Qiagen
QIAquick® PCR Purification Kit	Purification of PCR-products	Qiagen
QIAquick® Gelextraction Kit	Purification of DNA out of agarose-gels	Qiagen
RNA Bee	Isolation of total RNA	Ambion
Lineage Depletion Kit	Enrichment of Lin^{neg} progenitors	Miltenyi Biotec
Luciferase Reporter assay	Luciferase assay	Promega

2.3 NUCLEIC ACIDS

2.3.1 Oligonucleotides

The following oligonucleotides were used for cloning, sequencing, polymerase chain reaction (PCR), quantitative PCR (qPCR, Real-Time PCR) and complementary DNA (cDNA) synthesis. All oligos were purchased from Invitrogen.

Table 2: Primer sequences for cloning. Restrictionsites are underlined.

Name	*5´- 3´ sequence*	*Purpose of use*
miR-K12-11 fw BamHI	ATC**GGATCC**ATCTAGTCGCCCGTTATTGT	Cloning into expression plasmid
miR-K12-11 rev EcoRI	GAT**GAATTC**CACGCGTACGGTGGTCTCAT	Cloning into expression plasmid
miR-K12-7 fw BamHI	ATC**GGATCC**GCAATTTTTGTCGTATGCGC	Cloning into expression plasmid
miR-K12-7 rev EcoRI	GAT**GAATTC**GGATAGCCACCCACAATTGT	Cloning into expression plasmid
Jarid2 3´UTR fw SpeI	AGT**ACTAGT**GCCCGTGGTCGATTTATA	Cloning into pMIR-report
Jarid2 3´UTR rev HindIII	GGCG**AAGCTT**TGAAGTCTCCCTCCCAAG	Cloning into pMIR-report
hsa-miR-155 fw BamHI	AG**GGATCC**ACTATATGCTGTCACTCCAGCT	Cloning into expression plasmid
hsa-miR-155 rev EcoRI	CAA**GAATTC**CCAGTGACCAGATTATGATTAAC	Cloning into expression plasmid

Table 3: Primer sequences for Real-Time reverse transcriptase (RT) PCR.

Name	*5´- 3´ sequence*	*Purpose of use*
Mmu hprt fw	GCTGGTGAAAAGGACCTCT	Housekeeping gene (mus musculus)
Mmu hprt rev	CACAGGACTAGAACACCTGC	Housekeeping gene (mus musculus)
Mmu RPLP fw	CTCGCTTGCATCTACTCCGC	Housekeeping gene (mus musculus)
Mmu RPLP rev	AGAAAGGTTCGACGCTGACAC	Housekeeping gene (mus musculus)
Mmu GAPDH fw	GGTGAAGGTCGGTGTGAAC	Housekeeping gene (mus musculus)
Mmu GAPDH rev	GGGGTCTCGCTCCTGGAA	Housekeeping gene (mus musculus)
Mmu actinB fw	GAAATCGTGCGTGACATCAAAG	Housekeeping gene (mus musculus)
Mmu actinB rev	TGTAGTTTCATGGATGCCACAG	Housekeeping gene (mus musculus)
Jarid2 qPCR fw 2	CCCAAGTGTCCTCCACTAGC	Jarid2 gene (mus musculus)
Jarid2 qPCR rev 2	TGGGACTATTCGGCTGAGAC	Jarid2 gene (mus musculus)
c-myb RT fw	CTGTCAAAAGCCTACCCTTCTC	c-myb gene (mus musculus)
c-myb RT rev	TGGAGGGTAAGGTAGGTGCAT	c-myb gene (mus musculus)
Fos RT fw	AAACGGAGAATCCGAAGGGAA	Fos gene (mus musculus)
Fos RT rev	TATTTTGGCAGCCCAC	Fos gene (mus musculus)
Mmu Pu.1 fw	AGA TGC ACG TCC TCG ATA CT	Pu.1 gene (mus musculus)
Mmu Pu.1 rev	TTG TGC TTG GAC GAG AAC TG	Pu.1 gene (mus musculus)

Table 4: Primer sequences for cDNA synthesis. SL denotes stemloop.

Name	*5´ - 3´ sequence*
SL miR-21 TM	GTCGTATCCAGTGCAGGGTCCGAGGTATTCGCACTGGATACGACTCAACA
SL miR-K12-11	GTTGGCTCTGGTGCAGGGTCCGAGGTATTCGCACCAGAGCCAACTCGGACAC
SL hsa-miR-155	GTTGGCTCTGGTGCAGGGTCCGAGGTATTCGCACCAGAGCCAACACCCCT

Table 5: Primer sequences for Real-Time stemloop RT PCR.

Name	*5´- 3´ sequence*
miR-K12-11 fw	GCTGTTAATGCTTAGCCTGT
hsa-miR-155 fw	CAGCTTAATGCTAATCGTGAT
miR-21 fw	CGA TAG CTT ATC AGA CTG A
UniRev	GTG CAG GGT CCG AGG T

2.4 ANTIBODIES

2.4.1 Primary antibodies

The following tables list the used primary antibodies for immunofluorescence (IF), western blot, immunohistochemistry (IHC) and fluorescence activated cell sorting (FACS).

Table 6: Primary antibodies for IF and western blot.

Name	*Feature*	*Company*
Anti-Jarid2	Rabbit polyclonal antibody against Jarid2	Santa Cruz, sc-134548
Anti-β-actin	Mouse monoclonal antibody against β-actin	Santa Cruz, sc-47778

Table 7: Primary antibody for IHC.

Name	*Feature*	*Company*
PNA	Biotinylated Peanut Agglutinin (PNA) PNA binds preferentially to galactosyl (β-1,3) N-acetylgalactosamine	Vector Laboratories

Table 8: Primary antibodies for FACS analysis.

Name	*Fluorochrome*	*Clone*	*Company*
Anti-CD19	PE	1D3	Pharmingen
Anti-CD19	APC	6D5	BioLegend
Anti-B220	APC	RA3-6B2	BioLegend
Anti-CD3e	PE	145-2C11	BioLegend
Anti-CD11b	PE	M1/70	BioLegend
Anti-Gr1	APC	RB6-8C5	eBioscience
Anti-IgM	PE	RMM1	BioLegend

2.4.2 Secondary antibodies

The following secondary antibodies were used.

Table 9: Secondary antibodies.

Name	*Features*	*Company*
FITC anti rabbit IgG	FITC-conjugated rabbit IgG from goat	Santa Cruz Biotechnology
TexasRed anti Mouse IgG	TexasRed-conjugated mouse antibody from goat	Santa Cruz Biotechnology

2.5 PLASMIDS

2.5.1 Generation of retroviral vector pseudotypes

Following table summarizes retroviral vectors and packaging plasmids that were used to generate pseudotyped retroviruses.

Table 10: Retroviral vectors and packaging plasmids.

Vector	*Features*	*Reference*
SF91	SF91-enhanced green fluorescent protein (eGFP) γ-retroviral vector Encodes eGFP	(Schwieger et al., 2002; Schambach et al., 2006)
SF91 K12-11	SF91-eGFP γ-retroviral vector Encodes miR-K12-11 plus eGFP miRNA sequence is inserted into BamH/EcoRI restriction site	(Schwieger et al., 2002; Schambach et al., 2006)
SF91 miR-155	SF91-eGFP γ-retroviral vector Encodes hsa-miR-155 plus eGFP miRNA sequence is inserted into BamHI EcoRI restriction site	(Schwieger et al., 2002; Schambach et al., 2006)
#522	pEcoenv-I-puro Packaging construct Encodes ecotropic env gene EF1α-promoter	(Morita et al., 2000)
R690	pSV40 gag-pol Packaging construct Encodes MoMLV gag and pol genes SV40 promoter	(Beyer et al., 2002)

2.5.2 Luciferase assay plasmids

Following table lists plasmids that were used for luciferase reporter assays.

Table 11: Plasmids that were used for luciferase reporter assays.

Vector	*Features*	*Origin*
pCDNA3-GFP	Standard cloning vector Encodes GFP	Invitrogen
pCDNA3-GFP miR-K12-11	Encodes GFP plus miR-K12-11 miRNA sequence is inserted into BamHI/EcoRI restriction site	Invitrogen
pCDNA3-GFP miR-K12-7	Encodes GFP plus miR-K12-7 miRNA sequence is inserted into BamHI/EcoRI restriction site	Invitrogen
pCDNA3-GFP hsa-miR-155	Encodes GFP plus hsa-miR-155 miRNA sequence is inserted into BamHI/EcoRI restriction site	Invitrogen
pMIR-report™	pMIR-report™	Promega

Sensor miR-11	pMIR-report Positive control for miR-K12-11 Contains four binding sites (BS) for miR-K12-11	Promega
pMIR-report *JARID2*	pMIR-report Encodes 3´UTR of *JARID2* NM_004973 *JARID2* mRNA	Promega
pMIR-report *JARID2* m1	pMIR-report Encodes 3´UTR of *JARID2* Mutation of the first miR-K12-11/miR-155 BS BS I: 4169-4175 nt NM_004973 *JARID2* mRNA	Promega
pMIR-report *JARID2* m2	pMIR-report Encodes 3´UTR of *JARID2* Mutation of second miR-K12-11/miR-155 BS BS II: 4971-4977 NM_004973 Jarid2 mRNA	Promega
pMIR-report *JARID2* m1+m2	pMIR-report Encodes 3´UTR of *JARID2* Mutation of both miR-K12-11/miR-155 BS BS I: 4169-4175 nt and BS II: 4971-4977 NM_004973 *JARID2* mRNA	Promega

2.5.3 **Plasmids for miRNA expression analysis**

The following table lists plasmids that were used for diverse assays to analyze miRNA expression and function.

Table 12: Plasmids that were used for miRNA expression analysis.

Vector	***Features***	***Origin and reference***
pCMV-Sport 6 *JARID2*	Contains *JARID2* gene with shortened 3´UTR Contains first miR-K12-11 and hsa-miR-155 BS I: 4169-4175 nt NM_004973	ATCC catalog number 9121501 (Bolisetty et al., 2009)
pCMV-Sport 6 *JARID2* fl	Contains *JARID2* gene with fulllength (fl) 3´UTR Contains both BS for miR-K12-11 and hsa-miR-155 (BS I: 4169-4175 nt and BS II: 4971-4977 nt)	ATCC catalog number 9121501 (Bolisetty et al., 2009)
pCR2.1	TA-cloning Ampicillin and kanamycin resistance	Invitrogen

2.6 EUKARYOTIC CELL CULTURE

2.6.1 **Eukaryotic cell lines and primary cells**

Table 13 lists eukaryotic cell lines.

Table 13: Cell Lines.

Cell Line	*Features*	*Reference*
BCBL-1	PEL cell line KSHV positive, EBV negative	(Renne et al., 1996)
BJAB	Burkitt-Lymphoma cell line KSHV negative, EBV negative	(Steinitz & Klein, 1975)
RAJI	Burkitt-Lymphoma cell line KSHV negative, EBV positive	(Fadeel, 2005)
HEK 293T	Epithelial cell line, adherent Stable and constitutive expression of SV40 large T-antigen	(Graham et al., 1977)
NIH3T3	Mouse embryonic fibroblasts	(Jainchill et al., 1969)

The next table lists primary cells that were used in this work.

Table 14: Primary cells.

Primary cells	*Features*	*Origin/reference*
BM cells	Origin of C57BL/6 mice	C57BL/6, Jackson Laboratory

2.6.2 **Adherent cell culture**

Adherent cell lines were cultured in polysterene cell culture flasks or dishes in Dulbecco´s modified eagle medium (DMEM) supplemented with 1 % Penicillin-Streptomycin (Pen/Strep), 1 % glutamine, 1 % sodium pyruvat and 10 % fetal calf serum (FCS). Cells were cultured at 37°C with 5 % CO_2 and splitted when they reached a cell density of ~ 90 %. Cells were washed twice with phosphate buffered saline (PBS) and incubated with Trypsin/ethylenediaminetetraacetic acid (EDTA) for 3 - 5 min at 37°C until cells detached. Then, cells were re-suspended in DMEM. They were reseeded in a 1/10 ratio with fresh media with supplements.

2.6.3 **Subculturing suspension cells**

Suspension cell lines (BCBL-1, RAJI) were carried in RPMI 1640 (Roswell Park Memorial Institute 1640) supplemented with 10 % FCS and 1 % Pen/Strep at 37°C with 5 % CO_2. Cells were maintained by feeding them every 2 to 3 days. They were grown to a density of 1 – 2 x 10^6 cells/ml and then splitted 1:5 in fresh medium.

2.6.4 **Primary bone marrow cells**

BM cells were harvested from tibiae and femora of donor wt C57BL/6 mice (Ly5.2) that received an intraperitoneal injection of 5-fluorouracil (5-FU) five days before isolation; or BM cells were harvested from untreated C57BL/6 mice prior to negative lineage depletion. The 5-FU treatment as well as the lineage depletion is described in section 2.11.2 and 2.11.3, respectively.

Mice were etherized and sacrificed by cervical dislocation. To keep the mice semi-sterile they were immersed in 80 % ethanol. Under a sterile laminar flow bench BM cells were harvested by rinsing sterile PBS through tibiae and femora using syringe and canula. Prior to erilyse with Lyse-buffer (Pharmalyse 10 x), the harvested cells were centrifuged for 5 min at 300 x g. Then, cells were diluted in a density of 2 - 4 x 10^6 in 1 ml StemSpan™ Serum-Free Expansion Medium (SFEM) and cultured for 24 h.
Isolated BM cells were cultured in SFEM supplemented with 1 % glutamine, 1 % Pen/Step, 100 ng/ml mouse stem cell factor (mSCF), 100 ng/ml each human fms-related tyrosine kinase 3 Ligand (hFlt3-L) and human interleukin 11 (hIL-11), and 10 ng/mL mouse interleukin 3 (mIL-3). The following transduction with generated retroviruses is described in section 2.11.4.

2.6.5 **Long-term storage of cell lines**

For long-term storage of eukaryotic adherent cells, sub-confluent cells were detached using Trypsin/EDTA and centrifuged (500 x g, 5 min, 4°C). The cell pellet was re-suspended in FCS supplemented with 10% dimethyl sulfoxide (DMSO) (Sigma). The cell suspension was aliquotted in CryoPure tubes (Sarstedt) and slowly frozen in an isopropanol bath deposited at -80°C. This mild treatment reduces the formation of ice-crystals. After 24 h the frozen cell suspension was transferred into liquid nitrogen (-196°C) for long-term storage.

2.6.6 **Initiation of cell lines**

For initiation of a cell culture an aliquot was taken out of liquid nitrogen (-196°C). Cells were thawed quickly for 2 min at 37°C in a water bath. Ten ml of the appropriate cell culture medium was added and cells were resuspendend in this medium. After incubation for 30 min at 37°C and 5% CO_2 the medium was removed and cells were covered with fresh medium with supplements. Suspension cells were additionally centrifuged (1000 rounds per minute (rpm), 3 min, room temperature, Heraeus). The cell pellet was re-suspended in fresh medium plus supplements.

2.6.7 **Cell counting**

Cell density was determined using Neubauer Cell Counting chamber. Trypan Blue was used to selectively stain dead cells by mixing 1 volume Trypan Blue with 1 volume cell suspension for an incubation time of 5 min. Cells were counted under the light microscope (Leica) using 3 x 16 small quadrates. Cell number per ml was calculated using the average number of counted cells that were multiplied with factor 10^4.

2.6.8 **Transient transfection**

Transfection was performed with Polyethylenimine (PEI), a polymeric transfection agent, which condenses DNA into positively charged particles. This complex binds to anionic cell surface residues and is brought into the cell via endocytosis.

Transient transfection with PEI was performed according to the following protocol. 293T cells ($5x10^6$) were seeded into a 10 cm cell dish. After 24 h, cell culture medium was removed and cells were overlaid with 3 ml OptiMem. Then, 1 - 5 µg DNA was diluted in 1 ml OptiMem and mixed with 40 µl PEI (1 mg/ml). The mixture was incubated for 15 min at room temperature and subsequently added drop by drop to cells in medium. Cells were incubated for 8 h at 37°C. Then, supernatant was removed and transfected cells were overlaid with fresh medium plus supplements.

2.6.9 **Generation of pseudotype retroviral vectors**

Retroviral vector pseudotypes were generated by transient transfection of 293T cells using PEI plus plasmids expressing appropriate viral packaging proteins env (pEcoenv-I-puro; 3 µg (Morita et al., 2000)) and gag-pol (pSV40-gag-pol; 8 µg) (Beyer et al., 2002)) as well as the appropriate retroviral vector (SF91-miR-K12-11, SF91-hsa-miR-155 or SF91; 5 µg (Schwieger et al., 2002)). After 48 h, 72 h and 96 h, supernatant was harvested, sterile filtered through 0.22 µM Millex-GV Filter (Millipore) and used for transduction of NIH3T3 cells to determine the titer. The titer was evaluated using GFP expression analysis via FACS analysis (FACS Canto; BD Bioscience) three days post transduction of NIH3T3 cells (see also 2.6.10). Virus suspensions with a titer of $>1 \times 10^6$ infectious particles per ml were used for transduction of primary BM cells. Virus suspensions with a low titer ($<9 \times 10^5$) were discarded.

High-titer retroviral stocks were stored at -80°C.

2.6.10 **Transduction of cell lines**

After generation of pseudotype retroviral particles the filtered virus stock was used for transduction of NIH3T3 to determine titer and expression levels of miRNAs. Since the pseudotyped retroviruses express eco-env, the titration was performed on the mouse cell line NIH3T3. Four hours prior transduction 5×10^4 NIH3T3 cells were seeded into a 24-well plate. After sedimentation of cells on the plate, medium was removed and 500 µl fresh medium without supplements but with polybrene (8 µg/µL; Sigma-Aldrich, Taufkirchen) was added. An aliquot (20 µl, 100 µl) of retroviral stock was added to the cells. Immediately after centrifugation (28°C, 500 x g, 1 h) cells were incubated for 12 h at 37°C. Then, the medium-virus mix was removed and cells were covered with fresh medium plus supplements.

To determine the titer, FACS analysis was performed three days post transduction. The titer was calculated based on the volume of virus suspension (20 µl or 100 µl) and amount of seeded cells.
For miRNA expression analysis, GFP^+ cells were sorted and total RNA was extracted using RNA Bee (see 2.9.1).

2.6.11 Fluorescence-activated cell sorting (FACS)

FACS was used to separate GFP^+ BM cells from C57BL/6 mice or NIH3T3 cells. Flow cytometry was used to enumerate and define specific cell populations from splenic cells or BM cells. Prior to flow cytometry analysis or FACS, cells were collected, pelleted (1200 rpm, 3 min, room temperature; Multifuge 3 S-R) and washed with PBS. Finally cells were re-suspended in an appropriate volume of FACS buffer (PBS with 1 % FCS).
Cell sorting was performed in the Core Facility of the HPI on FACSAria (Becton Dickinson, Franklin Lakes, USA instrument). FACS analysis was performed on the FACSCanto (Becton Dickinson, Franklin Lakes, USA). Data was evaluated via FACSDiva software.

2.6.12 Luciferase reporter assay

A common method to analyze miRNA targets is the luciferase reporter assay. The 3´UTR of the gene of interest is inserted into the pMIR report vector (Promega), which encodes firefly luciferase gene upstream of 3´UTR of the gene of interest. The binding of the miRNA to the target site in the specific 3´UTR should result to a translational repression of the luciferase gene (see figure 10). This is measurable in luciferase activity. Firefly luciferase catalyzes the oxidation of luciferin in the presence of ATP, Mg^{2+} and molecular oxygen. Light is produced by converting the chemical energy of luciferin oxidation through an electron transition, forming the product molecule oxyluciferin.

For luciferase reporter assays, 293T cells (2×10^4) were seeded in 96-well plates. After 24 h cells were transfected with the pMIR-report construct, a miRNA expression construct and a ß-galactosidase (ß-gal) expressing construct for normalization purposes. The amounts of transfected DNA and reagents are listed in table 15.

Table 15: Protocol for luciferase reporter assay.

Reagents	***Concentration***
Luciferase Reporter Vector	5 ng
ß-Gal vector	50 ng
miRNA expression vector	50 ng
OptiMem	25 µl
PEI	1 µl

Transfections were done in technical duplicate, and at least three independent biological replicates were performed for each experiment. Lysates were prepared 24 h post transfection to measure luciferase and ß-gal activity. Cells were washed once in 50 µl PBS and then lysed in 100 µl 1 x RLB (Renilla Lysis Buffer). Cells were completely destroyed and the plate was frozen once at -80°C for at least 30 min. Prior to measurement of the luciferase activity, the lysates were thawed at room temperature for 30 min and homogenized by pipetting. The galactosidase activity was measured by transferring 50 µl lysate into a new 96 well plate and mixing with 50 µl 2 x Z-buffer (table 16) plus o-nitrophenyl-ß-D-galactopyranoside (ONPG) and freshly added ß-mercaptoethanol (7 µl/ml). Depending on the expression of ß-gal the incubation time at room temperature varies from a few minutes up to 1 h. Once a faint yellow color developed, the reaction was stopped by adding 150 µl of 1 M $NaCO_3$. Subsequently the absorption at 420 nm with a reference at 650 nm was measured with the microplate reader Synergy Mx using the Gen5 data analysis software.

Luminescence was measured by transferring 20 µl of lysate into a flat bottom white 96-well plate and adding 100 µl of the Renilla assay substrate solution. Luminescence was measured over 10 ms. The obtained light units were normalized by absorption of ß-gal activity.

Table 16: Z-Buffer with ONPG.

Components	***Concentration***
Sodium phosphate buffer pH 7.3	200 mM
$MgCl^{2+}$	2 mM
ONPG	1.33 mg/ml
ß-Mercaptoethanol (freshly added)	100 mM

In this work, the sensor vector miR-11 was used in every luciferase experiment as an internal control. This vector contains four perfectly complement binding sites to miR-K12-11. An expression construct of an irrelevant miRNA (miR-K12-7) served as a negative and normalization control, and was set to 100% (figure 10).

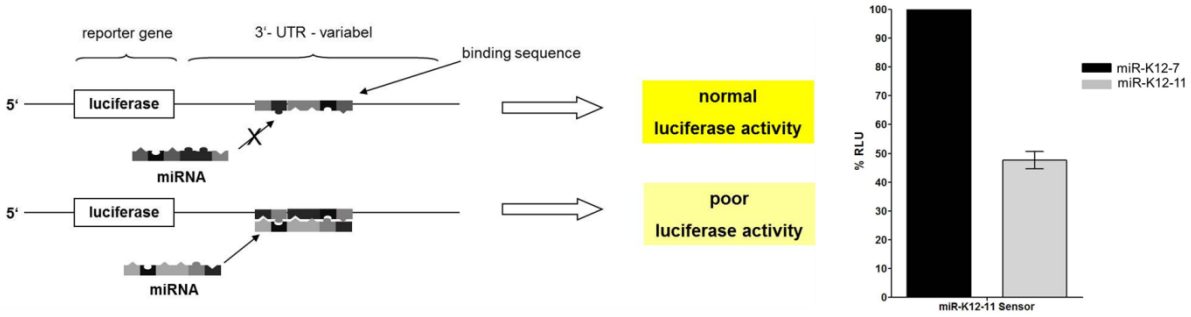

Figure 10: Sensor Vector. Left: Scheme of luciferase assay. The 3´UTR of the gene of interest is inserted into the pMIR report vector. A miRNA that do not bind to the sequence results in a normal luciferase activity, whereas the perfect binding results in poor luciferase. Right: The sensor vector was used as internal control. Expression of miR-K12-7 serves as negative control and was set to 100%. miR-K12-11 bind perfectly to the four binding sites that were cloned into the sensor vector. The luciferase activity leads to a reduction of 50% compared to the negative control. Results are from three independent experiments. (Scheme of luciferase: Dr. Nicole Walz; HPI; modified).

The efficiency of down-regulation of the luciferase activity of sensor miR-11 was investigated. The luciferase activity was reduced to 50%, confirming the efficacy of the luciferase reporter assay.

2.7 DNA-TECHNIQUES

2.7.1 Chemically competent bacteria

2.7.1.1 Bacteria and media for prokaryotic cell culture

Experiments were performed with the bacterial strain *Escherichia coli* (*E.coli)* DH5α (Genotype: F-, *dco*R, *rec*A1, *end*A1, *hsd*R17 (rk-, mk+), *sup*E44 1-, *thi*-1, *gyr* A96, *rel*A1). Bacteria were cultured in lysogeny broth (LB) medium (Lennox/Roth) or on LB-agar plates (40 g/L distilled H_2O (dH_2O) LB Agar). Media were sterilized by autoclaving for 20 min at 121°C. Selection of transformed bacteria was done by supplementing the LB-medium with appropriate antibiotics (100 µg/ml ampicillin or 50 µg/µl kanamycin).

2.7.1.2 Generation of chemically competent bacteria

Chemically competent bacteria were generated with the rubidium chloride ($RbCl_2$) method. A single colony of *E.coli* DH5α bacteria strain was inoculated in 500 ml LB_{KB}-medium (table 17) supplemented 8 mM $MgSO_4$ overnight (220 rpm, Innova® 43 Incubator Shaker Series).

The optical density (OD) correlates with the bacteria titer and was photometrically determined using a wavelength of 600 nm against medium as reference (1 OD = $8x10^8$ cells/ml). *E. coli* were continuously grown to an OD of 0.3 - 0.5 (Spectronic Genesys 10 Bio, Thermo Electron Corporation) followed by an incubation on ice for 15 min and were

subsequently centrifuged (300 x g; 5 min; 4°C). Supernatant was discarded and cells were re-suspended in 150 ml transformation buffer I (TFB I, table 18) and chilled on ice for 60 to 90 minutes. Centrifugation was repeated and cells were re-suspended in 30 ml ice cold TFB II (table 19). Aliquots of 200 µl were frozen in liquid nitrogen and stored at -80°C.
Following tables list the used buffers for the generation of chemically competent bacteria.

Table 17: LB_{KB} - media.

Components	*Concentration*
LB-Broth (Lennox, Roth)	10 g
KCl	5 ml
dH_2O	Filling up until 500 ml

Table 18: TFB I, pH 5,8.

Components	*Concentration*
Glycerol	22.5 ml (15% final concentration)
$CaCl_2$	1.5 ml (10 mM final concentration)
Kac	0.44 g (30 mM final concentration)
$RbCl_2$	1.81 g (100 mM final concentration)
$MnCl_2$	1.49 g (50 mM final concentration)
dH_2O	Filling up until 150 ml

Table 19: TFB II.

Components	*Concentration*
Glycerol	3.75 ml (15 % final concentration)
1 M 3 (N-morpholino)-propanesulfonic acid (MOPS)	250 µl (10 mM final concentration)
1 M $CaCl_2$	1.88 ml (75 mM final concentration)
$RbCl_2$	0.03 g (10 mM final concentration)
dH_2O	Filling up until 25 ml

2.7.2 **Transformation of chemically competent *E. coli***

Transformation of chemically competent *E.coli* was performed by the heat shock method. *E. coli* DH5α (100 µl) were thawed on ice for 10 min and subsequently added to ~ 50 ng plasmid-DNA or 10 µl of a ligation. Prior incubation on ice for 30 min, cells and DNA were carefully mixed. After flicking the tube, cells were transferred to a water bath (42°C) for 45 sec and immediately incubated on ice for 2 min. Subsequently, 900 µl LB-medium was added and the sample was incubated for 45 min in a shaking incubator at 37°C and 220 rpm (Innova® 43 Incubator Shaker Series). Afterwards the mixture was diluted in 5 ml LB-medium and then grown overnight at 37°C and 220 rpm (Innova® 43 Incubator Shaker Series) with appropriate antibiotics for amplification of a single plasmid in LB-medium, or plated onto LB-agar plates.

2.7.2.1 Blue-white screening

The Blue-white screening is based on a mutation in the lac Z-gene of bacteria (here: *E. coli* DH5α) that produce an enzymatic inactive protein (the Ω subunit). The protein misses 30 amino acids (α-region) at the N-terminus. The enzymatic activity can be recovered by transformation with a plasmid containing the missing α-region. In this work, the TA cloning vector pCR2.1 (Invitrogen) was used. Colonies were plated on 5-Bromo-4-Chloro-3-indolyl-ß-D-Galactopyranosid (XGal) and isopropyl β-D-1-thiogalactopyranoside (IPTG) containing agar plates (2.5 µl of 0.1 M IPTG, 40 µl of 20 mg/ml XGal). The lac repressor is inactivated by binding of IPTG leading to expression of the Ω subunit. Together with the α subunit the ß-gal gets active and hydrolyzes the chromogenic substrate XGal, which leads to blue staining of colonies. A successful ligation is indicated by whitish colonies. They contain vectors in which the sequence of the α- region is destroyed by insertion of an artificial DNA. Bacteria with self-aligned vectors are blue.

2.7.2.2 Culturing and storage

Agar plates

40 g LB-agar was diluted in 1 l dH_2O and autoclaved. Prior plating on bacteria plates, medium was cooled down and mixed with appropriate antibiotics. When the agar becomes jelly the plates were stored at 4°C.

Prior plating bacteria-suspensions onto agar plates, these suspensions were centrifuged (3000 rpm, 2 min, room temperature, Heraeus Biofuge pico), supernatant was removed and the cell pellet was re-suspended in 100 µl LB-medium. These agar plates were screened for clones after incubation overnight at 37°C.

Liquid culture

LB-medium was mixed with 1 l dH_2O prior autoclaving. *E. coli* DH5α were incubated in sterile LB-media supplemented with appropriate antibiotics (ampicillin or kanamycin) overnight at 37°C at 220 rpm (Innova® 43 Incubator Shaker Series).

Glycerol stock for long-time storage

Bacteria of a single colony were incubated in LB-medium with appropriate antibiotic overnight at 37°C and 220 rpm (Innova® 43 Incubator Shaker Series). Afterwards, cells were centrifuged (3000 x g, 5 min, Hereaus Biofuge fresco) and the cell pellet was re-suspended in 500 µl LB medium, transferred in 1.5 ml *CryoPure Tubes (*Sarstedt) and re-suspended in 500 µl sterile glycerol. Cells were stored at -80°C.

2.7.3 **Cloning**

In this work, particular PCR products were cloned. Whenever possible, the sticky end cloning strategy was performed. All generated constructs were confirmed by sequencing.

2.7.3.1 Ligation

Prior ligation, linearized vector DNA was treated with 1 Unit (U) of Calf Intestine Phosphatase (CIP, NEB) for dephosphorylization. 50 ng of vector DNA was mixed with a three- to fivefold molar amount according to the following formula.

$$\frac{ng\ (vector) * kb\ (insert) * 3 - 5\ molar\ amount}{kb\ (vector)} = ng\ (insert)$$

The standard protocol of a ligation reaction is shown in table 20.

Table 20: Protocol for ligation reaction.

Components	***Concentration***
Vector DNA	20 - 100 ng
Insert DNA	3 - 5x molar amount of vector DNA
T4-ligase reaction buffer 10x	2 µl
T4 ligase (1U/µl)	1 µl
dH_2O	Filling up until 10 µl

2.7.3.2 Quickchange mutagenesis

The mutation vectors pMIR-Jarid2 mut1, pMIR-Jarid2 mut2 and pMIR-Jarid2 mut1+2 were generated in accordance with the protocol of Stratagene Quickchange site-directed mutagenesis, using pMIR-Jarid2 as backbone vector.

2.7.4 Isolation of plasmid DNA from *E. coli*

Isolation of plasmid DNA was performed using peqGOLD Plasmid Miniprep Kit™ (peqlab) or Qiagen Plasmid Mini or Maxi-Kit (Qiagen). Small amounts of plasmid DNA were isolated from 3 ml cultures whereas larger amounts were prepared from 150 ml overnight cultures. Purification of plasmid DNA was performed according to manufacturer's instructions.
Purity and concentration of isolated DNA were determined photometrically using Nanodrop 1000 (peqlab). The isolated DNA was either used for analytical or preparative purposes. DNA was stored at 4°C for several weeks or at -20°C for several months.

2.7.5 Restriction of DNA

Restriction endonucleases (NEB and Fermentas) were used according to manufacturer's instructions. For analytic and preparative restrictions 0.5 - 2 µg DNA were digested and separated by gel-electrophoresis on 0.8 - 2 % agarose gel. For cloning approaches, DNA was gelextraced and used in ligation reactions.

2.7.6 **DNA sequencing**

Sanger´s generated DNA sequencing method was used to analyze DNA. The Sequencing Service from SeqLab was used. The samples were prepared according to the protocol of this service.

2.7.7 **DNA agarose-gel-electrophoresis**

DNA samples (PCR and restriction products) were separated using agarose gels for either analytic or preparative purposes. Gel-electrophoresis was performed with 1 x Tris-acetate EDTA buffer (TAE: 400 mM Tris-acetate; 20 mM EDTA; pH 8.5). Agarose concentrations reached from 0.8 - 2 % (0.8 %: 5 - 10 kbp fragments, 1 %: 1 - 5 kb fragments, 2 %: 0.2 - 1 kbp fragments). A 1 % agarose gel was prepared with 1 g agarose dissolved in 100 ml of 1 x TAE buffer and boiled in a microwave at 800 W for 4 min. After cooling down to ~ 60°C, 3 µl ethidiumbromide (EtBr) (10 mg/ml) was added. EtBr intercalates into DNA allowing a visualization of DNA fragments under UV light. DNA samples were mixed with 6 x loading dye (Fermentas) prior pipetting into gel-pockets. A 10 kbp DNA Gene-Ruler (Fermentas) was used to determine the specific DNA length. Electrophoresis was performed with a constant current of 90 V in an electrophoresis chamber (Bio-Rad) for ~ 80 min. The DNA was visualized by UV light (UV- Transilluminator GelDoc 2000, BioRad) and analyzed using Quantity One gel-documentary system (Quantity One, Bio-Rad).

2.7.8 **Purification of DNA**

PCR products and gel-excised DNA fragments were purified using the QIAquick PCR Purification and QIAquick Gel Extraction Kits (Qiagen), respectively, according to manufacturer's instructions.

DNA concentration was measured photometrically at 260/280 nm with the Nanodrop 1000 (peqlab). Purity was determined from the A_{260}/A_{280} ratio. An A_{260}/A_{280} ratio between 1.7 and 2.0 generally represents a high-quality DNA sample without protein contaminants.

2.8 POLYMERASE CHAIN REACTION

A standard PCR setup was as follows (table 21). Each PCR reaction was pipetted in 0.2 ml PCR reaction tubes (Sarstedt).

Table 21: Standard PCR reaction

Components	*Volume*
10 x DreamTaq PCR-Puffer (Fermentas)	2 µl
dNTPs mix(10 mM)	0.4 µl
Primer Fw (10 µM)	0.6 µl
Primer Rv (10 µM)	0.6 µl
DreamTaq Polymerase (5 U/µl; Fermentas)	0.1 µl
Template	2 µl (10 ng - 1 µg)
H_2O	14.3 µl

A standard PCR program is listed in the following table, but conditions varied among different primer pairs and templates.

Table 22: Typical PCR program.

Cycles	*Temperature*	*Time*	*Function*
1	98 °C	30 s	Dentature
30 - 35	92 °C	2 s	Denature
	55 - 60 °C	10 s	Annealing
	72 °C	7 s	Elongation
1	72 °C	1 min	Elongation
1	4 °C	∞	

PCR products were used directly or stored at 4°C for several days or at -20°C for several weeks.

2.9 REAL-TIME RT PCR

To measure mRNA expression levels, Real-Time RT PCR was used. In Real-Time PCR fluorescent signals are converted into a numerical value for each sample after each cycle. The cycle in which a specific amount of fluorescence exceeds background fluorescence is defined as the threshold Cycle (C_T). These C_T values are used to quantify template input making a precise and sensitive assay to analyze gene expression (Gibson et al., 1996).

Fluorescent signals in PCR were facilitated by using SYBR Green I which preferentially binds to double-stranded DNA. The DNA-dye-complex emits green light (λmax = 520 nm) when excited by wavelengths of about 480 nm. Since SYBR Green I binds the PCR product during each cycle, the relative fluorescence intensity is proportional to the increasing total amount of ds DNA in the PCR sample. However, SYBR Green I binds to every ds DNA. Hence, fluorescence signals may originate from unspecific ds DNA binding or primer-dimers. Therefore, an accurate primer design and a detailed establishment of primers (see 2.9.1).

2.9.1 **Real-Time RT PCR: Primer-Design**

The primer design involves several criteria. Non-template controls were included in each run to detect contaminations or primer dimer formation. Primer pairs were usually designed to span an exon/exon boundary, such that co-amplification of DNA contaminants can be disfavored.

In general primer design was performed using the NCBI software Primer-BLAST (http://www.ncbi.nlm.nih.gov/tools/primer-blast/index.cgi). The primer sequence varied in length (16 - 28 nt) and GC content (4 – 65 %). The lengths of amplicons were ~ 100 kbp. Primers were analyzed concerning specificity by using NCBI Blast (http://blast.ncbi.nlm.nih.gov/Blast.cgi).

Primer Evaluation

Prior to usage of primer pairs for Real-Time PCR, optimal PCR conditions were established using the following methods:

Gradient PCR

Primer pairs were analyzed for optimal temperature by conventional PCR. Employing a temperature gradient on the thermoblock (Mastercycler epgradient s, Eppendorf) allows evaluating the optimal annealing temperature. The PCR products were analyzed via agarose gel-electrophoresis. Only if PCR products showed distinctive, intensive bands in the correct size primer pairs were used for further testing.

Melting curve

Melting curve analysis is essential in the SYBR Green assay to exclude the possibility of primer dimer or multiple products. To evaluate the purity of the PCR product, the product is denatured by continuously increasing temperature. Since SYBR Green I is not able to intercalate into the ds DNA anymore, the fluorescence intensity decreases rapidly at a PCR product specific temperature, which is dependending on length and GC content of the PCR product. Therefore unspecific DNA products and primer dimers are detectable.

Standard curve

A standard curve allows the determination of primer-dependent PCR efficiency, which is essential for analysis. A standard curve was generated by using a serial dilution over at least five log ratios. Only primer pairs exhibiting an efficiency of 85 – 100 % were used for assays.

Agarose gel-electrophoresis

Finally, the specificity of the Real-Time PCR product was analyzed via agarose gel-electrophoresis.

2.9.2 **mRNA expression in GFP$^+$ BM cells: Real-Time RT PCR**

For mRNA expression analysis, total RNA derived from flow sorted GFP$^+$ BM cells was extracted using RNA Bee (AMS Biotechnology, Milton, UK) per the manufacter´s instructions (see 2.10.1). cDNA synthesis of each sample was performed using Superscript III (Invitrogen) per manufacter`s instructions in the presence of random hexamers (2.10.2). 15 ng of total RNA was added to the RT mix. The Real-Time PCR was performed on Rotor-Gene 6000™ (Qiagen) with 1.5 µl cDNA and evaluated via Software Rotor-Gene 6000™.
The table 23 lists the protocol for a Real-Time RT PCR:

Table 23: Protocol for Real-Time RT PCR

Components	***Volume***
PCR Mastermix 'SensiMix SybrGreen'	10 µl
Primer Fw (10 µM)	0.6 µl
Primer Rv (10 µM)	0.6 µl
Template cDNA	1.5 µl
H_2O	7.3

The standard Real-Time RT PCR program is shown in table 24.

Table 24: Real-time SYBR Green Program

Cycles	***Temperature***	***Time***	***Function***
1	95 °C	7 min	Dentature
45	95 °C	10 s	Denature
	55 - 58 °C	30 s	Annealing
	72 °C	7 s	Elongation
1	4 °C	∞	

mRNA expression levels of the genes of interest (here: Jarid2, fos, c-myb, Pu.1) were normalized using the housekeeping genes RPLP, Actin and GAPDH. For each primer pair, standard curves were generated (see 2.9.1) to assess efficiencies of primers. Calculations for relative quantification using three housekeeping genes were derived from algorithms published by Vandesompele et al. (Genome Biology 2002, 3: research 0034.1-0034.11) and from the geNorm manual which are available on the website http://medgen.ugent.be/~jvdesomp/genorm/example_calculations.xls.

2.9.3 **microRNA expression: Real-Time stemloop RT PCR**

In this work, Real-Time stemloop RT PCR using the Sybr Green method was performed to quantitatively detect miRNA expression (Chen et al., 2005). The characteteristic of Real-Time stemloop RT PCR is the specific so-called stemloop primer, which is added as reverse

primer to the RT reaction. Stemloop primers harbor an equal 5'-end, which allows formation of a stemloop and differ in the last 6 nucleotides at their 3'-end, which is complementary to the 3'-end of a specific miRNA. Figure 11 shows a schematic overview.

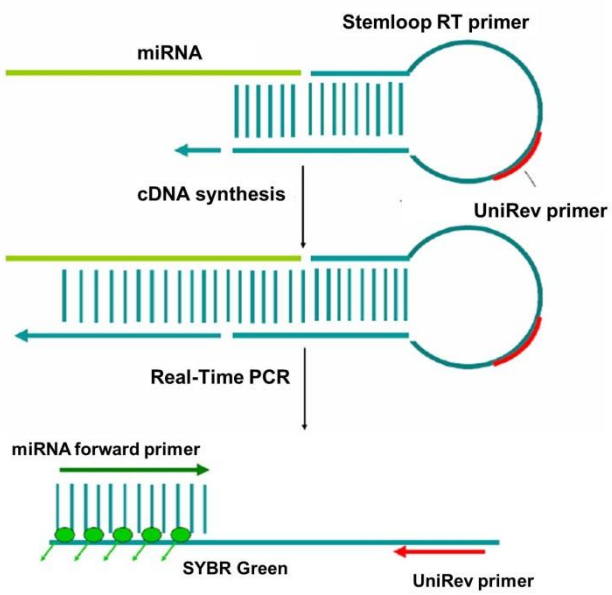

Figure 11: Principle of Real-Time stemloop RT PCR using Sybr Green. Detection of miRNA expression levels via Real-Time stemloop RT PCR. cDNA synthesis is performed using specific primers binding to the last 4 - 6 nt of a miRNA and fold into a stemloop structure at the 5' -end. Real-Time PCR is performed using a specific forward primer for the miRNA and a universal reverse primer, binding to a region within the loop of the stemloop primer.

For detection of miRNA expression levels total RNA of cultured cells was isolated using RNA Bee (AMS Biotechnology, Milton, UK) while RNA of paraffin embedded spleens was extracted using RNeasy FFPE Kit (Qiagen). For each sample the same input of total RNA (1 µg) was added to the RT mix together with the specific stemloop primers miR-21, hsa-miR-155 and miR-K12-11. cDNA synthesis was performed according to Varkonyi-Gasic (Varkonyi-Gasic et al., 2007). Following components were used for cDNA synthesis (table 25).

Table 25: Protocol for stemloop RT.

Components	***Volume***
dNTPs (10 mM)	0.5 µl
DEPC H_2O	11.15 µl
Stemloop RT-Primer (1 µM)	1 µl
Template (1 µg)	1 µl
5 x First Strand Buffer	4 µl
DTT (0,1 M)	2 µl
Superscript III (200 U/µl)	0.25 µl
RNase OUT (40 U/µl)	0.1 µl

cDNA synthesis was performed in the Thermocycler (AB Applied Biosystems, GeneAmp® PCR System 9700) by using following program (table 26).

Table 26: Pulsed RT program for stemloop cDNA synthesis.

Cycles	*Temperature*	*Time*
1	16°C	30 min
60	16 °C	30 s
	42 °C	30 s
	50 °C	1 s
1	4 °C	∞

After cDNA synthesis, RNAse H was added (0.4 µl RNAse H, 200 U/µl, Invitrogen). The mixture was incubated for 20 min at 37°C and subsequently inactivated by heating at 65°C for 10 min. Samples were used for Real-Time PCR or were stored at -20°C.

Real-Time PCR was performed on the Rotor Gene Q (Qiagen, Hilden Germany), using SensiMix SybrGreen. Following primer pairs were used: miR-K12-11 fw/UniRev, hsa-miR-155 fw/UniRev or miR-21 fw/UniRev. For each reaction, 1.5 µl cDNA was added to the Real-Time PCR mix. Real-Time PCR was performed as described above in 2.9.2 (table 24 and 25).

For evaluation of miRNA expression in transductants, results were normalized to the respective standard curve. RNA isolated from BCBL-1 and RAJI were used as positive controls for miR-K12-11 and hsa-miR-155, respectively. The efficiency of both primer pairs was evaluated using a ten-fold serial dilution of BCBL-1 and Raji cDNA.

Expression levels of transductants were calculated using $2^{-\Delta CT}$, in which the control sample was either BCBL-1 for miR-K12-11 or RAJI for hsa-miR-155 expression. Each experiment was performed using three biological replicates, in which each sample was analysed in duplicate.

The miRNA expression level in splenocytes was normalized to miR-21 and related to the appropriate positive control sample using the $2^{-\Delta\Delta CT}$ method (Livak, 2001; Pfaffl, 2001). The specific GFP rate of each sample was included into the calculations by dividing the GFP percentage by the measured relative copy number.

2.10 RNA-TECHNIQUES

2.10.1 RNA isolation

RNA isolation was performed with a modified method based on the publication from Chomczynski and Sacchi (Chomczynski & Sacchi, 1987). Total RNA was isolated via RNA Bee (Ambion) according to manufacturer's instructions. Purification of total RNA from

formalin-fixed, paraffin-embedded (FFPE) tissue sections was performed using RNeasy FFPE Kit (Qiagen) according to manufacturer's instructions. RNA was further purified when necessary with RNeasy Mini Kit (Qiagen) according to manufacturer's instructions.
Finally, RNA was quantified using Nanodrop 1000 (peqlab). RNA concentration was determined at a wavelength of 260 nm. RNA concentration correlates with OD, thus an A260 reading of 1.0 is equivalent to about 40 µg/ml of RNA. The purity of RNA is determined by A260/A280 ratio. The value of 1.8 to 2.0 indicates pure RNA without protein contaminants.

2.10.2 cDNA-synthesis

In this work, the Superscript III reverse transcriptase enzyme (Invitrogen) was used to transcribe mRNA into cDNA according to manufacturer's instructions. In general, 1 µg RNA was initially used employing random primers. cDNA synthesis was performed in the Thermocycler GeneAmp PCR System 9700 (AB Applied Biosystems,). Afterwards the samples were incubated with RNAse H (NEB) for 20 min at 37°C followed by an inactivation for 20 min at 65°C. Then the samples were analyzed via Real-Time RT PCR to evaluate expression levels (see 2.8).

2.11 PROTEIN TECHNIQUES

2.11.1 Western blot

Whole-cell lysates were harvested 48 h post transfection. Lysates, corresponding to about 5×10^5 cells, were separated on standard SDS-PAGE (10 %-gels) and transferred onto PVDF-membranes (Millipore). Blots were probed using antibodies directed against Jarid2 (Santa Cruz, sc-134548) or, as a loading control, actin (Santa Cruz, sc-47778).

2.11.2 Immunohistochemistry

In this work the paraffin sectioning was performed.
Sterna were fixed in Calfix (ProTaqs, Quartett GmbH, Berlin) and needed to be decalcified prior paraffin embedding. For paraffin embedding, the organs (spleen, lymphnodes, decalcified sterna) were placed into tissue cassettes (Diapath, Martinengo, Italy), hydrated and incubated in 55 % ethanol. Samples were dehydrated (Leica ASP300, Nussloch). Paraffin-embedded tissue blocks can be stored at room temperature. Histological samples were cut in 3 - 4 µm sections via microtome and air dried at room temperature. Before sections can be stained and treated with aqueous agents, they require deparaffinization and rehydration. After incubation for 25 min at 56°C the sections were soaked for 5 min in Ottix Plus (Xylol-substitute; Diapath, Martinengo) and immediately transferred in Ottix Shaper

(alcohol-substitute, Diapath, Martinengo). Afterwards sections were soaked ten times in Ottix Shaper. Finally they were ready for staining.
Hematoxylin and eosin staining (H&E) was performed according to standard laboratory protocols. Sections were hydrated and then dipped into Mayer´s hemalm (Thermo Scientific, Braunschweig) and agitated for 30 sec. Subsequently the sections were rinsed with water for 1 min and then stained with eosin solution for 10-30 sec. Finally the sections were dehydrated.

For PNA (Vector Laboratories, Burlingame, CA) staining, the dewaxed slides were incubated with 1 : 100 dilution of the primary antibody for 45 min. PNA staining leads to a brownish colour and therefore enables the estimation of both GC number per section as well as relative area of GC per section. Detection was performed using ABC Elite Peroxidase Kit plus DAB-Kit (DAKO) and counterstained with Mayers hemalm.
The establishment of the protocols for the PNA staining as well as the performance of sample preparations and stainings was done in co-operation with Gundula Pilnitz-Stolze (HPI).

Samples were analyzed using Zeiss microscope (Axioplan2 imaging) with the objective lens of 10x/0.45 Zeiss Plan-APOCHROMAT. Pictures were taken using Jenoptik ProgRes C12 and Imagic Jenoptikss CxxPlus. The samples were analyzed using Image Access Enterprise, Adobe Photoshop CS4 (Adobe, San Jose, CA) and PixelClassifier (Nikon).

2.12 MOUSE EXPERIMENTS

BM transplantations were performed in C57BL/6 mice (Jackson Laboratory, Maine, USA). C57BL/6 mice were bred in the Heinrich-Pette-Institute animal quarters under SPF conditions. Animal experiments were handled in accordance with good animal practice. All animal experiments were approved by the Hamburg Office of Health (permit no. FI87/04 and 79/08).

2.12.1 Workflow description

In this work, a retroviral mediated gene transfer was employed to force expression of miR-K12-11 and hsa-miR-155 and GFP in isolated HSCs.
At first, retroviral vectors were generated. The pri-miRNAs miR-K12-11 and hsa-miR-155 were amplified and cloned into the retroviral vector SF91 downstream of the LTR promoter and GFP. The vector encoding only GFP was used as control. Then, generated retroviral vectors were used for transfection of 293T cells, together with gag-pol and env genes (see 2.6.9). The co-transfection led to the production of infectious particles, the retroviral stock.

High-titer retroviral stocks were used for transduction of HPCs that were isolated from donor mice (see 2.11.4). After transduction the cells were injected into lethally irradiated mouse recipients (see 2.11.5).

2.12.2 5-Fluorouracil treatment

5-FU is a pyrimidine analog and is a common drug in the treatment of cancer. It is toxic against highly proliferating cells and leads to the enrichment of resting progenitor cells in the BM. Donor wt C57BL/6 mice (Ly5.2) received an intraperitoneal injection of 5-FU (150 mg/kg (GRY-Pharma GmbH)). The injection was performed by Maike Schwieger or Birte Niebuhr (Forschungsgruppe Carol Stocking, HPI). Five days post 5-FU treatment mice were etherized and sacrificed via cervical dislocation and immersed in 80% ethanol to keep them semi-sterile. BM cells were harvested under the laminar flow hood.

2.12.3 Lineage depletion

Progenitor cells from donor mice (Ly5.2) were enriched via lineage depletion Kit (Miltenyi Biotec) according to manufacturer's instructions. Mice were etherized and sacrificed via cervical dislocation and immersed in 80% ethanol to keep them semi-sterile. BM cells were harvested by rinsing cells thouroughly out of tibea and femur via syringe and canula under a laminar flow hood. Lineage negative cells were enriched via lineage depletion Kit.

2.12.4 Transduction of primary BM cells

Produced pseudotyped retroviral stocks (see 2.6.9) were titered prior to transduction of primary BM cells. Virus stocks with a titer of $>1x10^6$ infectious particles per ml were used for transductions of primary BM cells. BM cells were harvested from tibiae and femora of donor wt C57BL/6 mice that received an intraperitoneal injection of 5-FU five days before isolation (see 2.11.2); or BM cells were harvested from untreated C57BL/6 mice prior negative lineage depletion (see 2.11.3). Three independent BM transductions and transplantations were performed. Two independent experiments were performed using 5-FU and one experiment was done with lineage depletion (Myltenyi Biotech).

The efficacy of virus transduction of primary cells can be increased using the recombinant human fibronection-fragment RetroNectin® (TaKaRa, Bio Inc.). Coating was performed overnight using 10 µg RetroNectin®. Prior transduction, RetroNectin® was removed and wells were blocked with 2 ml BSA with subsequent washing with 3 ml HBSS. For BM transductions, virus particles were fixed onto RetroNectin® coated non-tissue 35-mm culture plates (bacteria tissue plate) by spinoculation for 4 x 30 min at 400 x g at 4°C. Virus suspensions were removed and 0.5×10^6 BM progenitors per well were suspended in StemSpan SFEM medium (StemCell Technologies) with supplements (see 2.6.4) and

incubated for 12 h at 37°C. A second plate was prepared for transduction using same protocol: Four rounds of transductions were repeated after 24 h. Then, virus suspension was removed and 0.5 x 10^6 BM progenitors per well were suspended in StemSpan SFEM medium (StemCell Technologies) with supplements and incubated for 12 h at 37°C. Cells were washed and re-suspended with PBS. Finally cells were re-suspended in PBS in a concentration of ~2 x 10^6 per 300 µl PBS. A small aliquot was used for FACS analysis to determine the transduction rate via measurement of GFP expression.

2.12.5 Allotransplantation

Since an efficient engraftment of donor cells (Ly5.2) requires the extraction of recipients HSCs (8-12 weeks old mice, Ly5.1), the mice were lethally irradiated (9 Gray) in an open cesium-137-radiant source for a time-period of 24 min. The irradiated mice were transplanted 4h post radiation. Transduced BM cells (~ 1 x 10^6) supplemented with untreated splenic cells (~ 5 x 10^4) of wt C57BL/6 mice (Ly5.1) were re-suspended in 300 µl PBS without supplements. These cells were transplanted into lethally irradiated C57BL/6 mice by tail vein injection. Prior injection the tail was warmed up via heating lamp. The transplantation was performed by Maike Schwieger of Birte Niebuhr (Forschungsgruppe Carol Stocking, HPI).

After transplantation the mice received the antibiotic solution Baytril® through drinking water to prevent infections (1 ml oral solution Baytril® 2.5 % contains 25 mg Enrofloxacin, which is a synthetic antiinfective of the fluoroquinolone class, Bayer Health Care, Leverkusen). Baytril® is bactericidal for different bacteria and mycoplasma. Baytril® (0,1 mg/mL) was added to the drinking water for a time-period of 21 days post transplantation.

In case of pathological symptoms like apathy, weight loss, breathing difficulties, motorically limited (paralysis) or abnormalized posture, the mice were etherized and sacrificed via cervical dislocation. Mice without these symptoms were sacrificed after a time-period of 12 - 16 weeks.

2.12.6 Analysis of mice

Transplanted Mice were sacrificed 12 - 16 weeks post transplantation. Mice were etherized and sacrificed via cervical dislocation.

2.12.6.1 Blood analysis

For blood analysis mice were etherized and subsequently punctuated at the mandibular vein using a lancet (Accu-Chek, Roche, Mannheim). The blood was collected into an EDTA-test tube. Blood parameters were measured at the Hemavet 950FS (Drew Scientific Inc., Oxford, Connecticut) using 20 µl of the collected blood. Prior to blood analysis the blank value was measured using control blood that was provided by Drew Scientific Inc.. In

general the following parameters were in focus: White blood cell (WBC), red blood cell (RBC), hemoglobin (Hb) and Hematocrit (HCT).

2.12.6.2 Analysis of organs

Sacrificed mice were fixed on a mat using four canulas. The mice preparation started with a Y-cut skin incision. Thorax, abdomen and lymphnodes were exposed. Peripheral lymphnodes were removed, fixed with 4 % formalin containing 1 % acetic acid and long-time stored at 4°C. In some cases these samples were used for IHC.

After opening the peritoneum the organs of the abdomen (spleen, liver, kidney, stomach, intestine, urinary bladder, and genitals) were phenotypical analyzed. Then the spleen was removed, immediately chilled on ice and weighed. Subsequently after weighing the spleen was cut into two pieces. Whereas one specimen was fixed in 4 % formalin containing 1 % acetic acid, the other one was chilled in PBS on ice for FACS analysis and cell sort later on. FACS analysis require single cell suspensions. Thus, spleens were prepared by pressing through a 100 µm microstrainer. Erythrocytes were depleted via lysis buffer (Pharm Lyse (BD)). Splenocytes were stained with conjugated antibodies for 1 h in PBS supplemented with 1 % FCS. In some cases one third of the spleen was transferred in CryoTubes, freezed in liquid nitrogen and after a few hours stored in -80°C for long-time storage. These pieces have been used for RNA extraction via RNA Bee at a later date.

The exposure of thorax leads to the analysis of lymphnodes, heart and lung. The thymus was analyzed in size.

For histologic inspection of BM, sterna were dissected and fixed in a formalin containing solution specifically developed for fixation of iliac crest trephine biopsies (Protaqs Calfix, Quaratett) and appropriately decalcified (Protaqs Calless, Quaratett) before paraffin embedding (performed by Gundula Pilnitz-Stolze (HPI)). To analyze BM cells at FACS, femur and tibiae were removed from the mouse. BM cells were harvested by rinsing PBS through the bones via canula and syringe. Cells were re-suspended in PBS and used for FACS analysis or cell sort. For FACS analysis, cells were stained with conjugated antibodies for 1 h in PBS supplemented with 1 % FCS.

2.13 DATABASES AND SOFTWARE

Diagrams and figures were designed with Adobe Photoshop CS Version 8.0.1 and Microsoft Powerpoint.

Evaluation, analyzes, sequencing analyzes and cloning strategies were performed with the software program CLC Workbench. Primer design was done with the program Primer Blast (http://www.ncbi.nlm.nih.gov/tools/primer-blast/).

Real-Time PCR was evaluated with the Rotor-Gene 6000™ Software.

Literature research was performed with PubMed Medline (http://www.ncbi.nlm.nih.gov/) miRNA sequence analysis was performed with miRBASE (http://microrna.sanger.ac.uk/sequences/).

IF and IHC were evaluated using the program Image J (http://rsbweb.nih.gov/ij/) and the PlugIn Cell Count (http://rsbweb.nih.gov/ij/plugins/cell-counter.html)..

Samples of histochemistry were analyzed using Jenoptik ProgRes C12 and Imagic Jenoptik CxxPlus. The PixelClassifier (Nikon) was used to evaluate the formation of germinal centers.

All statistical analyzes were performed applying student`s two-tailed t-test using GraphPad Prism 5.03 software.

3 RESULTS

KSHV expresses miR-K12-11 that shares 100 % seed sequence with the cellular miR-155. There is strong evidence that miR-K12-11 has evolved to mimic hsa-miR-155 functions, since miR-155 plays a critical role in immune response. It is thought that KSHV utilizes this mimicry to modulate B-cell differentiation and B-cell response. Furthermore, a constitutive expression of miR-K12-11 probably has an important impact on virus-induced tumorigenesis.

To explore miR-K12-11 functions *in vivo*, phenotypic alterations were monitored in a mouse model, in which retroviral-mediated gene transfer was combined with BM transplantation to force expression of miR-K12-11, hsa-miR-155 or GFP alone (negative control) in HPCs. If the observed seed sharing is sufficient to allow miR-K12-11 to engage the same contingent of host transcripts, similar phenotypes should ensue upon forced expression of the two miRNAs in murine HPCs. This study provides evidence if miR-K12-11 is a functional ortholog of hsa-miR-155 in the context of hematopoiesis and lymphopoiesis with regard to KSHV infected B-cells.

3.1 EXPERIMENTAL SET UP

To explore the functions and mimicry of miR-K12-11 *in vivo*, three gamma-retroviral vectors were generated that express either GFP alone or GFP together with pri-miRNA hsa-miR-155 or miR-K12-11. Figure 12 illustrates the general experimental set up. After generation of retroviral vectors, infectious pseudotyped retroviral particles were produced (see 3.2 and 3.3). These infectious particles were used for transduction of isolated progenitor cells from donor mice, which were subsequently transplanted into lethally irradiated mouse recipients (see 3.4.). Mice were sacrificed 12 - 16 weeks post transplantation. Since miR-155 plays a critical role in hematopoiesis and immune response (Eis et al., 2005; Costinean et al., 2006; Thai et al., 2007), this study focused on the analysis of lineage commitment during hematopoiesis and investigated the immuno-phenotypic profile in lymphoid organs such as bone marrow and spleen (see section 3.5). Alterations in splenic structure were also explored. Additionally, target identification was an important aspect in this study (see section 3.6), which gain insight into possible molecular mechanisms underlying the phenotype.

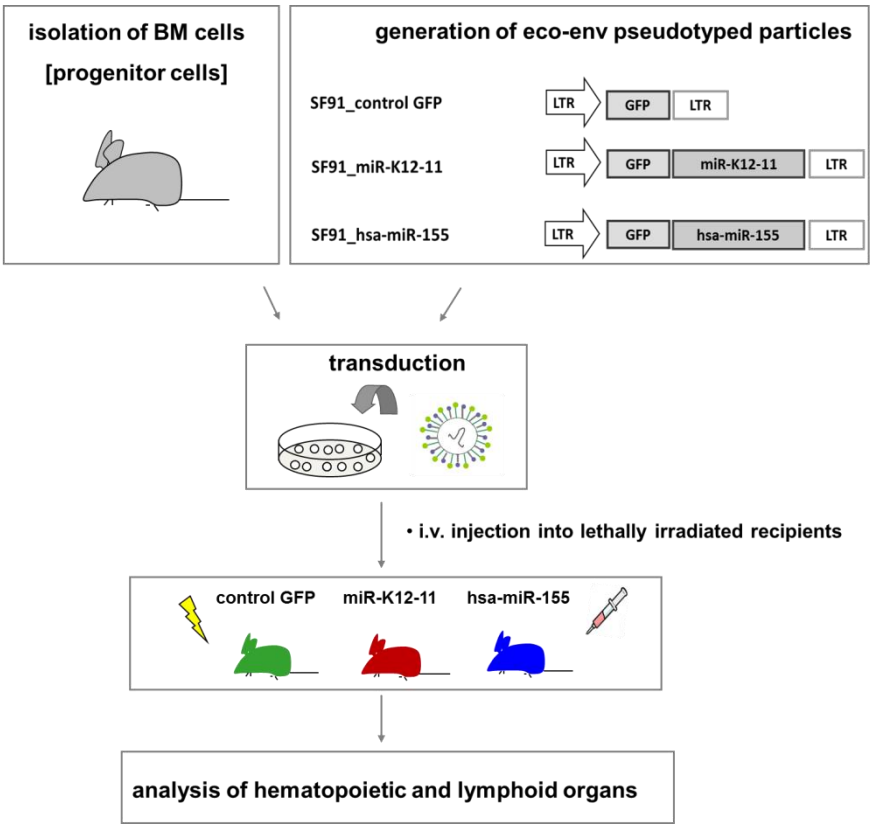

Figure 12: Experimental set up. Pri-miRNA sequences of miR-K12-11 and hsa-miR-155 were cloned into gamma-retroviral vectors. The control vector encodes for GFP alone. Either the progenitor cells were enriched via 5-FU treatment and then isolated from donor mice or the isolated hematopoietic progenitor cells (HPCs) were subjected to lineage depletion prior to transduction with pseudotyped retroviral particles. The transplantation of these transduced progenitor cells was performed by injection into the tail vein (intravenous (i.v.)). After 12 - 16 weeks, mice were sacrificed and analyzed.

3.2 CLONING STRATEGY TO GENERATE RETROVIRAL VECTORS

The gamma-retrovirus SF91 was used as a vehicle to deliver genes of interest, here pri-miRNAs and GFP, into murine HPCs. This vector possesses several important features. Firstly, SF91 encodes for GFP, which is a commonly used reporter gene to detect transduced cells via fluorescence microscopy or FACS. Secondly, SF91 contains long terminal repeat (LTR) sequences that signal for incorporation into the host genome. This is a prerequisite to obtain a stable gene expression in transduced cells. Furthermore the 5´LTR sequence acts as an RNA pol II promoter, controlling the transcription of the reporter gene and the inserted genes, here GFP and the appropriate miRNA. The promoter is constitutively active, leading to a sustained expression of GFP and miRNA. Notably, GFP and the miRNA are encoded on the same transcript, which is controlled by the LTR promoter. A scheme of generated constructs is mapped in figure 13.

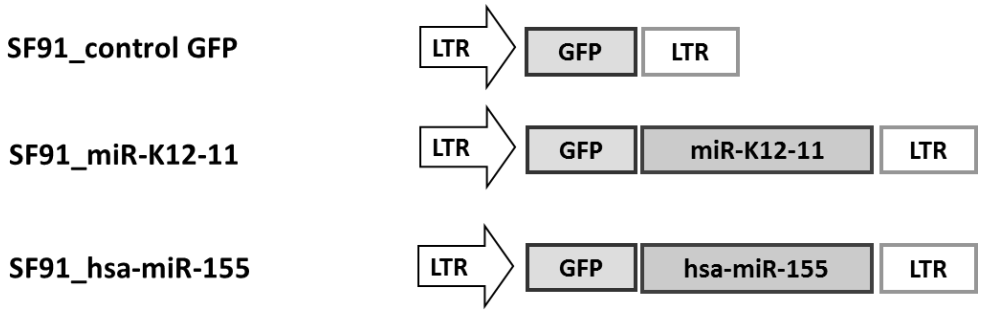

Figure 13: Depiction of gamma-retroviral vectors. Constructs express the reporter gene GFP plus miR-K12-11 or hsa-miR-155, or GFP alone. 5´long terminal repeat (LTR) acts as a RNA pol II promoter. The LTR sequences contain signals for the incorporation into the host genome. The pri-miRNA sequences were inserted downstream of the promoter and the GFP gene. GFP and miRNA were encoded on the same transcript.

Pri-miRNA sequences of miR-K12-11 and hsa-miR-155 were amplified by PCR from DNA of the PEL cell line BCBL-1 and the EBV positive Burkitt-lymphoma-derived cell line RAJI, respectively, and inserted into EcoRI and BamHI restriction sites downstream of the 5´LTR and GFP gene into SF91. The miRNA expression cassette containing miR-K12-11 or hsa-miR-155 hairpin sequence is flanked ~ 150 bp upstream and downstream from the mature miRNA sequence.

3.3 SUCCESSFUL GENERATION OF INFECTIOUS PARTICLES

High-titer stocks of pseudotyped retroviral particles were generated by transient co-transfection of 293T cells with the generated retroviral vectors and packaging constructs, encoding gag-pol and eco-env genes. The titer of produced infectious particles was determined by calculating GFP-transduction rates in infected cultures. Virus suspensions with > 1 x 10^6 infectious particles per ml were considered as high-titer retroviral stocks and used for retroviral transduction of murine HPCs.

Before starting the *in vivo* experiment, transduced NIH3T3 cells were analyzed regarding their GFP and miR-K12-11 or hsa-miR-155 expression to prove the functionality of generated retroviral particles. Whereas GFP expression was measured via FACS analysis or fluorescent microscopy, mature miRNA expression levels were estimated using Real-Time stemloop RT PCR.

GFP expression validates successful transduction

NIH3T3 cells were transduced with each generated viral stock and then analyzed for GFP expression. The figure 14 shows representative fluorescence microscopy images after transduction.

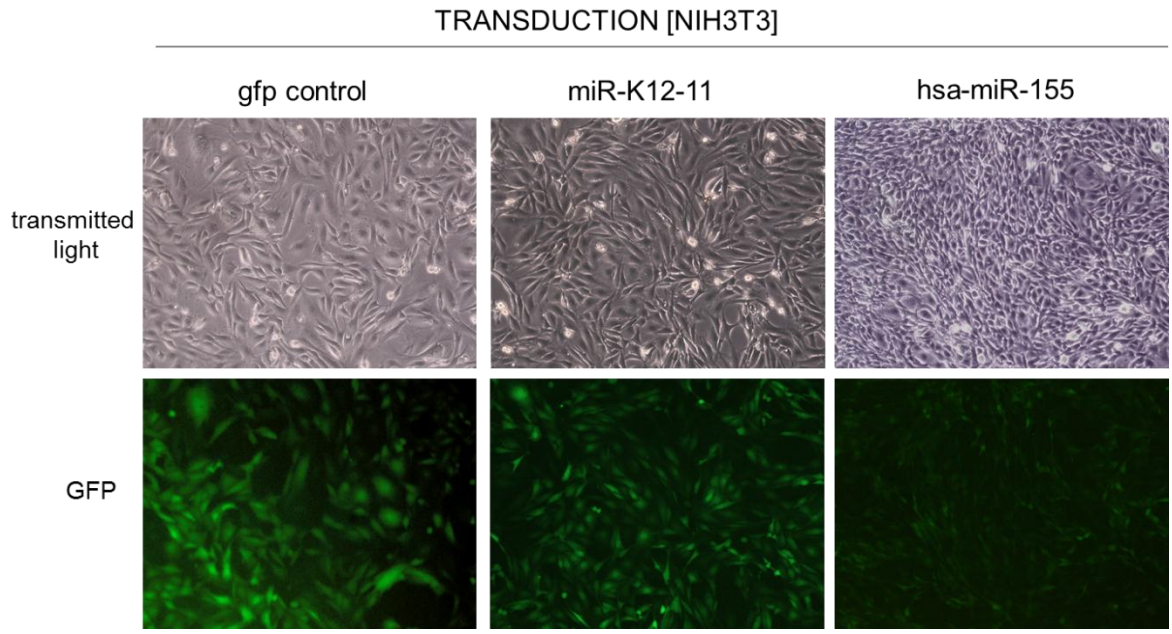

Figure 14: Transductants expressed GFP. Shown are representative images of fluorescence microscopy after transduction of NIH3T3 cells with produced virus stock (control gfp, miR-K12-11, hsa-miR-155). Cells were analyzed 72 h post transduction. Each experiment resulted in GFP expression verifying the success of transduction.

GFP expression was detected in each experiment with each construct providing first indication that generated retroviral particles are functional.

Efficient expression of miRNAs

Next, expression levels of mature miR-K12-11 and hsa-miR-155 were analyzed via Real-Time stemloop RT PCR of GFP^+ flow sorted transductants (NIH3T3) (figure 15), since GFP expression alone does not prove the functionality of the generated constructs.

It was aimed to achieve an expression level that resemble the level of miR-K12-11 during KSHV infection; and resemble the hsa-miR-155 expression during EBV infection or upon B-cell activation during B-cell response. Therefore, miRNA expression in transductants was compared to representative tumor cell lines of B-cell origin. Whereas the PEL cell line BCBL-1 was used as positive control for miR-K12-11, the EBV-positive lymphoma cell line RAJI was used as positive control for hsa-miR-155. The relative copy number of the respective miRNA of GFP^+ flow sorted transductants was related to the specific positive cell line, BCBL-1 or RAJI, using the $2^{-\Delta CT}$ method.

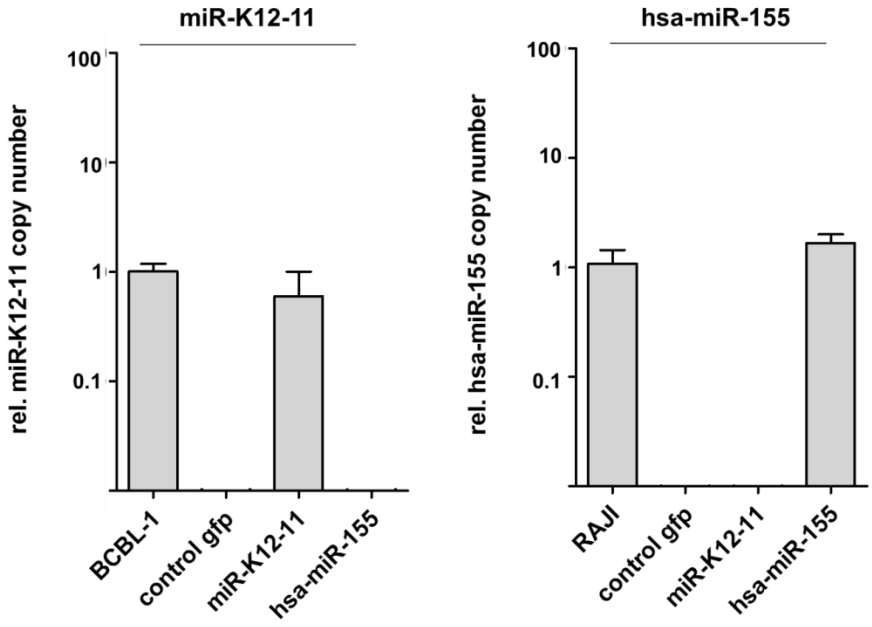

Figure 15: Efficient miRNA expression in transductants. Detection of ectopic miRNA expression in transductants (NIH3T3 cells). Total RNA was extracted from flow sorted GFP^+ cells followed by detection of miRNA expression levels using Real-Time stemloop RT PCR. BCBL-1 and RAJI RNA was used as a positive control for miR-K12-11 or hsa-miR-155 expression, respectively. The rel. copy number was evaluated using $2^{-\Delta CT}$. Expression levels of positive controls were set to 1 rel. copy number. Experiments were done using three biological replicates, in which each sample was analyzed in duplicate. Transductants express the appropriate miRNA, whereas control cells express none of the miRNAs.

miR-K12-11 expression was detected in all transductants infected with miR-K12-11 retroviral stocks. GFP^+ sorted transductants showed a relative copy number of 0.7 (+/- 0.6), a comparable level to endogenous miR-K12-11 expression of the KSHV positive control cell line BCBL-1 (rel. copy number: 1.0 (+/-0.3)). As expected, miR-K12-11 was not detectable in transductants infected with control gfp stocks or hsa-miR-155 stocks.
Additionally, hsa-miR-155 expression was measured in all transductants that were infected with hsa-miR-155 retroviral stocks. These transductants showed 1.6 (+/-0.57) rel. copy number; which is comparable to the endogenous hsa-miR-155 expression level of the positive control RAJI (1.06 (+/-0.6) rel. copy number).

These data verify the functionality of all three generated retroviral stocks and revealed a comparable mature miRNA expression level to those in representative tumor cell lines of B-cell origin.

3.4 HEMATOPOIETIC RECONSTITUTION

miRNA and GFP expression was confirmed *in vitro*, indicating the functionality of generated retroviruses. Therefore, the produced high-titer stocks were further used for

transductions of isolated and enriched HPCs, following transplantation of lethally irradiated mouse recipients.

3.4.1 **Successful retroviral transduction of isolated progenitors**

The success of transduction of HPCs was monitored via FACS analysis for GFP expression. In this thesis work, three independent transplantation experiments were performed. In the first two experiments, HPCs were isolated from 5-FU treated mice, which have increased levels of early progenitors. In the third experiment, BM cells were isolated from untreated mice and enriched for HPCs by depletion of cells expressing lineage-specific markers. Table 27 lists detected GFP rates of transduced progenitor cells of each experiment.

Table 27: Transduction rates of isolated progenitor cells. Prior to transplantation the transduction rates of progenitor cells were measured via FACS analysis, which validates the success of transduction.

Experiment	*Type of experiment*	*control gfp*	*miR-K12-11*	*hsa-miR-155*
Experiment 1	5-FU	14 %	17 %	7 %
Experiment 2	5-FU	6 %	13 %	/
Experiment 3	Lineage depletion	30 %	25 %	13 %

The obtained transduction rates of 5-FU treated cells were low, ranging from 6 - 17 %, although especially high-titer stocks were applied. One explanation for the lower transduction rates in 5-FU treated cells might be a reduced effective MOI since a high number of cells were needed to be infected, which are further on not exclusively progenitor cells. This might be circumvented using the lineage depletion experiment, in which specifically progenitor cells were enriched. Hence, a lower number of cells needed to be infected, increasing thereby the effective MOI. These transductions reached the highest efficiencies for all three constructs (13 % - 30 %).

3.4.2 **Transplantation of progenitor cells into mouse recipients**

We lethally irradiated mouse recipients prior transplantation to ensure the engraftment of transduced HPCs. These cells are capable of generating new blood and lymphoid cells in lethally irradiated mice. Table 28 summarizes the number of transplanted and analyzed mice per experiment and per mouse cohort.

Table 28: Number of transplanted animals. Isolated HPCs from donor mice were transduced and subsequently transplanted into lethally irradiated mouse recipients. The table summarizes the number of transplanted and analyzed mice.

Experiment	*Type of experiment*	*control gfp*	*miR-K12-11*	*hsa-miR-155*
Experiment 1	5-FU	7	7	7
Experiment 2	5-FU	3	14	/
Experiment 3	Lineage depletion	6	3	9

For this project 16 control mice, 24 mice that express miR-K12-11 as well as 16 mice expressing hsa-miR-155 were analyzed.

3.4.3 **GFP and miRNA expression in mouse recipients**

In this study, mice were sacrificed 12 - 16 weeks post transplantation. To validate the functionality of the gamma-retrovirus *in vivo*, GFP and miRNA expression was analyzed in harvested BM cells and splenocytes.

Splenocytes express GFP

GFP expression was analyzed in harvested splenocytes via FACS analysis (figure 16).

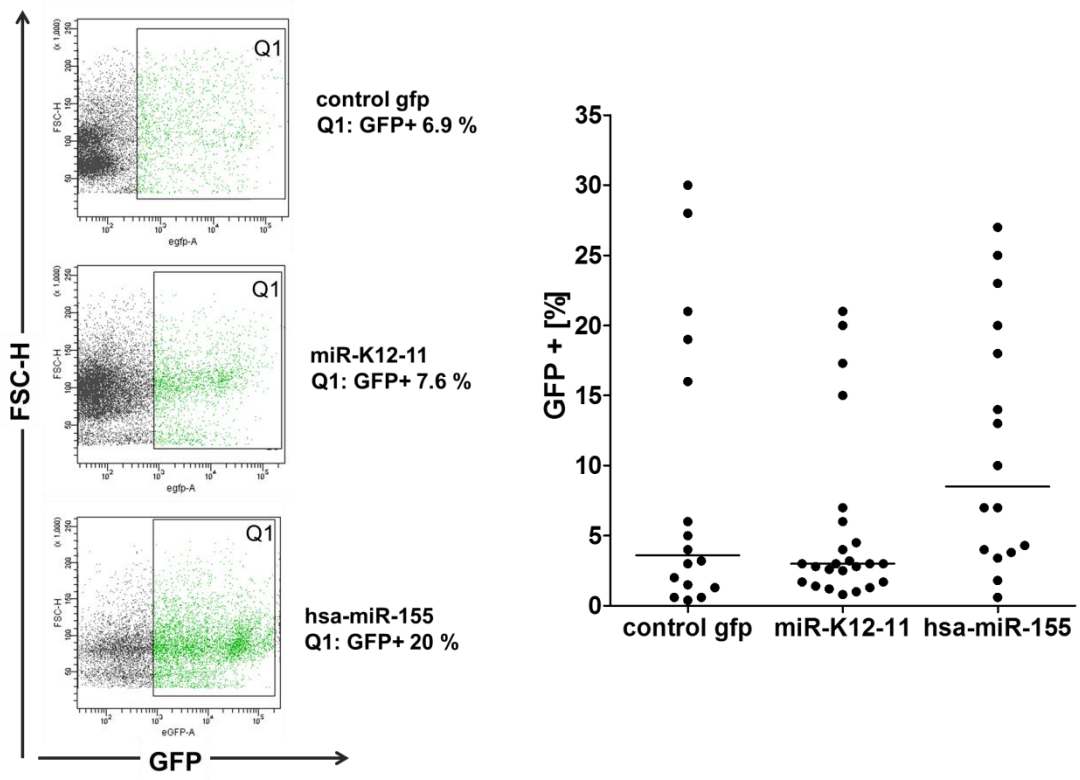

Figure 16: Splenocytes express GFP. GFP expression in harvested splenocytes was analyzed using FACS analysis. Left: Representative dot plot from one mouse of each mouse cohort. Q1 denotes the GFP^+ population. Right: Each mouse expressed GFP in splenocytes. Each dot represents one mouse (control gfp: n=16; miR-K12-11: n=24; hsa-miR-155: n=16).

GFP expression in harvested splenocytes of each mouse was detected after a long time-period of 12 - 16 weeks post transplantation. The findings validate successful transplantation and hematopoietic reconstitution.

Higher GFP content in splenic compartment compared to BM compartment

Next, GFP rates of BM and splenic compartments were compared (figure 17). Homing to the BM compartment of transplanted HPCs leads to a first accumulation of these cells in the BM. Comparing GFP rates in BM and spleen after 12 - 16 weeks gain insight into processes like *e.g*. homing of transplanted cells to BM that arose to mature cells and then migrated to spleen.

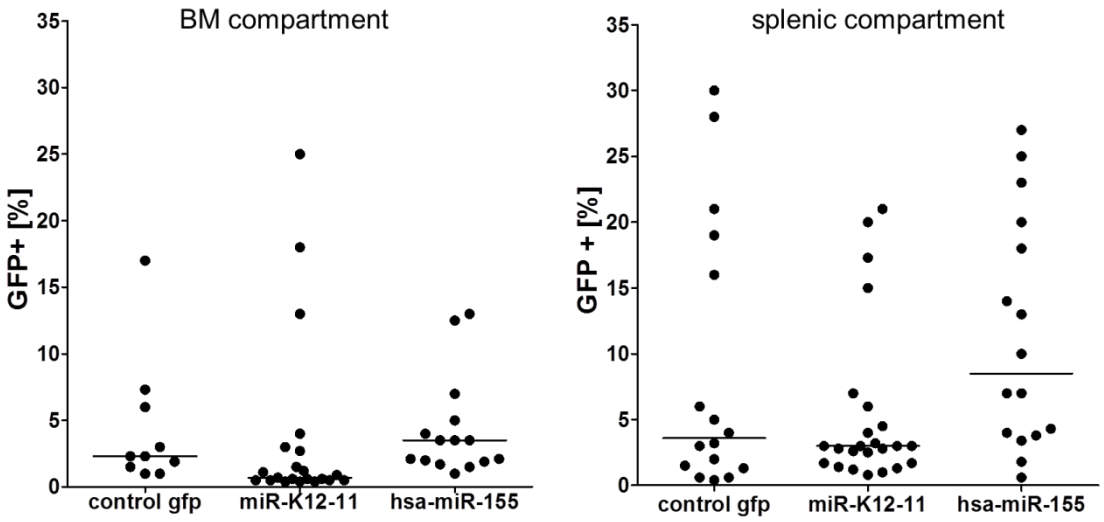

Figure 17: Splenocytes have a higher GFP rate compared to BM compartment. GFP expression in BM cells (left graph) and splenocytes (right graph) indicate successful transplantation and engraftment of transduced progenitor cells. GFP rates were higher in the splenic compartment compared to BM compartment. One dot denotes one mouse. (BM compartment: control gfp: n=10; miR-K12-11: n=21; hsa-miR-155: n=15. Splenic compartment: control gfp: n=16; miR-K12-11: n=24; hsa-miR-155: n=16).

Comparing GFP rates in BM and splenic compartment, it is apparent that BM cells have a lower GFP^+ content in all three mouse cohorts compared to splenocytes. This result may be explained by two different scenarios: (a) Cells of the BM are precursors of those of the spleen. Thus, although transduced HPCs would first give rise to GFP^+ cells in both BM and spleen, these cells cannot be replenish themselves and thus would be eventually lost – first in BM and then spleen. This would be observed if the transduction efficiency of ST- or LT-HSCs was too low. (b) Cells of the BM are predominantly of myeloid origin, whereas those of the spleen are primary lymphoid. If transplanted cells preferentially give rise to lymphoid cells and miRNA expression imparts a proliferation or survival advantage of lymphoid cells, one may expect more GFP^+/miRNA expressing cells in the spleen as in the BM. But as this is observed with the control vector, this scenario is unlikely.

Lineage depletion resulted in higher GFP rates in splenocytes

To answer the question whether lineage depletion or 5-FU treatment results in a higher GFP rate, analysis was continued by comparing the rates of the two different types of experiments (figure 18). The upper graphs show GFP rates in BM cells and compare 5-FU treated cells with lineage depleted cells, whereas the lower graphs depict GFP rates in splenocytes comparing 5-FU and lineage depletion.

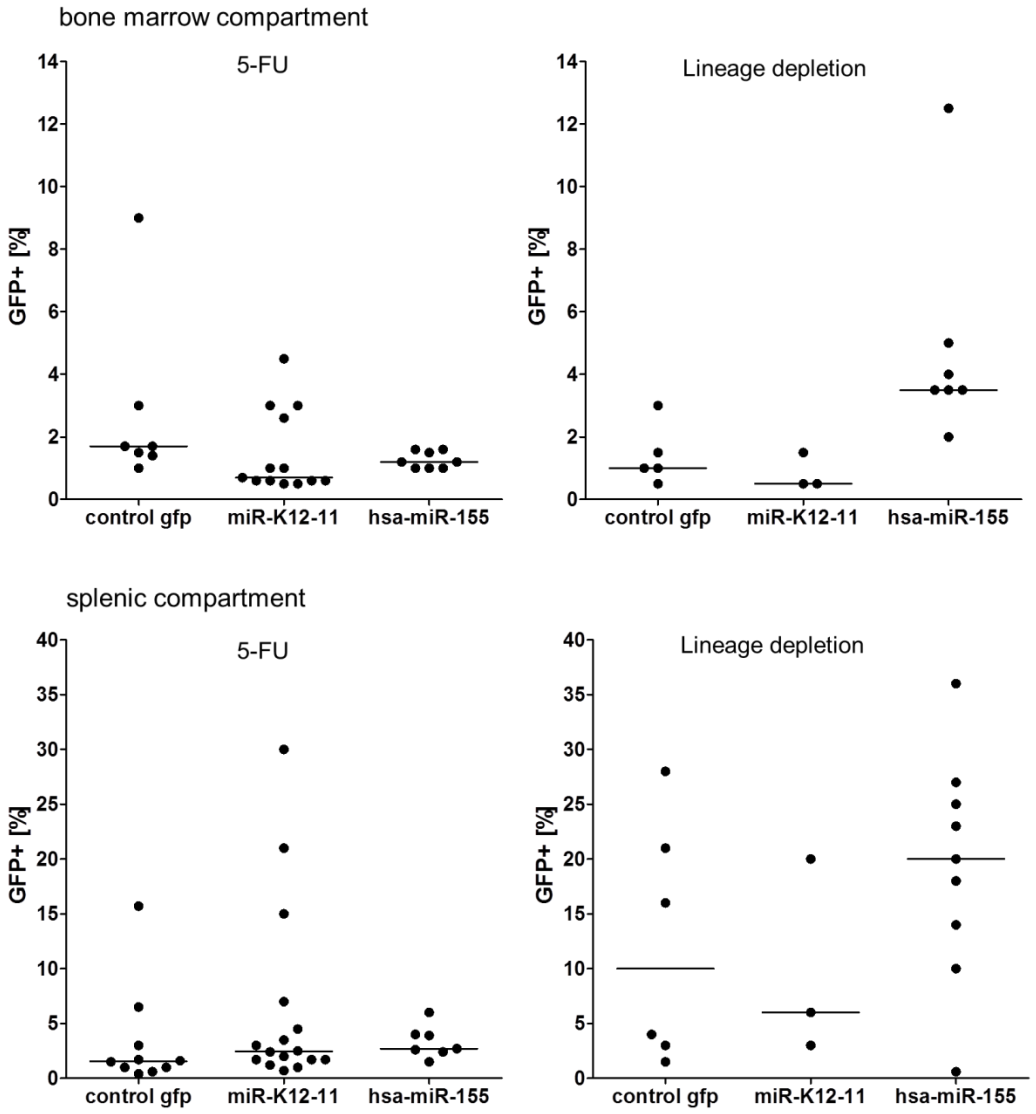

Figure 18: Comparison of GFP rates between 5-FU treated cells and depleted cells in BM and spleen. GFP expression was detectable in bone marrow (upper graphs) and spleen (lower graphs). Splenocytes revealed higher GFP rates compared to BM cells. The lineage depletion resulted in a slight increase of GFP rates. Upper graphs: BM cells exhibited a low GFP rate. hsa-miR-155 mice showed a higher GFP content when cells were enriched via lineage depletion. Lower graphs: Lineage depletion resulted for all constructs to a higher GFP content compared to the 5-FU experiment in the spleen. Each dot denotes one mouse.

Comparing the efficacy of transduction rates after 5-FU treatment and lineage depletion in transplanted mice, it is obvious that the latter method led to a higher GFP rate in splenocytes. GFP rates in the BM compartment showed no significant differences

comparing both methods, except for the hsa-miR-155 mice. Remarkably, BM cells and splenocytes of hsa-miR-155 mice showed in the lineage depletion experiment a higher GFP^+ rate compared to 5-FU treated cells. Although the transduction rates of the hsa-miR-155 construct were lowest (see table 27, section 3.4.1), GFP rates were highest in splenocytes in the lineage depletion experiment, compared to the other two mouse cohorts. This provides indication that hsa-miR-155 expression probably induces pro-survival or anti-apoptotic pathways leading to an expansion of these cells in spleen and BM.

Efficient miRNA expression in splenocytes

Expression of the appropriate mature miRNA in mouse recipients was validated by Real-Time stemloop RT PCR, using extracted RNA from paraffin embedded spleens (figure 19). Three mice of each miRNA mouse cohort and one control mouse were investigated. The miRNA expression level in splenocytes was calculated using the $2^{-\Delta\Delta CT}$ method, normalizing to miR-21 (Livak, 2001; Pfaffl, 2001). The specific GFP rate of each sample was included into calculations by dividing the GFP percentage by the measured relative copy number.

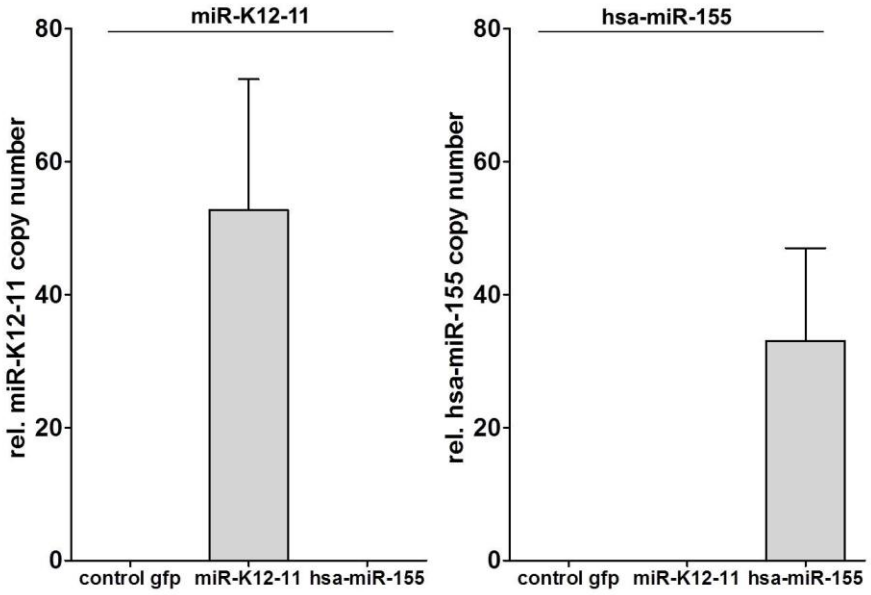

Figure 19: miRNA expression in harvested splenocytes. Total RNA was extracted from paraffin embedded spleens and miRNA expression levels were detected using Real-Time stemloop RT PCR. miR-21 was used as endogenous control. Three mice from each miR-K12-11 and hsa-miR-155 expressing mouse cohort and one control gfp mouse were analyzed. Splenocytes of BM transplanted mice express the appropriate miRNA: miR-K12-11 or hsa-miR-155. None of those miRNAs was detected in the control.

The expression of miR-K12-11 and hsa-miR-155 expression confirms an active promoter in the *in vivo* situation. miR-K12-11 expression was only detected in miR-K12-11 mice with 80, 23 and 45 rel. copy number. hsa-miR-155 expression in hsa-miR-155 mice was

similar variable as detected in miR-K12-11 mice (30, 60 and 11 rel. copy number); and also only measurable in hsa-miR-155 mice.

Together, the data clearly demonstrate the success of transplantation, engraftment as well as hematopoietic reconstitution. Moreover, the experiments validate the functionality of generated gamma-retroviruses that express GFP along with miR-K12-11 or hsa-miR-155. Thus, generated gamma-retroviruses are useful vehicles to force expression of the respective miRNA in mice.

3.5 PHENOTYPIC ALTERATIONS IN MIRNA EXPRESSING MICE

Mice were monitored for differences in blood components, organ morphology as well as immuno-phenotypic changes.

3.5.1 Blood analysis – no changes in cellular blood components

In this study, an automated complete blood count (CBC) was performed to quantify specific cellular components that circulate in the blood.

For this purpose, etherized mice were punctuated at the mandibular vein to collect blood. The blood was analyzed using the Hemavet. A CBC allows the detection of abnormally high or low counts of blood cells, and provides therefore first evidence for increased immune response or a disease. For example a high count of white blood cells (WBCs) provide first indication if mice have an infection or developed a disease like *e.g*. leukemia. Because no significant difference in any of analyzed cellular components was detected, only exemplary data from WBCs and red blood cells (RBCs) are shown in figure 20.

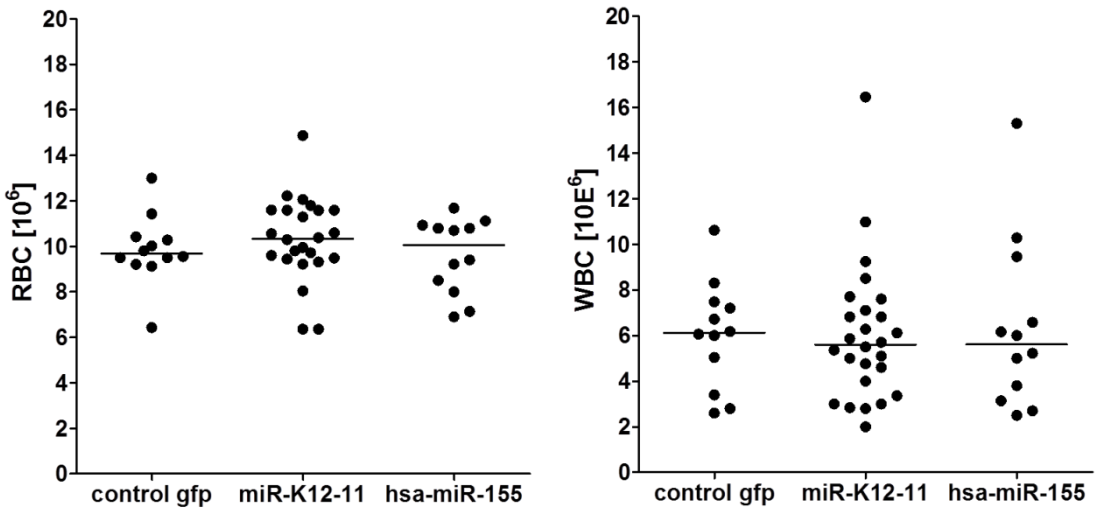

Figure 20: CBC indicates no differences in blood components. Punctuation at the mandibular vein was performed to collect blood for hematologic analysis via Hemavet. Analysis of red blood cells (RBCs) and white blood cells (WBCs) showed no changes compared to control mice. One dot denotes one mouse (control gfp: n=12; miR-K12-11: n=24; hsa-miR-155: n=12).

These findings provide no evidence, that miRNA expression in these mice facilitate the development of a disease *e.g.* like leukemia, or promote an inflammatory response.

3.5.2 **Expansion of B-cell fraction in the bone marrow**

To answer the question if miRNA expression facilitates expansion of a specific cell type in the BM compartment, FACS analysis was performed. This technique enables the distinction of different cell types by using different antibodies that mark a specific lineage like B-cells (B220, CD19), erythroid (Ter119) as well as myeloid cells (CD11b/Gr1).

The immuno-phenotypic profile was analyzed in BM cells harvested from tibiae and femora. Notably, percentage of GFP^+ cells in BM and spleen were 0.5 % -13 %. From this analysis, only mice exhibiting a GFP rate of at least 1 % were taken into account.

3.5.2.1 No expansion of erythroid cell fraction in miRNA expressing mice

First, the percentage of erythroid cells in the BM was analyzed using Ter119 as a lineage marker for these cells. For this purpose, GFP^+ cells (miRNA expressing cells) were gated and further analyzed for their Ter119 expression (figure 21).

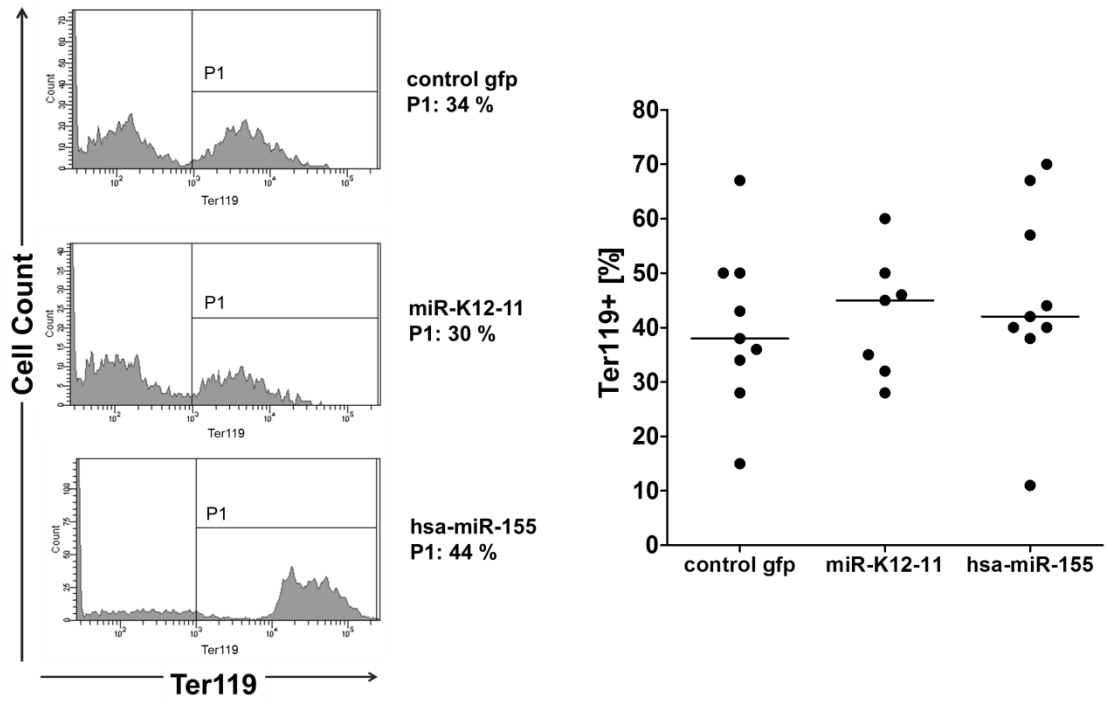

Figure 21: No change in percentage of erythroid cells in miRNA expressing BM cells. BM cells harvested from tibiae and femora were characterized using flow cytometry. GFP^+ cells were gated and analyzed for Ter119 expression. Left: Representative histograms of one mouse of each mouse cohort. P1 denotes the $Ter119^+$ cell fraction. Right: Graph shows the percentage of positive Ter119 cells in bone marrow cells of each analyzed mouse. All three mouse cohorts showed similar median percentage of Ter119 expressing cells. One dot represents one mouse. (control gfp: n=9; miR-K12-11: n=7; hsa-miR-155: n=9).

The number of erythroid cells in the BM of all analyzed mouse cohorts showed similar percentage. The median percentage value of the number of erythroid cells showed 38 % (+/-15.8 %), 45 % (+/-11.2 %) and 42 % (+/-17.7 %) in control mice, miR-K12-11 and hsa-miR-155 mice, respectively. No abnormality was observed.

3.5.2.2 Decrease of myeloid cell population in miR-K12-11 expressing mice

The analysis was continued with the myeloid cell fraction. BM cells were subjected to FACS analysis to estimate the percentage of GFP^+ cells that express both Gr1 and CD11b (figure 22).

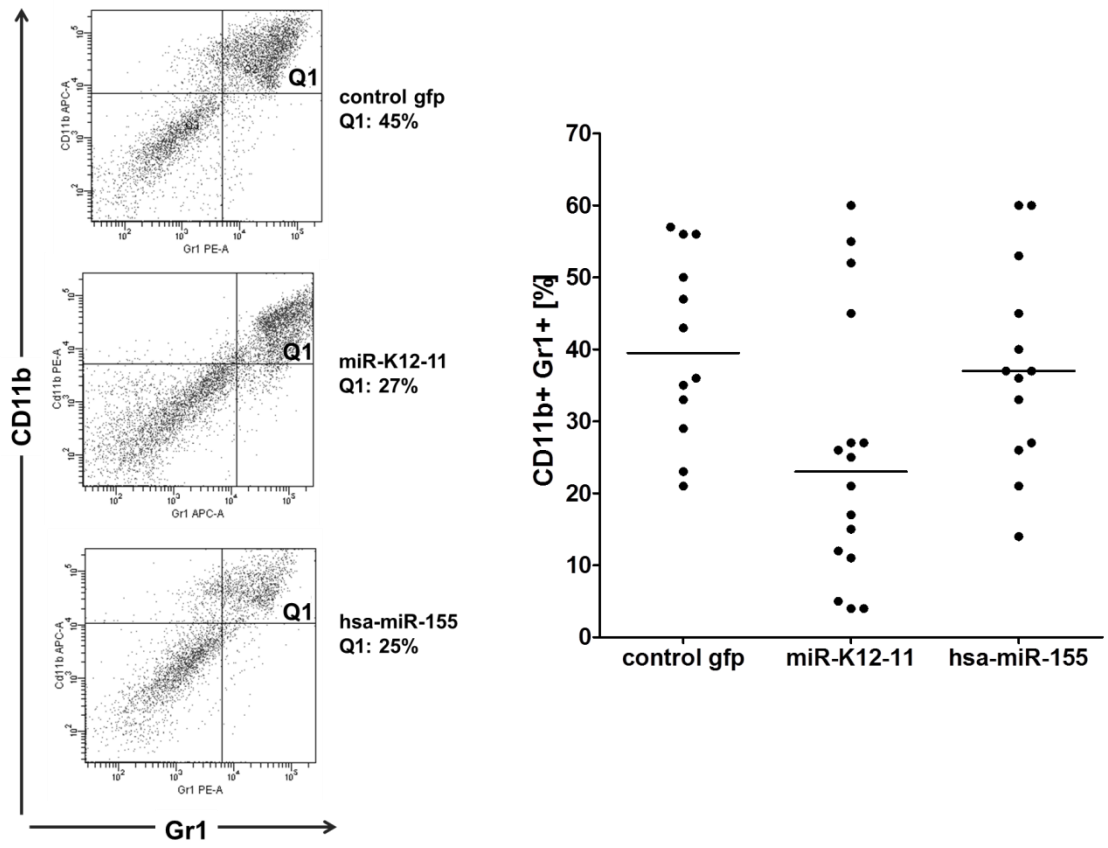

Figure 22: Decreased myeloid cell fraction in miR-K12-11 expressing mice. BM cells harvested from tibiae and femora were characterized using flow cytometry. GFP^+ cells were gated and analyzed for CD11b and Gr1 expression. Left: Representative dot plot of one mouse of each mouse cohort. Double positive cells ($CD11b^+Gr1^+$) are located in quadrate Q1. Right: Number of myeloid cells ($CD11b^+Gr1^+$) was decreased in miRNA expressing mice compared to control mice. One dot represents one analyzed mouse (control gfp: n=12; miR-K12-11: n=16; hsa-miR-155: n=13). Whereas miR-K12-11 mice showed a significant decrease of the myeloid fraction compared to control mice, hsa-miR-155 mice showed only a slight decrease.

Notably, miR-K12-11 mice showed a significant decrease of the number of myeloid cells (22 %; +/-18%) compared to control mice (40 %; +/-12 %). A similar phenotype to miR-K12-11 mice was observed in hsa-miR-155 mice, but less pronounced (35 %; +/-13 %). These findings infer that the myeloid lineage is disfavored when miR-K12-11 is ectopically expressed, and that a similar trend might exists in hsa-miR-155 expressing cells.

3.5.2.3 Increased number of B-cells in BM compartment

The observed underrepresentation of myeloid cells raised the question if other lineages, like B-cells, might be favored. Therefore, the cell lineage study was continued with an analysis of the B-cell population in GFP^+ BM cells using B220 and CD19 antibodies (figure 23; left and right panels respectively). Both proteins are expressed on the surface of B-cells and are therefore commonly used for B-cell identification.

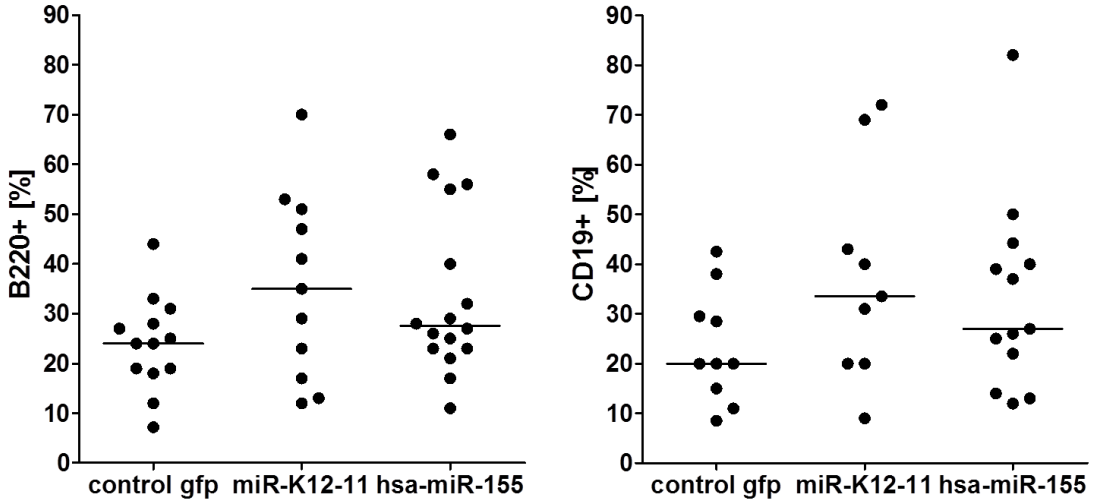

Figure 23: B-cell fraction was increased in the BM compartment of miRNA expressing mice. BM cells harvested from tibiae and femora were characterized for the immuno-phenotypic profile of lymphocytes using flow cytometry. B220 (left graph) and CD19 antibodies (right graph) were applied to analyze the B-cell fraction. GFP^+ gated BM cells from miRNA-expressing mice revealed a slight increase in number of B-lineage cells compared to GFP control mice. Each dot denotes one mouse (B220: Left graph; control gfp: n=13; miR-K12-11: n=11; hsa-miR-155: n=16 and CD19: Right graph; control gfp: n=10; miR-K12-11: n=9; hsa-miR-155: n=13).

The $B220^+$ population is moderately increased in miRNA expressing mice. miR-K12-11 mice showed a median percentage of 35 % (+/-18.7 %) whereas the hsa-miR-155 mice exhibited a lower content with 28 % of $B220^+$ (+/-16.4 %) cells. The control mice showed the lowest percentage of $B220^+$ cells with 24 % (+/-9 %). Using CD19 antibody, a similar phenotype was observed. In miR-K12-11 mice, 34 % (+/-18 %) of GFP^+ gated cells were positive for CD19 expression. hsa-miR-155 mice showed 27 % (+/-16 %) of $CD19^+$ cells, whereas the control mice exhibited the lowest content with 20 % (+/-9 %). B-cells were slightly overrepresented in miRNA expressing mice in the BM compartment.

3.5.3 **Increased pre-B-cell fraction**

The finding of moderately augmented B-cells in the BM led to the question if miRNA expression influences the transition of B-cells during their development. Thus, FACS analysis was continued to answer the question if miR-K12-11 or hsa-miR-155 expression might influence the B-lineage, for instance by facilitating differentiation toward later B-cell stages, or, by inducing a B-cell block in the BM compartment. Figure 24 shows the expression pattern of CD19 and CD43 during B-cell development in the BM compartment, which highlights the distinction between early and later B-cell stages when applying CD19 antibody in combination with CD43. $CD19^+CD43^+$ cells mark earlier B-cell fractions

whereas $CD19^{+}CD43^{-}$ cells define the later B-cell stages, like small pre-B-cells and immature B-cells.

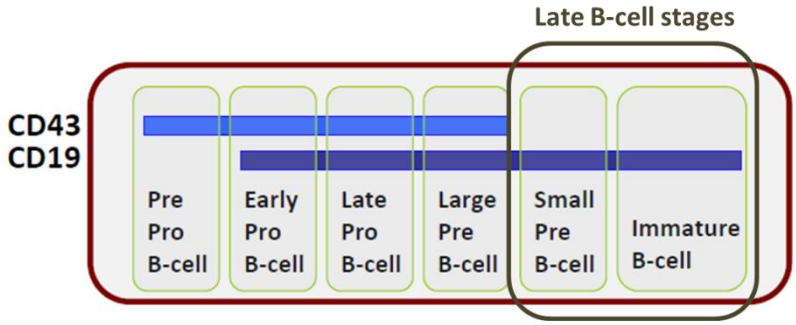

Figure 24: CD19/CD43 expression allows distinction between early and late B-cell stages. Different cell surface expression allows discrimination of different B-cell stages in the bone marrow. $CD19^{+}CD43^{-}$ expression defines early B-cells like early pro-B-cells, late pro-B-cells and large pre-B-cells. Small pre-B-cells and immature B-cells express CD19 but lack CD43 antigen (figure was designed according to Hardy et al. (Hardy et al., 2007)).

To answer the question if miRNA expression influences B-cell development, $GFP^{+}/CD19^{+}$ cells were first gated and then analyzed for their CD43 expression. The following graph and histograms depict the results when gating GFP^{+} and $CD19^{+}$ cells (figure 25). Shown are the percentage of cells that express CD19 but lack CD43 antigen, hence the later B-cell fractions, like small pre-B-cells and immature B-cells.

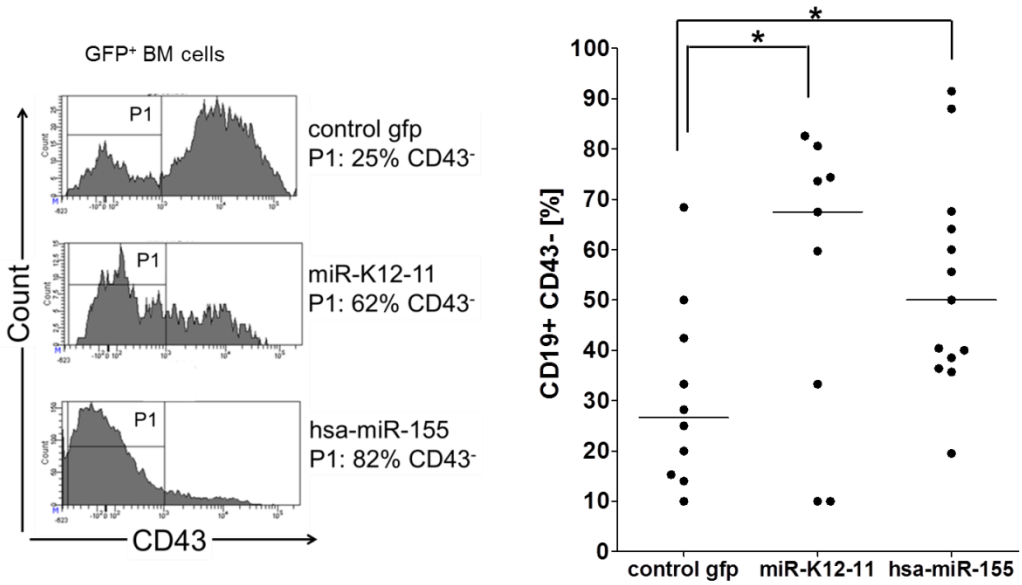

Figure 25: Increased number of later B-cells. CD43 expression evaluated by flow cytometry on $GFP^{+}/CD19^{+}$ gated BM cells revealed a significant increase of the later B-cell population ($CD19^{+}CD43^{-}$) in the BM of miRNA expressing mice, indicating a shift toward the later B-cells if the appropriate miRNA is expressed. Left: Histograms of representative miRNA expressing and control mice represent the increased B-cell fraction in the $GFP^{+}/CD19^{+}$ gated BM cells of miRNA expressing mice. Gate P1 indicates the $CD43^{-}$ population. Right: The graph shows the significant increased fraction of pre-B-cells in miRNA exressing mice. One dot represents one mouse (control gfp: n=10; miR-K12-11: n=9; hsa-miR-155: n=13).

Strikingly, a significant increase of later B-cells ($CD19^+/CD43^-$) in $GFP^+/CD19^+$ cells in both miRNA expressing mouse cohorts was detected. The histograms represent the result of one mouse of each mouse cohort, whereas the graph shows the percentage of $CD19^+/CD43^-$ cells of each analyzed mouse. miR-K12-11 mice revealed 68 % (+/-28 %) of later B-cells, hsa-miR-155 showed 50 % (+/-20 %) compared to 28 % (+/-18 %) of the control mice. These findings indicate that ectopic expression of the respective miRNA in murine progenitor cells induces a shift from early pro-B-cells toward later B-cell stages ($CD19^+/CD43^-$).

To answer the question whether pre- or immature B-cells or both were expanded in the BM compartment, FACS analysis was continued using B220 and IgM antibodies. The scheme in figure 26 maps the expression pattern of IgM and B220 during B-cell development in the BM compartment, highlighting that immature B-cells express both, IgM and B220. The double staining allows therefore the distinction between pre-B-cells and immature B-cells. The graph in figure 26 depicts the results when using IgM antibodies by gating GFP^+ and $B220^+$ cells.

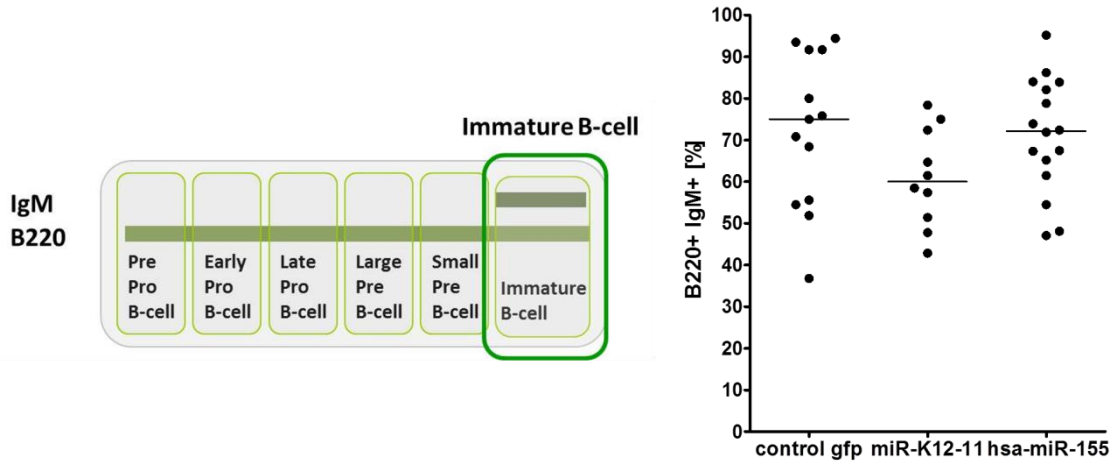

Figure 26: No increase of the immature B-cell fraction. Left: Schematic drawing of the expression pattern during B-cell development concerning the cell surface proteins IgM and B220. Employing both antibodies allows the discrimination of different B-cell stages in the bone marrow. $B220^+IgM^+$ expression defines immature B-cells (modified to Hardy et al. (Hardy et al., 2007)). Right: IgM expression evaluated by flow cytometry on $GFP^+/B220^+$ gated BM cells revealed no significant increase or decrease of the immature B-cell population in the BM of miRNA expressing mice. One dot represents one mouse (control: n=13; miR-K12-11: n=10; hsa-miR-155: n=16).

Interestingly, the number of immature B-cells was not significantly increased in the BM compartment. Whereas miR-K12-11 mice revealed only a moderate decrease of the immature B-cell population (60 %; +/-12 %) compared to the control group (75 %; +/-18 %), hsa-miR-155 mice showed no change in the percentage of immature B-cells (72 %; +/-13 %).

Collectively, the B-cell population was increased in the BM in miR-K12-11 or hsa-miR-155 expressing mice, although only moderately. But this observation is in line with the observed slight underrepresentation of the myeloid lineage. In addition, the sub-populations of $B220^{+}/IgM^{+}$ population was not significantly increased, but strikingly $CD19^{+}/CD43^{-}$ (pre-B-cell) cells were significantly increase in their number.

3.5.4 **Phenotypic changes of spleens in miRNA expressing mice**

Spleens from euthanized mice were removed, then weighed and finally cut into two pieces. Whereas one piece was embedded into paraffin, the second one was used for FACS analysis. Spleens were compared with respect to immuno-phenotypic changes, morphology and GC development.

3.5.4.1 Splenic weight

The first step when analyzing spleens included the weighing to detect for example an enlarged spleen, called splenomegaly (figure 27). The abnormal extension of a spleen can have multiple causes; one example is the development of a lymphoma, because these cells can accumulate in the spleen, which result in splenomegaly.

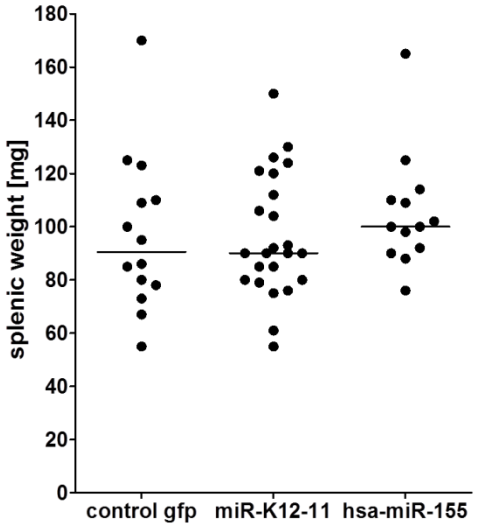

Figure 27: No change in the weight of spleens. Spleens were weighed to estimate weight alterations. The median value of all mouse cohorts was similar. One dot represents one mouse (control gfp: n=14; miR-K12-11: n=24; hsa-miR-155: n=13).

Spleens of miRNA expressing mice showed no differences in weight compared to control mice. miR-K12-11 mice and control mice had a weight of 90 mg (median value); the hsa-miR-155 mice exhibited a weight of 100 mg. A splenomegaly owing to miRNA expression was therefore not observed. These findings suggest that miRNA expressing mice did not develop lymphoproliferative diseases like leukemia or lymphoma.

3.5.4.2 Expansion of B-cell fractions in spleens

Next, the question should be answered if miRNA expression affects different cell populations in the spleen, as this was observed in the BM compartment (see section 3.5.2). For this purpose, spleens were purged through a strainer followed by single cell analysis via FACS. Each analysis was performed by gating GFP$^+$ cells followed by analysis of their immuno-phenotypic profile using diverse antibodies. Notably, percentage of GFP$^+$ cells in the bone marrow and spleen reached 0.5 % - 30 %. From this contingent, only mice exhibiting a GFP rate of at least 1 % were taken into account.

To address the question if or to what extent miRNA expression affects the B-cell population in splenocytes, flow cytometric immuno-analysis was performed. B220 and CD19 antibodies were used to detect the B-cell fraction. First, CD19$^+$ cells were analyzed (figure 28).

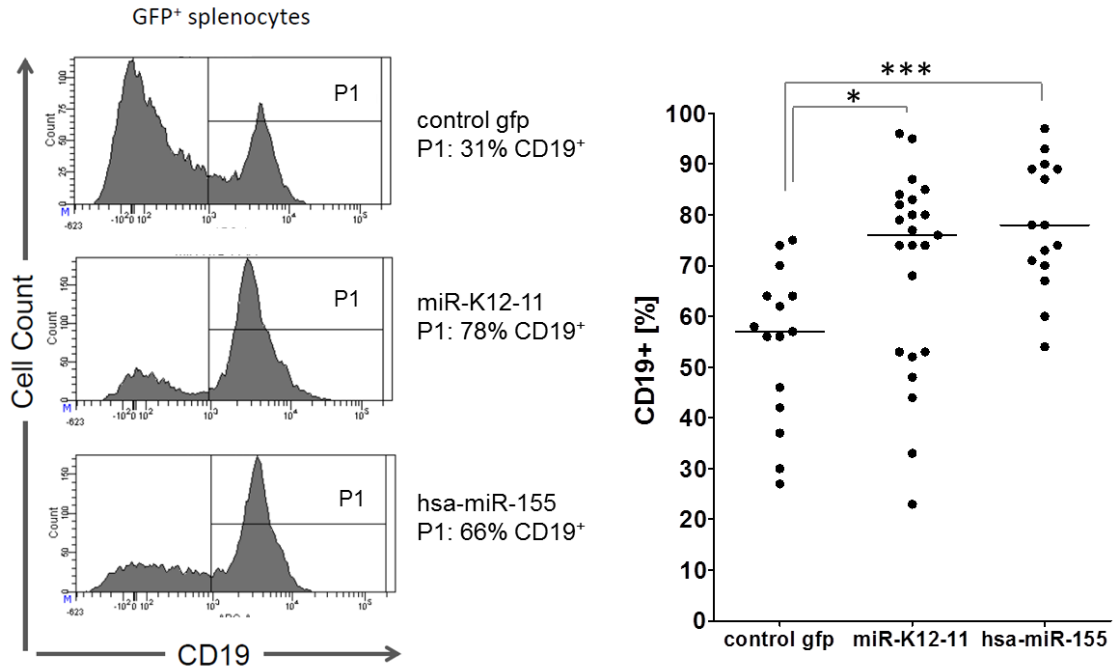

Figure 28: Expansion of CD19$^+$-cell fraction in spleens of miRNA expressing mice. Left: Representative histograms of one mouse of each mouse cohort. The histograms represent CD19 expression of GFP$^+$ splenocytes. Gate P1 denotes CD19$^+$ fraction. Right: Distribution of percentage of CD19$^+$ cells on GFP$^+$ gated splenocytes is shown in the graph. One dot represents one mouse (control: n=15; miR-K12-11: n=23; hsa-miR-155: n=15). Flow cytometry analysis revealed an expansion of percentage of B-cells in miRNA expressing mice using the B-cell marker CD19 on GFP$^+$ splenocytes. B-cell fraction was significantly increased when the appropriate miRNAs were expressed.

Interestingly, GFP$^+$ splenocytes of miRNA expressing mice showed a significant increase in the number of B-cells in GFP$^+$ splenocytes. Gate P1 denotes CD19$^+$ population in the GFP$^+$ splenocytes and shows that miRNA expressing mice had an increase of CD19$^+$ cells

(the two lower histograms) compared to control mice (upper histogram). The percentage of CD19$^+$ cells in GFP$^+$ splenocytes is plotted in the graph (right panel). hsa-miR-155 mice showed a median value of 75 % (+/-12 %) of positive B-cells; miR-K12-11 mice showed the same trend (72 % (+/-19 %) as hsa-miR-155 mice, whereas the control mice had a lower B-cell content (55 % (+/-14 %)). These findings revealed a significant increase in the number of CD19$^+$ B-cells when miRNAs are expressed.

Next, the analysis was continued using B220 antibodies as a second B-cell marker (figure 29). This analysis was conducted to confirm the observed B-cell expansion when using CD19 antibodies.

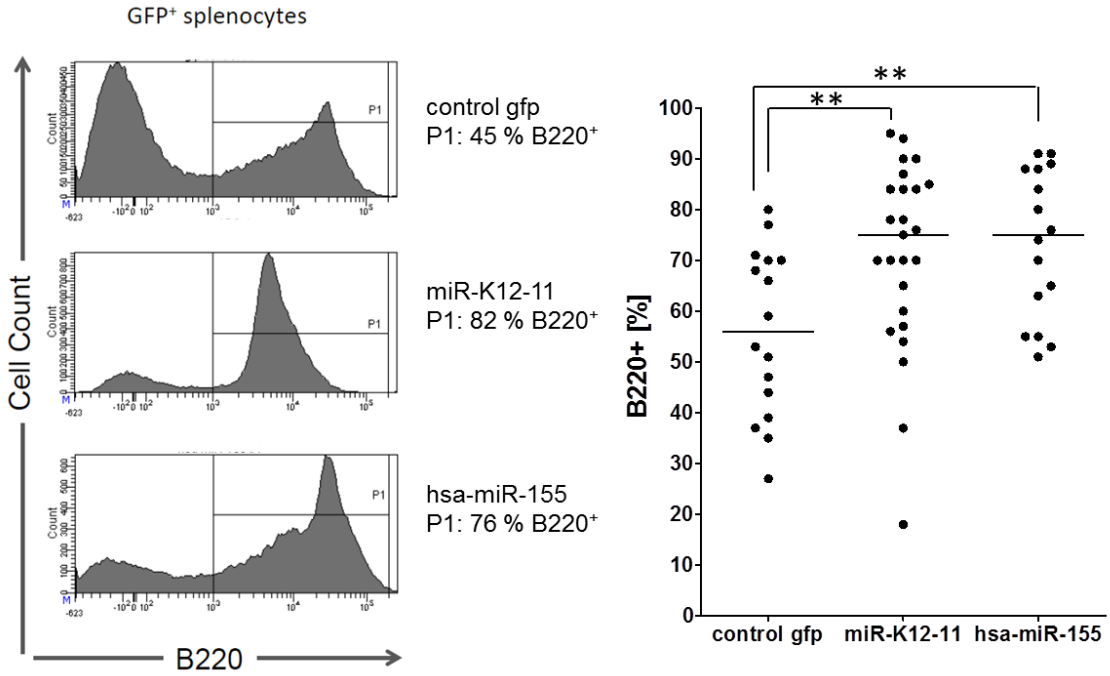

Figure 29: Expansion of B220$^+$-cell population in miRNA expressing mice. Left: Representative histograms of one mouse of each mouse cohort. GFP$^+$ splenocytes were first gated and then analyzed for B220 expression. Flow cytometry analysis revealed an expansion of B-cells in miRNA expressing mice using the B-cell marker B220. Right: The percentage of B220$^+$ cells in GFP$^+$ splenocytes is shown in the graph. One dot represents one mouse (control: n=16; miR-K12-11: n=25; hsa-miR-155: n=16).

The expansion of the B-cell fraction in GFP$^+$ splenocytes of miRNA expressing mice when using CD19 antibodies was confirmed using a second B-cell marker, namely B220. The representative histograms of one mouse of each mouse cohort highlight the shift toward B220$^+$ splenocytes. Gate P1 denotes the B220$^+$ population in GFP$^+$ splenocytes and highlights the increased B-cell fraction in miRNA expressing mice (two lower histograms). The percentage of B220$^+$ cells in GFP$^+$ splenocytes of each mouse is plotted in the graph. In comparison, the GFP$^+$ population of miR-K12-11 and hsa-miR-155 mice showed a

median value of 75 % (+/-18 % and +/-14 %) of $B220^+$ cells in GFP^+ splenocytes, whereas the control mice represented a lower median of 55 % (+/-16 %) of $B220^+$ cells.

3.5.4.3 T-cells are underrepresented in the spleen

It is conceivable that another cell lineage is underrepresented while B-cells are expanded. To prove this notion, FACS analysis was extended using CD3 antibodies to estimate the proportion of T-cells in splenocytes (figure 30).

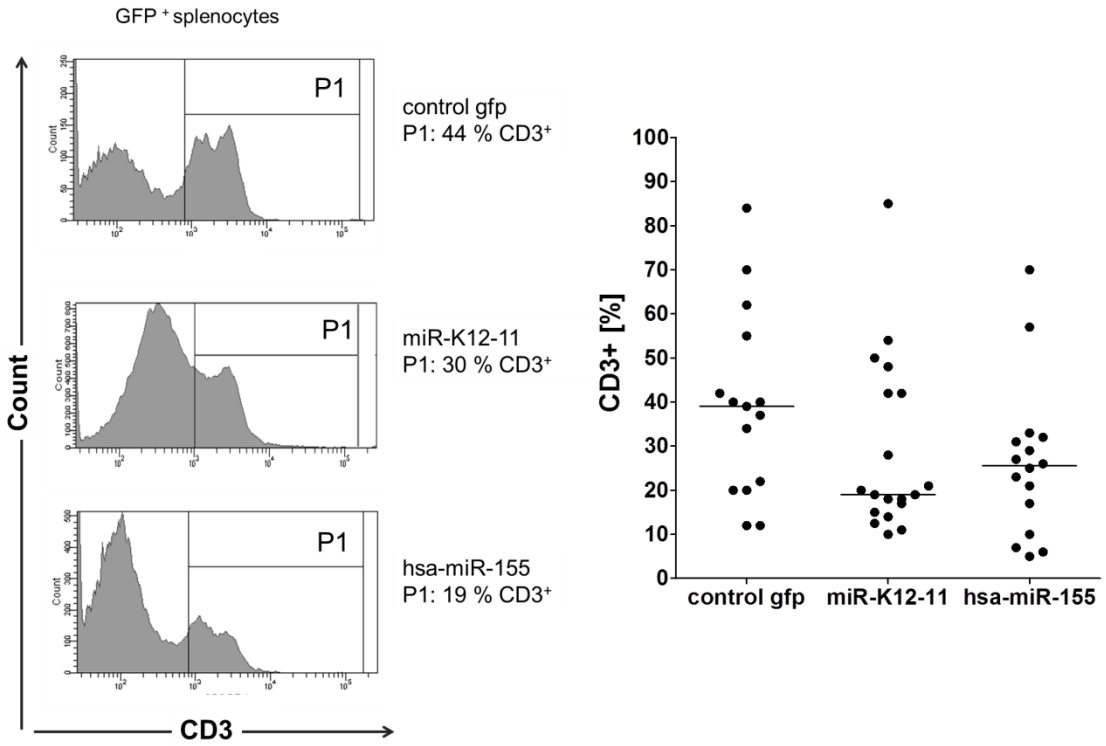

Figure 30: T-cell fraction is decreased in miRNA-expressing mice. Flow cytometry analysis showed a decrease of T-cells in miRNA expressing mice when using the T-cell marker CD3. Left: Representative histograms of one mouse of each mouse cohort. Gate P1 denotes $CD3^+$ population in GFP^+ splenocytes. Right: The graph shows the distribution of T-cells in GFP^+ splenocytes. One dot represents one mouse (control: n=15; miR-K12-11: n=19; hsa-miR-155: n=16).

Interestingly, T-cells are underrepresented in GFP^+ splenocytes in miRNA expressing mouse cohorts. In comparison, miR-K12-11 and hsa-miR-155 mice represented a median value of 18 % (+/-20 %) and 22 % (+/-18 %) of $CD3^+$ cells, whereas the control mice showed 40 % (+/-20 %). The average number of T-cells was decreased approximately 1.8 and 2.2 fold in hsa-miR-155 and miR-K12-11 mouse cohorts, revealing a moderate but not statistically significant decrease.

Taken together, these findings indicate an influence of both miRNAs in the B-cell lineage, leading to an expansion of B-cells among splenocytes; whereas T-lineage cells are possibly disfavored in their commitment or survival, resulting in a decrease of the T-cell population.

3.5.5 **Increased number of GCs in spleens**

In this thesis work, splenic structure, such as red pulp, white pulp and mantle zone, was investigated via H&E staining. Spleens were embedded into paraffin prior to H&E staining. Representative images from spleens highlight the observation that formations of GCs were increased (figure 31).

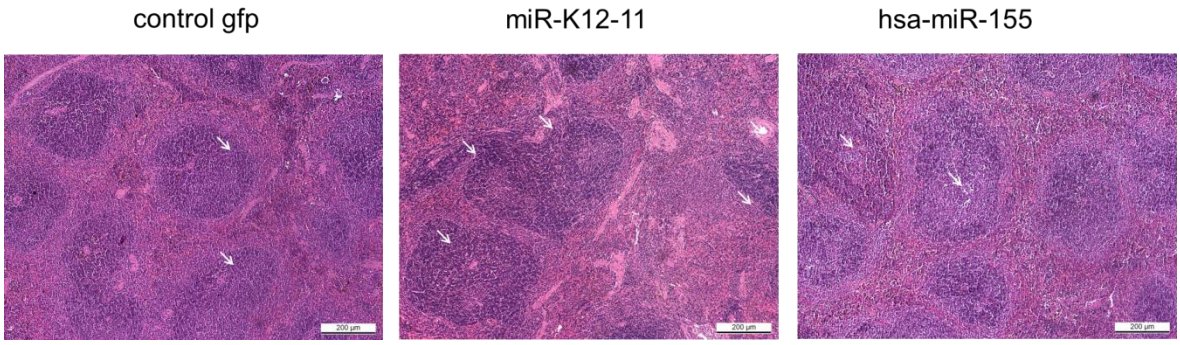

Figure 31: Enhanced GC formation in miRNA expressing mice. H&E stainings indicate an increased GC formation in miRNA expressing mice. White arrows mark GCs.

Lymphoma or tumor cells were not detected in H&E stainings, but it is apparent that GC formation was increased in miRNA expressing mice. GCs are sites of antigen-driven B-cell switch recombination and selection that generate high-affinity memory B-cells. Interestingly, Thai et al. revealed a role of miR-155 in GC response (Thai et al., 2007), which underscores the observation of the enhanced GC formation in these miRNA expressing mice. The analysis was continued regarding GC development using PNA to stain GCs.

Enhanced GC formation in miRNA-expressing mice.

The GC B-cell is a discrete cell population that expresses PNA. Thus, any activated B-cell in the GC can be probed with PNA highlighting specifically the region of the GC (figure 32).

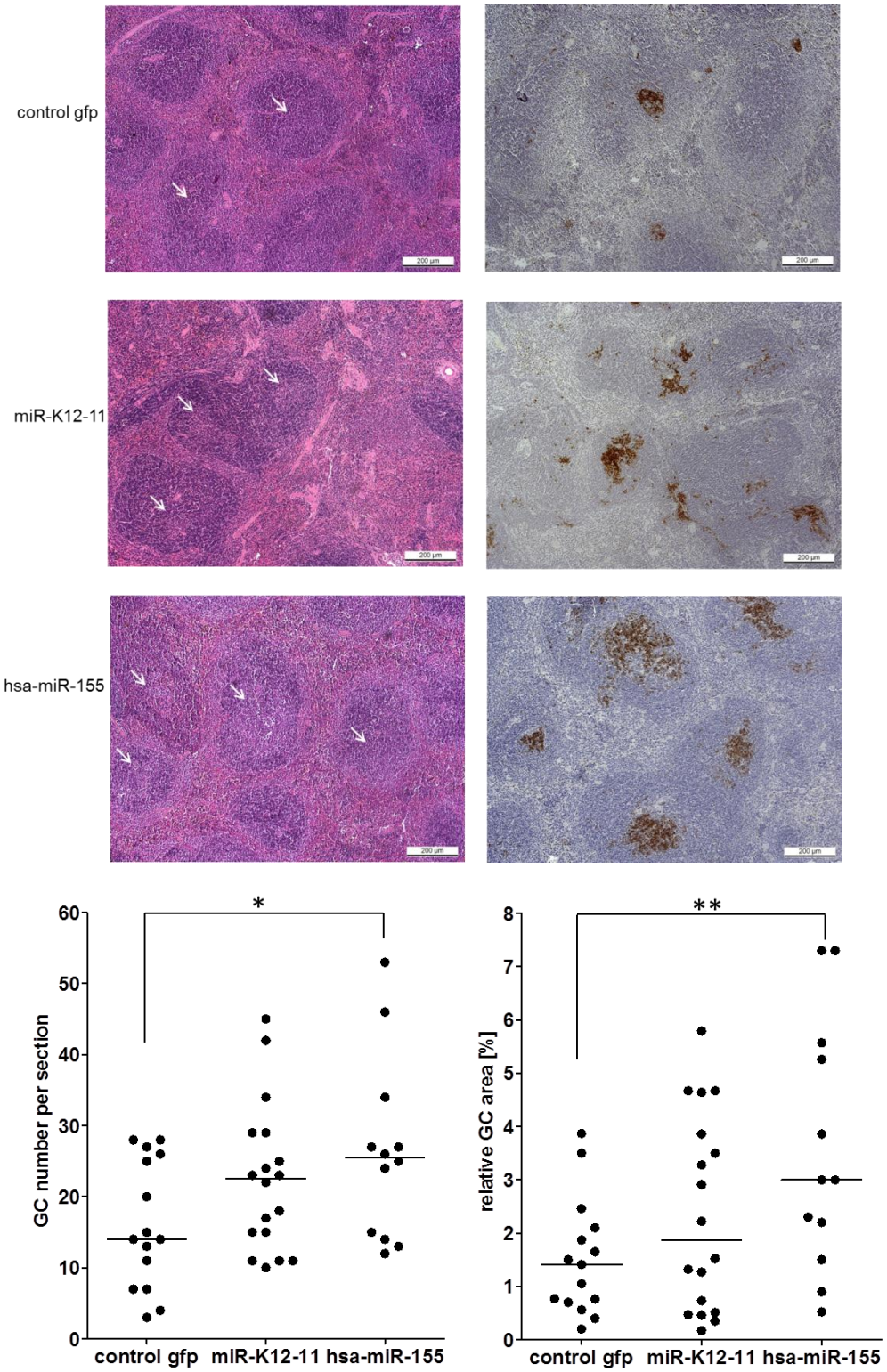

Figure 32: Enhanced GC development in miRNA expressing mice. Upper figure, H&E staining and IHC indicate an increased GC formation in miRNA expressing mice. Left: H&E staining: White arrows indicate GCs. Right: IHC: PNA staining was used to estimate GC number and relative GC area per section (PNA: brownish). Stainings of one representative mouse per mouse cohort. Lower figure: Evaluation of GC number and relative area was performed via Pixel Classifier (Nikon NIS elements). Each dot denotes one mouse. Left: Number of GCs was calculated by summing up GCs per section. Right: The relative GC area was evaluated by surrounding each GC as region of interest (ROI), summing up the total GC area and normalizing it to the area of the splenic section. The hsa-miR-155 mouse cohort showed a significant increase in GC number as well as relative GC area compared to the control mice. The miR-K12-11 mice displayed the same phenotype, but less pronounced.

The number of GCs was calculated by summing up all GCs per section (left graph). A significant increase in the GC number was observed in hsa-miR-155 mice (26; +/-12) compared to control mice (16; +/-9). A similar trend was observed in miR-K12-11 mice. They showed also an increase in GC number (22; +/-10), however this was not statistically significant. Notably, the p-value for the GC number in the miR-K12-11 mouse cohort was 0.07, and thus just above the significance mark of 0.05.
Next, the relative GC area was evaluated by surrounding each GC as region of interest (ROI), summing up the total GC area and normalizing it to the area of analyzed splenic section and calculating the percentage of GC per area (right graph). hsa-miR-155 mice showed a significant increase of GC area (2.4 %; +/-2.2 %) compared to the control group (1.52 %; +/-1 %). miR-K12-11 mice showed an increase (3.5 %; +/-1.5 %), however this increase was not significant.

Comparing all three mouse cohorts, hsa-miR-155 mice showed in GC number and GC area evaluations a significant increase compared to control mice. miR-K12-11 mice had the same phenotype as hsa-miR-155, however less pronounced and thus not statistically significant. These observations indicate an enhanced formation of GC when one of the miRNAs is expressed.

3.6 CONFIRMING TARGETS AND VALIDATING A NOVEL ONE

After analyzing phenotypic alterations, cellular targets were investigated to gain insight into possible cellular mechanisms that underlie the observed phenotype. On the one hand, putative targets were investigated with regard to their mRNA expression *in vivo*. On the basis of conservation between hsa-miR-155 and miR-K12-11, recently identified miR-155 targets were investigated, which are furthermore associated with B-cell development. This approach seems to be most promising to confirm miR-K12-11 targets with biological relevance in the context of KSHV infection in B-cells. On the other hand, we aimed to investigate *JARID2* as a novel target of miR-K12-11.

3.6.1 **Repressed mRNAs in miRNA expressing BM cells**

In this work, the mRNA expression levels of *Sfpi1*, *c-Myb* and *Fos* were validated, since these genes have been shown to play a role in B-cell development and immune response and are further verified as a target of miR-155 *in vitro* (Gottwein et al., 2007; Rodriguez et al., 2007; O'Connell et al., 2008; Imig et al., 2011). The expression levels of these mRNAs were measured to answer the question if and to what extent these genes were expressed in the *in vivo* situation. For this purpose, RNA from flow sorted GFP^+ BM cells (miRNA expressing cells) was first extracted followed by Real-Time RT PCR.

PU.1 (human gene symbol: *SPI1*; mouse gene symbol: *Sfpi1*) is one of the three candidates that were analyzed during this work (figure 33). *SPI1* was already validated as a target of hsa-miR-155 (O'Connell et al., 2008). It is thought that this gene plays an important role in the early B-cell development for progression toward later B-cell stages. It seems that the expression level is an essential factor for this B-cell lineage commitment. Whereas high *SPI1*/*Sfpi1* expression correlates with myeloid lineage, a low level is important to commit the cells toward B-cells (Matthias & Rolink, 2005; Nutt & Kee, 2007).

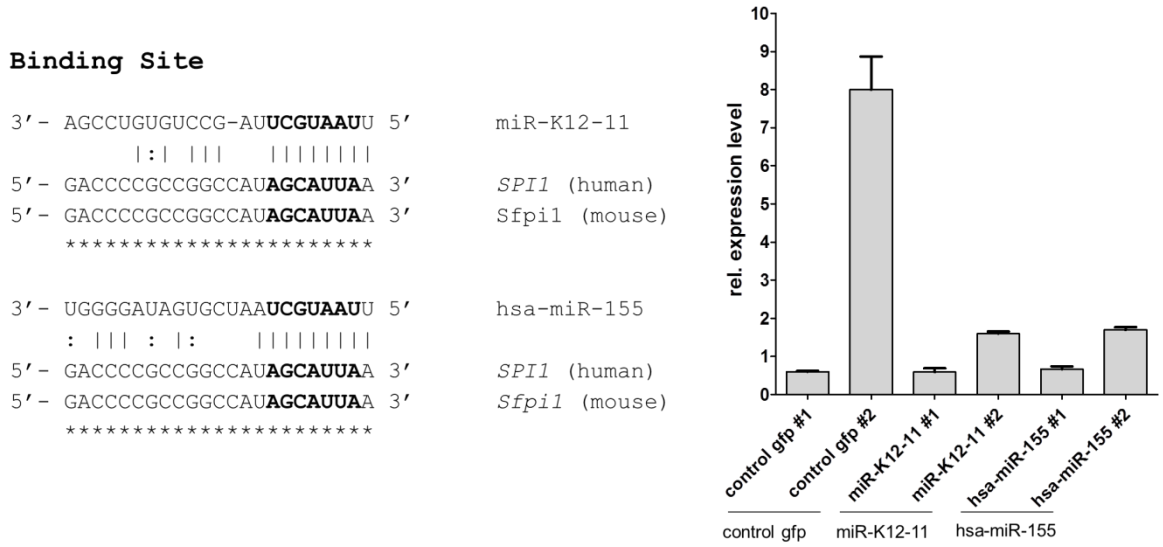

Figure 33: *Sfpi1* expression level in miRNA expressing BM cells. Left: *SPI1/Sfpi1* 3´UTR contains one seed match site for miR-K12-11 and hsa-miR-155. The alignment depicts the binding-sequences (BS) of the mature miRNA to the 3´UTR. The seed region and the BS of the 3´UTR is marked with bold letters and asterisks depict conserved region between mouse and human mRNA (*SPI1*: NM_011355; *Sfpi1*: NM_011355.1). Right: Real-Time RT PCR analysis of total RNA derived from flow sorted GFP^+ BM cells from two mice of each mouse cohort. The mRNA level of *Sfpi1* was normalized to endogenous level of *Actin*, *Gapdh* and *Rplp*.

The comparison of control mouse #2 with miRNA expressing mice revealed a repression of this mRNA in miRNA expressing BM cells, whereas the comparison of control #1 with the miRNA expressing BM cells revealed no repression. This finding is not consistent with previous reports that validated a repression of *SPI1/Sfpi1* by miR-155 expression.

The expression analysis was continued by investigating *c-Myb*, which is a cellular proto-oncogen (figure 34). The 3´UTR of *c-Myb(*mouse)/*c-MYB*(human) harbors two binding sites for each miRNA, making the gene to a putative target of miR-K12-11 and hsa-miR-155. And indeed, *c-MYB* was validated as a target of hsa-miR-155 (Imig et al., 2011). *C-MYB* is an interesting target in regard to KSHV biology, since its expression is tightly coordinated during B-cell development, in particular the pre-B-cell commitment (Bender & Kuehl, 1987; Bender et al., 1987; Imig et al., 2011). This mRNA needs to be repressed

during transition from the pre-B-cell to immature B-cell stage (Imig et al., 2011). Notably, when comparing the 3´UTRs of mouse and man, there are differences between these species. Whereas the binding site 1 is conserved within the 3´UTR of *c-MYB*, the binding site 2 exhibits some non-conserved sequences. Nevertheless the important seed region is conserved in both binding sites.

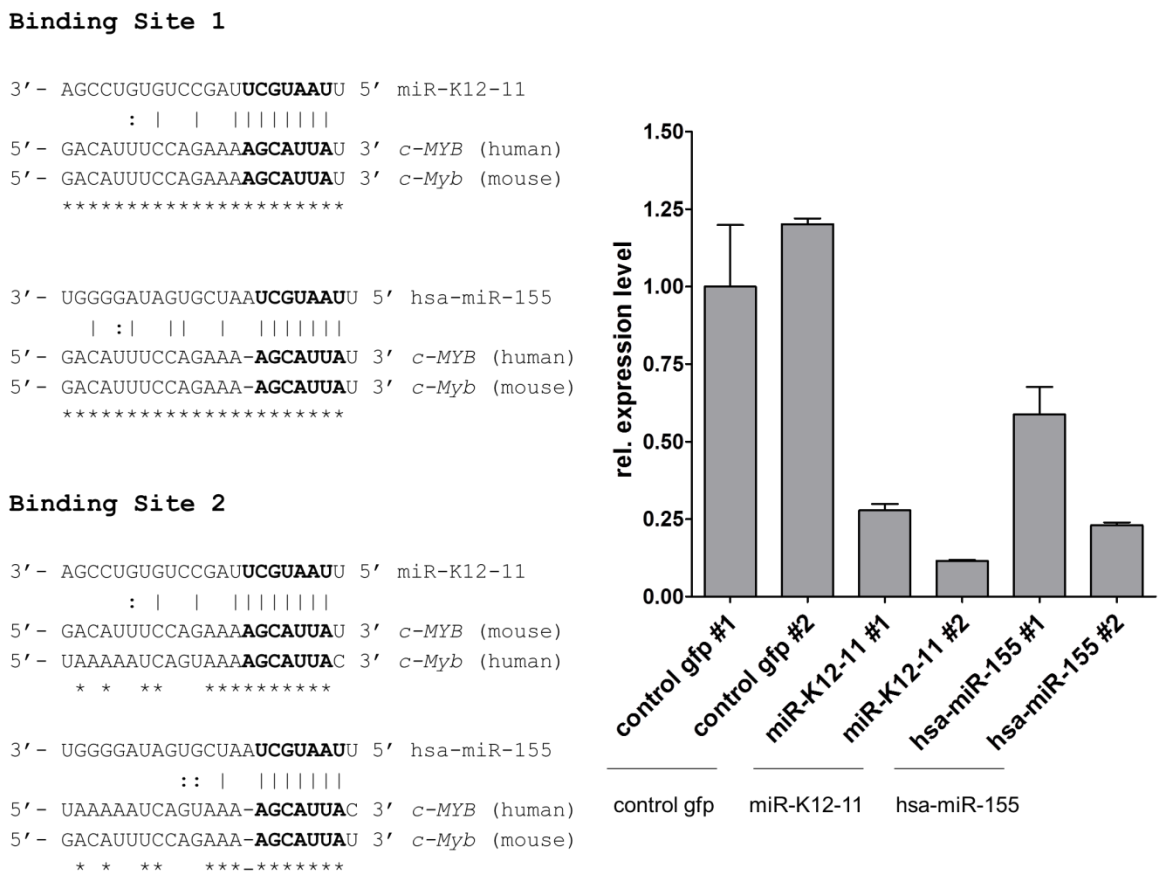

Figure 34: Repressed c-myb expression level in miRNA expressing BM cells. Left: The alignment depicts the binding sites (BS) of the mature miRNA to the 3´UTR. *C-MYB/c-Myb* 3´UTR contains two seed match sites for each miR-K12-11 and hsa-miR-155. Seed region and the BS in the 3´UTR is marked with bold letters and stars depict conserved region between mouse and human mRNA (*c-MYB*: NM_005375; *c-Myb*: NM_010848). Although binding site 2 exhibits some non-conserved sequences, the important seed region is conserved. Right: Real-Time RT PCR analysis of total RNA derived from flow sorted GFP^+ BM cells from two mice of each mouse cohort. The mRNA level of c-Myb was normalized to endogenous level of *Actin*, *Gapdh* and *Rplp*. *C-Myb* expression was repressed in miRNA expressing BM cells.

C-Myb expression is repressed in miRNA expressing BM cells when comparing the expression level with the control. This finding is consistent with previous data that demonstrated a hsa-miR-155 mediated repression of *c-MYB* (Imig et al., 2011).

The study was extended with analyzing the expression of gene *Fos*, which is a cellular proto-oncogene with important functions during hematopoiesis (Gonda & Metcalf, 1984; Bender et al., 1987; Liebermann & Hoffman, 1994; Thomas et al., 2005). This gene is further associated with innate immunity and B-cell differentiation. The 3´UTR of *Fos*(murine)/*FOS*(human) mRNA contains one binding site for both miRNAs (figure 35). Previous data from *in vitro* studies validated that *FOS* is a shared target of hsa-miR-155 and miR-K12-11 (Gottwein et al., 2007).

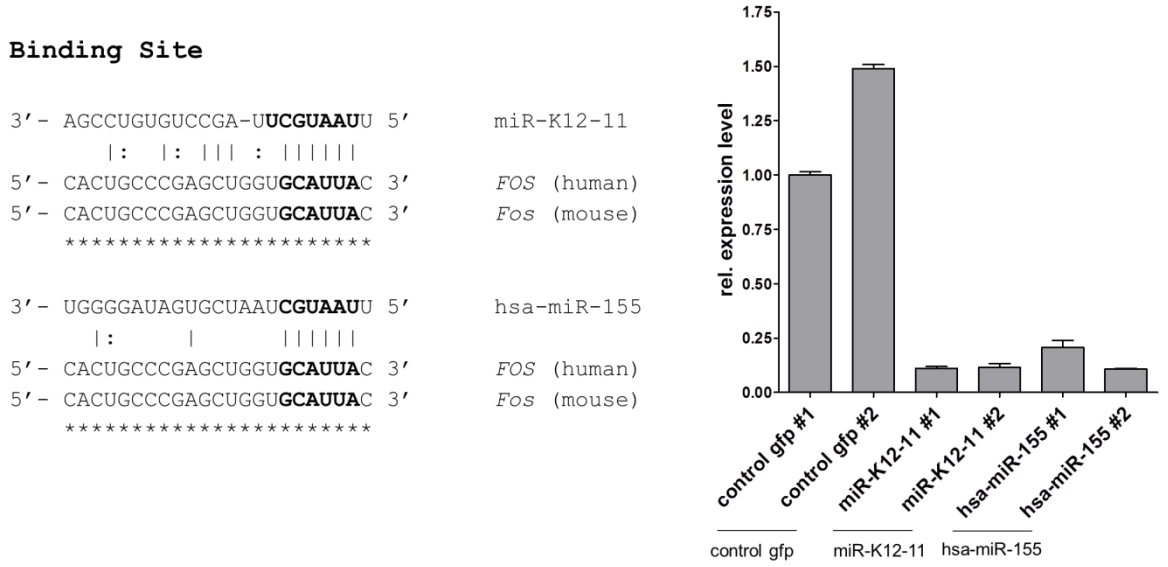

Figure 35: Repressed *Fos* expression level in miRNA expressing BM cells: Left: *Fos/FOS* 3´UTR contains one seed match site for each miR-K12-11 and hsa-miR-155. The alignment depicts the binding-sequences (BS) of the mature miRNA to the 3´UTR. Seed region and the BS in the 3´UTR is marked with bold letters and stars depict conserved region between mouse and human mRNA (*FOS*: NM_005252; *Fos*: NM_010234). Right: Real-Time RT PCR analysis of total RNA derived from flow sorted GFP^+ BM cells from two mice of each mouse cohort. The mRNA level of *Fos* was normalized to endogenous level of *Actin*, *Gapdh* and *Rplp*. *Fos* expression was repressed in miRNA expressing BM cells.

Our data revealed a strong reduced level of *Fos* transcripts in miRNA expressing BM cells. All miRNA expressing BM cells showed a repressed mRNA expression level of *Fos* compared to the control. This observation is in line with previous data that revealed a repression mediated by both miRNAs (Gottwein et al., 2007).

3.6.2 *Jarid2* – a novel target of miR-K12-11

JARID2 garnered our considerable interest, since it plays an important role in hematopoiesis, cell differentiation and myeloid disorders (Majewski et al., 2008; Shen et al., 2009; Puda et al., 2012). JARID2 recruits the histonemethyltransferase polycomb repression complex 2 (PRC2) to histone tails, which trimethylates 'Lys-27' of histone H3 (H3K27me3) (Li et al., 2010; Islam et al., 2011; Zhang et al., 2011). Importantly, H3K27-me3 is a mark for heterochromatin; hence JARID2 is thought to have an impact in the transcriptional silencing via mediating PRC2 occupancy on the genome.

The 3´UTR of the *JARID2*(human)/*Jarid2*(murine) gene contains two perfect seed match sites for miR-K12-11 and hsa-miR-155 (figure 36), indicating that *JARID2* might be a target gene for both miRNAs. Several studies postulated that *JARID2*/*Jarid2* is a target of miR-155 in human and mouse cells (Costinean et al., 2006; O'Connell et al., 2008; Bolisetty et al., 2009; Xu et al., 2010a; Gottwein et al., 2011a). With the exception of a single nucleotide exchange in binding site 1, *Jarid2* is perfectly conserved between mouse and human. So far, neither the regulation by miR-K12-11 nor the effect of both miRNAs on the protein level has been validated so far.

The functional validation of miRNA targets includes luciferase reporter assays. To demonstrate a direct interaction between miRNAs and 3´UTRs, the seed regions in the *JARID2*-reporter vector were mutated. Therefore, three different plasmids were generated. Whereas *JARID2* mut1 harbors mutations in the first seed (4169-4175 nt), the *JARID2* mut2 contains a mutated seed of the second match (4971-4977 nt). The third mutant construct, *JARID2* mut1+mut2, has both seed matches mutated (4169-4175 nt and 4971-4977 nt). An expression construct expressing an irrelevant miRNA, here miR-K12-7, lacks canonical binding sites in the 3´UTR of *JARID2* and was used as a negative control for normalization. The *JARID2*-reporter vector was co-transfected with the appropriate miRNA expression vector into 293T cells and luciferase activity was measured 24 h post transfection.

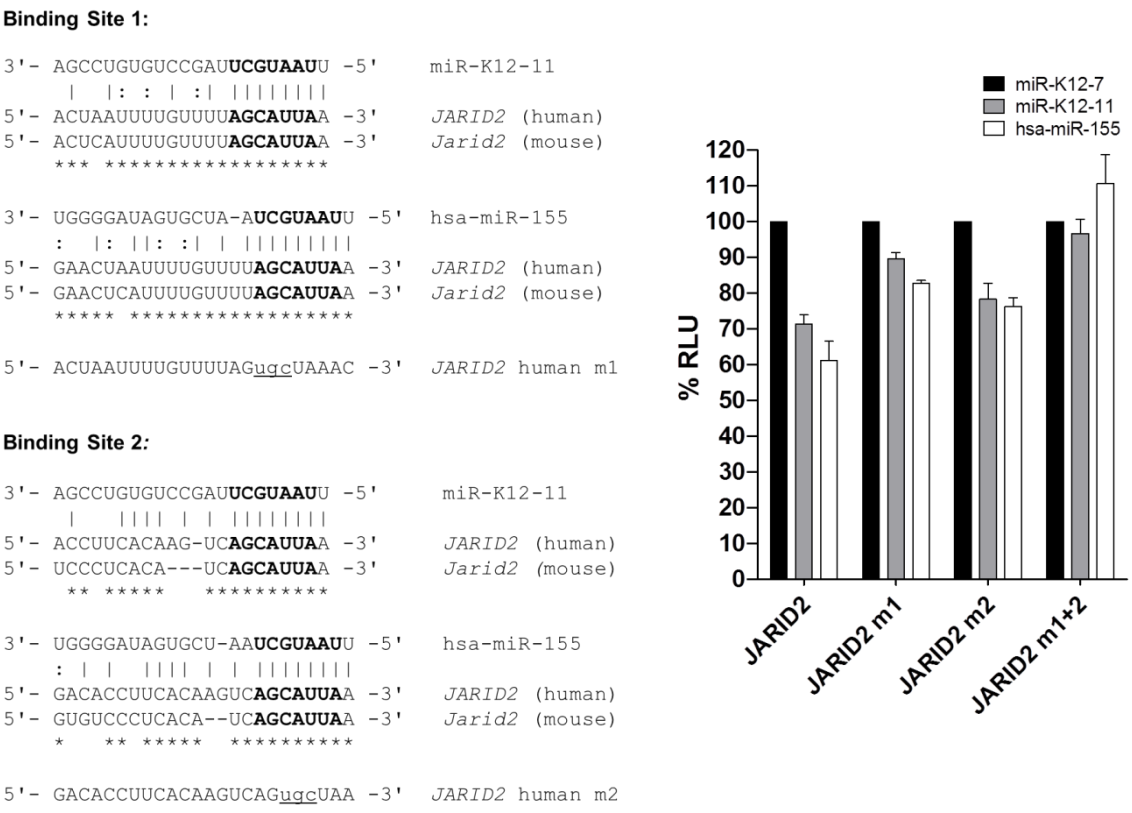

Figure 36: miR-K12-11 and hsa-miR-155 can directly repress *Jarid2* mRNA. Left: *JARID2*/*Jarid2* 3´UTR contains two seed match sites for each miR-K12-11 and hsa-miR-155. The alignment depicts the two mature miRNAs and the two binding sites (BS) (*JARID2*: NM_004973, *Jarid2*: NM_001205043). Seed region and the BS in the 3´UTR is marked with bold letters and stars depict conserved region between mouse and human mRNA. The mutation sequences in the mutated *JARID2* vectors are marked with underlined, small letters. Right: miR-K12-11 and hsa-miR-155 targets *JARID2*. Luciferase reporter assay revealed a reduction in luciferase activity when the appropriate miRNAs were overexpressed. 293T cells were co-transfected with pMIR-*JARID2* or the mutated pMIR-*JARID2* vectors together with one of the miRNA expression vector. The co-expression with the mutated *JARID2*-vectors abolished the reduced luciferase activity.

We observed a reduction to 73% and 60% activity when miR-K12-11 and hsa-miR-155 were ectopically expressed, respectively. Note, the co-transfection with miR-K12-7 was used as negative control and the measured luciferase activity was set to 100%.
Luciferase activity reduction was found to be reverted using the single mutation vectors (*Jarid2* mut1; *Jarid2* mut2). The miRNA mediated repression was completely abolished when both binding sites were mutated (*Jarid2* mut1+2). These results indicate that *Jarid2* expression is seed match dependent.

To investigate if these findings are biological relevant, the JARID2 protein level was explored when overexpressing the respective miRNAs. Because miRNA-mRNA interaction can destabilize and degrade its target mRNA, a repressed protein translation should be measurable. Thus, we continued to analyze the effect of the miRNA expression

on the protein level using western blot analysis (figure 37). Because there are no cell lines with an endogenous high level of JARID2 expression, we made use of an IMAGE Clone that expresses a shorter *JARID2* transcript variant containing the first binding site (pCMV-Sport-Jarid2, ATCC number 9121501, nt 1-4968 (NM_004973)). For this experiment three different negative controls were used: an empty miRNA-expression vector encoding only for GFP, the miR-K12-7 and EBV encoded miR-BART5, both without a canonical binding site in the 3´UTR of *JARID2*. JARID2 protein levels were determined 48 h post transfection (figure 37).

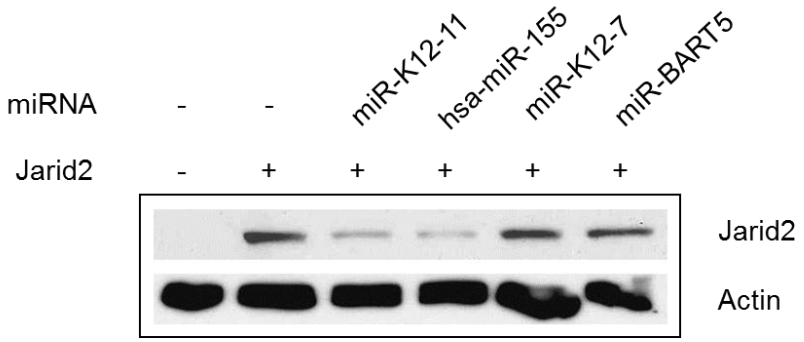

Figure 37: Reduced level of JARID2 protein. JARID2 protein level was reduced when hsa-miR-155 or miR-K12-11 is overexpressed. 293T cells were co-transfected with JARID2 expression vector (ATCC number 9121501, nt 1-4968 (NM_004973)) and miR-K12-11 or hsa-miR-155 expression vector. Western blot depicts the reduced protein level when the appropriate miRNAs were overexpressed. The protein level was not affected when the cells were co-transfected with the control vectors, designated as miR-K12-7, EBV miR-BART5 or mock.

The JARID2 protein level in hsa-miR-155 and miR-K12-11 cells was reduced compared to control cells (co-transfection with miR-K12-7, EBV miR-BART-5, or mock), indicating that both miRNAs have the potential to negatively regulate JARID2 protein expression.

To address the question, if miRNAs have also the ability to repress the *Jarid2* transcript level *in vivo*, RNA from GFP^+-flow sorted BM cells was extracted followed by Real-Time RT PCR (figure 38).

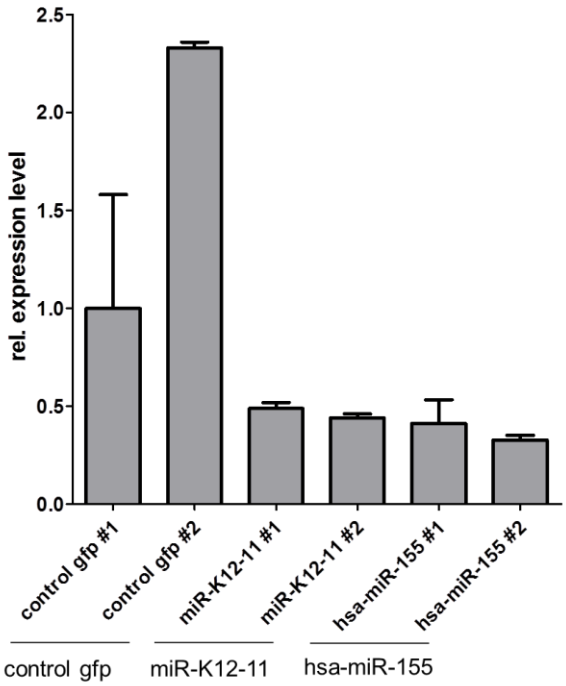

Figure 38: Repressed *Jarid2* mRNA level in the GFP$^+$ BM cells of miRNA-expressing mice. Real-Time RT PCR of total RNA derived from GFP$^+$ BM cells from two mice of each mouse cohort. *Jarid2* mRNA expression level were normalized to endogenous level of *Actin*, *Gapdh* and *Rplp*. *Jarid2* mRNA was downregulated in the GFP$^+$ BM cells of miRNA-expressing mice.

The obtained results show a reduced *Jarid2* transcript level in all miRNA expressing cells compared to the control mice. These results indicate that hsa-miR-155 as well as miR-K12-11 might target *JARID2 in vivo*.

Collectively, the results of the luciferase reporter assay, the western blot assay as well as the Real-Time RT PCR indicate that both miRNAs, hsa-miR-155 and miR-K12-11, can directly target *JARID2 in vitro* and *in vivo*.

4 DISCUSSION

KSHV is a human gamma-herpesvirus linked to the development of at least three malignancies, namely KS, PEL and MCD. Pathogenesis related to KSHV is often observed in the context of host immune-suppression. One of the most relevant questions in KSHV biology addresses the identification of genes and mechanisms that establish and maintain latency and promote tumorigenesis. Since nearly all KSHV-associated tumor cells are latently infected, the latent genes are thought to have a critical impact on tumorigenesis. With regard to this, the KSHV miR-K12-11 represents an interesting case because it is expressed during latency and has been suggested to be a functional ortholog of hsa-miR-155 – a cellular miRNA that functions in hematopoiesis and immune response as well as in tumorigenesis (Eis et al., 2005; Costinean et al., 2006; Rodriguez et al., 2007; Thai et al., 2007; O'Connell et al., 2008).

State of knowledge at the beginning of this study

Numerous studies investigating KSHV were performed to identify genes and unravel mechanisms involved in latency in B-cells and lymphomagenesis. This is a challenging task because established B-cell lines are poorly permissive to infection by KSHV, which is a paradox since KSHV is lymphotropic *in vivo*. So far, there is no suitable system available that contributes to a comprehensive understanding of latency and virus-induced tumorigenesis in the context of KSHV infection in B-cells. Consequently, key questions of how KSHV establishes and maintains latency in B-cells and which virus-host interactions provoke tumorigenesis are still not answered (Wen & Damania, 2010; Boshoff, 2011).

In contrast to KSHV, EBV *in vitro* model systems are available to explore mechanisms of latency, as well as processes of virus-induced host cell transformation. Extensive studies have demonstrated that EBV has evolved a complex system using different latent transcriptional programs to gain access to the memory B-cell reservoir by hijacking normal B-cell biology (Laichalk et al., 2002; Souza et al., 2005; Thorley-Lawson, 2005; Roughan & Thorley-Lawson, 2009). Since memory B-cells are long-lived cells, EBV and KSHV are thought to establish long-term reservoirs of infection in this specific cell type.

Because EBV is the closest relative of KSHV in humans, it is thought that KSHV´s host interactions are overall similar to those of EBV, even though latent proteins of EBV and KSHV are not conserved and gene expression patterns are different during latent infection. Nevertheless, it is assumed that mechanisms of how the two viruses gain access into the memory B-cell pool are conserved (Thorley-Lawson, 2005; Boshoff, 2011). In analogy to results obtained for EBV, it is conceivable that viral gene products supplant cellular signals required to allow latently infected cells to transit through the GCs,

resulting in differentiation into plasma or memory B-cells. EBV and KSHV infected B-cells probably require the activation of multiple pathways, involving mechanisms such as strong BCR signaling and induction of anti-apoptotic and pro-survival pathways to avoid apoptosis of negative selected B-cells resulting in transition through GCs.

New perspectives regarding virus-host interactions arose after the discovery of virus-encoded miRNAs. An attractive hypothesis is that one function of EBV and KSHV miRNAs is to repress genes that play roles in B-cell response, which in turn may serve to reprogram infected naïve B-cells toward memory B-cells. It has been assumed that the miRNAs hsa-miR-155 and miR-K12-11 have an important impact in these processes. Whereas EBV uses pathways to strongly enhance the human miR-155 expression during infection, KSHV expresses its encoded miR-K12-11. Since this viral miRNA might be a functional analog of hsa-miR-155, it likely replaces functions of hsa-miR-155. This putative mimicry attracted considerable interest, since miR-155 has an influence in hematopoiesis, pre-B-cell development, GC formation and immune response (Costinean et al., 2006; Rodriguez et al., 2007; Thai et al., 2007; O'Connell et al., 2008). All these cellular processes are mechanisms that may contribute to KSHV persistence in B-cells. Furthermore, hsa-miR-155 is overexpressed in a number of human tumors, which suggests that miR-K12-11 may also contribute to cellular transformation.

At the time when this work started, it was not known if and to what extent the shared seed sequence would result in the mimicking of *in vivo* functions and if miR-K12-11 is capable of influencing hematopoiesis, B-cell development and differentiation as well as lymphomagenesis. To address this issue, a side-by-side study was designed using a BM transplantation mouse model to force expression of hsa-miR-155 or miR-K12-11 in HPCs.

4.1 STUDY DESIGN

To explore functions of miR-K12-11 as well as its mimicry of hsa-miR-155, a “top down” approach was employed, while a “bottom up” approach would represents another strategy to identify miRNA functions (see review (Grundhoff & Sullivan, 2011)). Both have their strengths and drawbacks.

The “bottom up” approach is comprised of methods such as computational prediction to identify mRNA binding sites that are combined with experiments to confirm these targets, such as cDNA expression profiling or RISC/Ago studies. The latter method is based on the miRNA-mRNA complex that is incorporated into RISC. These complexes are purified and mRNAs residing in the enriched complexes are identified, for example by sequencing. Experiments using cDNA expression profiles are often combined with miRNA-overexpression experiments to detect repressed mRNAs. Disadvantages of these

approaches are, for example, the generation of large datasets or the detection of false positive targets that might repress mRNAs with no selective advantage to the virus. The overexpression of miRNAs might generate a bias due to displacement of endogenous miRNAs whereby low affinity target sites may appear to be functionally important. Additionally, only limited information with regard to the biological consequences of the identified targets are provided. The “bottom up” approach, including high-throughput screenings, is beneficial when there is no existing hypothesis concerning functions and targets of the miRNA, providing first evidence for putative cellular processes regulated by miRNAs.

The here-applied “top-down” approach can be used when assumptions about targets and functions exist. This approach can be extremely powerful when phenotypes or putative functions are first identified, confirmed in the context of infection, and then employed to identify biological relevant targets. Nevertheless the “top down” approach has drawbacks as well, for instance the complex and time-consuming experimental set up (Grundhoff & Sullivan, 2011).

We hypothesized that miR-K12-11/hsa-miR-155 expression in HPCs would alter processes involved in hematopoiesis and the immune response. Additionally, we reasoned that constitutive expression might promote tumorigenesis. These assumptions were based on the known biology of KSHV infection and KSHV-associated disease, as well as on previous mouse studies that had investigated functions of miR-155 (Costinean et al., 2006; Rodriguez et al., 2007; Thai et al., 2007; O'Connell et al., 2008).

To verify these assumptions, we designed a mouse model in which hematopoietic progenitor cells were transduced with retroviral vectors encoding miR-K12-11 or hsa-miR-155, and subsequently transplanted into lethally irradiated C57BL/6 mice. Of note, these transplanted progenitors have the potential to reconstitute the BM compartment of irradiated recipients, which is a prerequisite to explore the effect of miRNA expression with regard to hematopoiesis, lineage commitment and B-cell response. Changes in lineage and cell frequencies resulting from miRNA expression were monitored via FACS technology. Thereby, we sought to determine the consequence of miRNA expression on several aspects of hematopoiesis, *e.g.* like enhanced proliferation, survival or favored lineage commitment. Furthermore, morphological changes in spleen tissues were analyzed. Another aspect of this study was the investigation of putative miRNA targets to understand how the miRNAs might influence cellular processes that underlie the observed phenotypes, and if miR-K12-11 and hsa-miR-155 share such targets.

The study was performed in C57BL/6 mice, hence in a murine cellular background. One might suspect that the study of the KSHV miR-K12-11 in a murine cellular background is sub-optimal, due to the fact that miR-K12-11 is expressed by a herpesvirus that infects humans. Therefore, one may argue that it makes more sense to explore its functions regarding virus-host interactions in a humanized mouse model. However, since miR-K12-11 is a putative functional ortholog of hsa-miR-155 (Gottwein et al., 2007; Skalsky et al., 2007), a miRNA that is highly conserved between mammals, we reasoned that miR-K12-11 should likewise be functional when tested in a murine system. The mature murine miR-155 differs only in one nucleotide exchange at position 12 with the hsa-miR-155, which is highlighted in figure 9 (see section 1.9). This nucleotide is not involved in base-pairings at the canonical target sites, and therefore is probably not crucial for binding and downregulation of target mRNAs. The above strongly suggests that relevant targets are conserved between human and mouse, hence hsa-miR-155 should be fully functional in a murine cellular background. This is underscored by data by Reith and colleagues, in which miR-155-mediated repression of *FOS* mRNA was demonstrated in mouse, human and rat (Dunand-Sauthier et al., 2011). Therefore, if a viral miRNA indeed represents a functional homologue of a conserved host miRNA, it should likewise be able to orchestrate the same processes in different species, resulting in the same phenotypes. We therefore assume that our mouse model reveals phenotypic alterations caused by targeting mRNAs that are relevant during KSHV infection.

Although data from mouse studies provide important indications for mechanisms in the human system, the results require cautious interpretation. Much of knowledge in HSC differentiation and commitment into immune cell lineages comes from mouse studies, but there are also species-specific variations in expression patterns of antigens and transcription factors during these processes (Payne & Crooks, 2007). This caveat has to be considered when results are transferred from mouse to man.

4.2 PREPARATORY STUDY

For this study, we aimed to achieve miR-K12-11 expression levels in transduced cells that are similar to those in a KSHV-infected cell. It seems reasonable to assume that miR-K12-11 expression levels during KSHV infection are similar to hsa-miR-155 expression levels upon B-cell activation and, furthermore, that hsa-miR-155 levels upon B-cell activation are similar to those seen in EBV infected B-cells. EBV-infected cells with a type III latent expression profile utilize latent protein LMP-1 to upregulate hsa-miR-155 (Gatto et al., 2008; Lawrie et al., 2008; Yin et al., 2008a). Our goal was therefore to achieve miR-155 expression levels that resemble the situation in EBV-infected cells or in activated B-cells.

To investigate miR-K12-11/hsa-miR-155 expression levels in transductants, NIH3T3 cells were transduced with generated retroviral particles and analyzed with regard to their respective miRNA expression level by Real-Time stemloop RT PCR. The measured miRNA expression levels in transductants were compared to the miRNA expression level of representative tumor cell lines of B-cell origin, here PEL (BCBL-1) and the EBV-positive Burkitt-lymphoma cell line (RAJI), and turned out to be similar. These findings suggest that miRNA expression levels in transductants are comparable to the situation during KSHV or EBV infection or upon B-cell activation.

Because not sufficient amounts of RNA from GFP^+ sorted BM or splenocytes could be extracted, the miRNA expression level *in vivo* could not be estimated. Thus, the measured miRNA expression levels in NIH3T3 cells should be interpreted with caution, as it is not clear, if the expression levels *in vitro* and *in vivo* are comparable. However, the findings provide evidence that the miRNAs are neither overexpressed nor insufficiently expressed. These results provided a strong basis for studying miRNA functions in a mouse model, as it appears to resemble expression levels of the respective miRNA in KSHV- or EBV-infected cells, or even in activated B-cells.

4.3 SUCCESFUL HEMATOPOIETIC RECONSTITUTION

After validation of adequate miRNA expression levels in transduced NIH3T3 cells, the retroviral stocks were used to transduce HPCs that were subsequently grafted into mouse recipients. Three different mouse cohorts were generated that expressed GFP plus miR-K12-11 or hsa-miR-155, or GFP alone (negative control).

After 12 - 16 weeks post-transplantation, the first steps comprised the detection of GFP and miRNA expression in hematopoietic (or myeloid and lymphoid) cells of donor mice, verifying both the success of hematopoietic reconstitution and an active vector promoter in the mouse cells.

First, we succeeded in detecting GFP expression via FACS analysis in two lymphoid organs, namely spleen and BM. The next step included the evaluation of miRNA expression in splenocytes. For this purpose, RNA from paraffin embedded spleens was extracted followed by Real-Time stemloop RT-PCR. We succeeded in detecting the respective miRNA in each sample, but observed a high variance in their expression levels. This variation might originate from the employed samples, because the paraffin embedded splenocytes included GFP^+ as well as GFP^- cells. Thus, to compare the miRNA expression of each positive cell, the measured relative copy number was divided by the GFP percentage. Nevertheless, this might not exactly represent the expression level in each positive cell, thereby generating a bias. Moreover, diverse proportions of cell

populations in these samples can further increase this bias, because it is conceivable that specific vector-promoter activities in distinct cell types lead to different miRNA expression levels.

Taken together, although there is a caveat when interpreting the miRNA expression levels, the detected co-expression of GFP and miRNA in harvested splenocytes of miRNA expressing mice validated successful engraftment as well as an active vector-promoter in mouse recipients.

4.4 PHENOTYPIC ALTERATIONS UPON MIRNA EXPRESSION

After validation of GFP and miRNA expression in transplanted mice, the recipients were monitored for phenotypic alterations with regard to CBC, morphological changes in spleen (weight and histology), and immuno-phenotypic profiles in spleen and BM (FACS analysis). Whereas examination concerning CBC and splenic weight did not show any change compared to the control mice, the splenic structure and immuno-phenotypic profile revealed alterations.

Increased pre-B-cell fractions in the BM compartment

The cell lineage study was first performed for BM cells to evaluate the influence of miRNA expression on early stages of hematopoiesis. miRNA expressing mice showed a slight decrease of the myeloid lineage, whereas the B-cell lineage was moderately increased. This moderate increase toward B-cell lineage cells assumed that more pronounced phenotypes might exist among the sub-populations of B-cells in the BM. Indeed, the number of small pre-B-cells was significantly increased in both miRNA expressing mouse cohorts. FACS analysis allowed the distinction between early and late B-cell stages when using CD19, CD43, B220 and IgM antibodies (see figure 39) and revealed a shift from pro-B-cells/large pre-B-cells ($CD19^+/CD43^+/B220^+/IgM^-$) to small pre-B-cells ($CD19^+/CD43^-/B220^+/IgM^-$) in both miRNA expressing mouse cohorts (see also appendix suppl. figure 3). The population of immature B-cells ($CD19^+/CD43^-/B220^+/IgM^+$) did not show any significant changes. These data provide strong evidence that expression of miR-K12-11 and hsa-miR-155 might orchestrate pathways that have an impact on lymphopoiesis, particularly by supporting the pre-B-cell population.

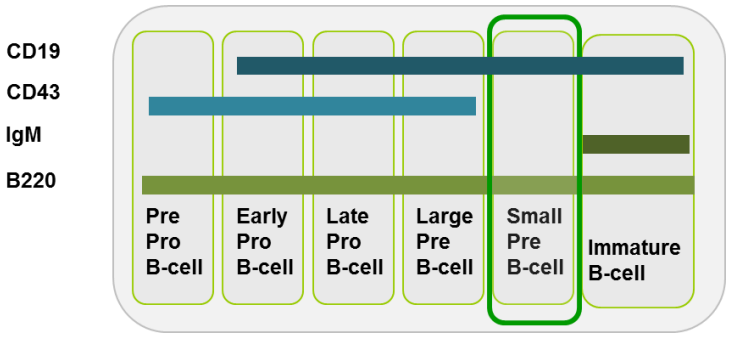

Figure 39: Differential expression of surface markers during B-cell development. Specific B-cell stages in the BM are discriminable due to distinct protein expression profiles in each cell type. $CD19^{+}CD43^{-}B220^{+}IgM^{-}$ expression denotes small pre-B-cells. The green box marks the fraction of small pre-B-cells, which are increased in miRNA expressing mice. (Figure: (Hardy et al., 2007); modified).

The findings of an increase of pre-B-cells upon miR-K12-11/hsa-miR-155 expression is in line with data from transgenic miR-155 mice generated by the group of Carlo Croce (Costinean et al., 2006). Splenocytes of transgenic miR-155 mice expressed high levels of *VpreB1* mRNA compared to control cells, which is consistent with the observed pre-B-cell accumulation, since VpreB1 is selectively expressed in the pre-B-cell state. The transgenic miRNA mice generated by Costinean et al. express hsa-miR-155 under the control of a V_H promoter-Ig heavy chain Eμ enhancer, which becomes active at early pro-B-cell stages (Costinean et al., 2006).

The group of David Baltimore employed an experimental set up that, like our study, used stable transduction (O'Connell et al., 2008). However, there were also major differences compared to our study design, including the type of vector that was used (gamma-retroviral vector versus foamy virus), time-point of analysis and usage of mouse strains (C57BL/6 versus FVB/N and C57BL/6). This may explain, at least in part, why the author's observations were markedly different from ours and those of Costinean et al: O'Connell and colleagues observed a myeloid disorder with no increase in B-cell fractions. The authors attributed the differences in their findings of a myeloid disorder in contrast to the pre-B-cell expansion in Croce´s transgenic miR-155 mouse model to the use of different promoters: *i.e.* sustained expression in all HPCs (as in our system) versus restricted miRNA expression in B-cell committed cells (Costinean et al., 2006; O'Connell et al., 2008). Since our mouse model showed a similar phenotype compared to Croce´s transgenic miR-155 mice, but no myeloproliferative disorder like in Baltimore's report, it is unlikely that the lineage-restricted promoter is the reason for the different phenotypes. It is more likely that several factors such as the time point of analysis, expression level of miRNAs or the specific mouse strain background lead to the distinct, yet different phenotypes.

Expansion of B-cells and enhanced GC formation in spleen

The lineage study was extended to splenocytes, in which we observed a significant increase of B-cell numbers compared to control mice.

The observed expanded B-cell fractions in spleen is in line with a study by Boss et al. that was published while this work was in progress. They used a humanized Nod/Scid mouse model, whereas our system studied the miRNAs in a murine cellular background. Remarkably, even though the two studies used entirely different mouse strain backgrounds, the major findings – *i.e.* expansion of B-cells in the spleen – are the same. Whereas both studies also did not find any significant imbalance in myeloid/erythroid and B-cells in the BM, we additionally detected a significant overrepresentation of pre-B-cells (see section above), a B-cell population which was not investigated by Boss et al.. Furthermore, due to a fundamental difference between the two experimental systems, we were able to generate additional data regarding GC reactions: Whereas our miRNA mouse cohorts showed an increased GC formation, no such effect could be observed in the Nod/Scid mice used by Boss et al.. This is because Nod/Scid mice do not efficiently reconstitute human T-cells after BM transplantation; hence they are not capable of inducing T-cell dependent GC formation.

In the context of GC formation, our findings were in line with data from Thai and colleagues, who published in *Science* that miR-155 expression influences GC reactions by controlling cytokine reaction (Thai et al., 2007). They generated miR-155 'knock out' and 'knock in' mice and observed that miR-155 has the potential to regulate GC responses via modulation of cytokine expression, in particular TNFα and LTα. Their 'knock out' mice lacked an efficient GC response after stimulation via lipopolysaccharide (LPS). It is likely that similar mechanisms occur in our mouse recipients, which may be responsible for the observations we made in the hsa-miR-155 and miR-K12-11 mouse cohorts. However, we did not specifically test expression of these cytokines due to a too low amount of sorted GFP^+ B-cells.

One question arose when observing the GC alterations in spleen despite the low number of GFP positive cells in this organ (1 % - 30 %). How is it possible that this low percentage of GFP positive, hence miRNA expressing cells, can induce gross changes in GC formation in the spleen? One possible explanation might be that hsa-miR-155 or miR-K12-11 molecules are secreted through so-called 'exosomes'. These are vesicles that protect small RNA molecules from degradation by RNAses and transport molecules to neighboring cells, which was shown for EBV-encoded miRNAs (Pegtel et al., 2010). Thus, miRNAs may act in a paracrine-like fashion. Another possible scenario might involve paracrine signaling via cytokine expression (such as TNFα and LTα) to induce GC reaction, as it has been shown in miR-155 'knock-in' and 'knock-out' mice (Thai et al.,

2007) (see section above). It is likely that one or both of these scenarios occur in our mouse model to trigger the formation of GC.

Taken together, the results provide evidence that both miRNAs play a critical role in B-lymphopoiesis and B-cell differentiation as well as GC reaction, and that the viral miRNA phenocopies hsa-miR-155 when expressed in HPCs *in vivo*. The observed altered phenotype is schematically depicted in figure 40.

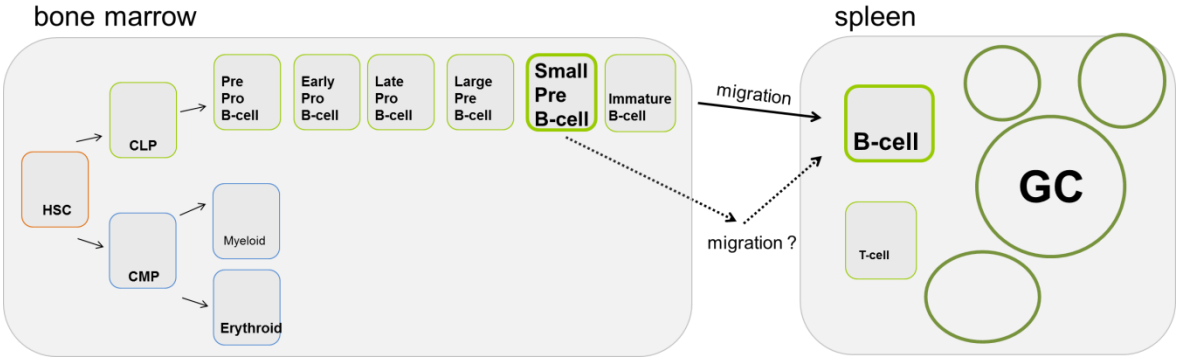

Figure 40: Schematic drawing of the altered phenotype in miRNA expressing mice. The figure depicts a simplified model of B-cell biology and highlights the observed phenotype in miRNA expressing mice. In the BM the small pre-B-cell fraction was augmented whereas the myeloid population was decreased. The B-cells were increased in the splenic compartment. One explanation for the detected increased B-cell population in the spleen might be a triggered migration of BM B-cells to the splenic compartment. It is possible that miRNAs support migration of pre-B-cells; but this has not been proven so far. The formation of GCs was increased in miRNA expressing mice. The population of T-cells was underrepresented.

It is noteworthy that transient expression of miR-K12-11 during KSHV infection is conceivable, since this was observed for miR-155 in normal lymphopoiesis; miR-155 is expressed at moderate level in HSCs, at high levels in GC B-cells and at much lower levels in mature B-cells (Gibcus et al., 2009; O'Connell et al., 2010). Expression of miR-155 is rapidly induced in B-cells upon stimulation (Vigorito et al., 2007; Fernando et al., 2012). Likewise, EBV-infected cells transiently upregulate hsa-miR-155 expression at the time when the latent transcriptional program III is induced and EBV expresses its latent protein LMP-1, but later shut off LMP-1 transcription when the virus adopts a type I or type 0 expression profile in memory B cells. My own previous observations in *de novo* infected SLK (uninfected endothelial cells derived from a KS lesion) cells support the notion that miR-K12-11 expression is likewise transient, with an expression peak at day five post infection and rapidly declining miRNA expression levels thereafter (Dahlke et al., unpublished data from master thesis, see appendix, suppl. figure 1). This may resemble the expression pattern of miR-155 during B-cell response and represents a plausible

strategy for KSHV to gain access to the memory B-cell reservoir, where downregulation of miR-K12-11 may serve to minimize the risk of tumor development.

4.4.1 **Seed sharing is sufficient to mimic functions *in vivo***

Next, we sought to answer the question if miR-K12-11 mimics functions of hsa-miR-155 *in vivo*. Since our study design allows the comparison of mice that express either miR-K12-11 or hsa-miR-155, the study allows important insights into the viral mimicry *in vivo*. If seed sharing is indeed sufficient, the same phenotypic alterations should ensue.

Both miRNA mouse cohorts developed similar alterations when expressing one of the miRNAs, underscoring the hypothesis that KSHV utilizes hsa-miR-155 mimicry. These results are in line with recently published data from the study by Boss and colleagues in which the authors observed a very similar phenotype in the humanized mouse model for miR-K12-11 as well as hsa-miR-155 (Boss et al., 2011).

Nevertheless, at least in our study, although the phenotypes between miR-K12-11 and hsa-miR-155 were of generally the same type, they were pronounced differently. When comparing the two miRNA expressing mouse cohorts, it was apparent that the phenotype in BM was more distinct in miR-K12-11 mice, whereas the hsa-miR-155 mice showed a more pronounced phenotype in spleen. However, the reason for this observation is not known. One explanation might be a favored transport of hsa-miR-155 by exosomes compared to miR-K12-11 transport, thereby affecting more cells. But so far, there is no indication for exosome transport of miR-K12-11 and/or hsa-miR-155.

Other reasons might be either quantitative differences (miRNA concentration) or qualitative miRNA differences (*i.e.* non-canonical targeting of host transcripts by the non-conserved nucleotides outside of the seed region) or a combination of both (figure 41). Because we were not able to compare the absolute miRNA expression level in GFP^+ flow sorted BM cells or splenocytes (see section 4.2, due to the low amount of extracted RNA), we cannot exclude the possibility that a lower copy number of miR-K12-11 might be the reason for the less pronounced phenotype in the spleen. It is indeed conceivable that a distinct miRNA concentration may results in different phenotypes. Qualitative differences may also cause the different pronounced phenotypes. Whereas seed sharing results in an overlapping set of targets of both miRNAs, differences in the non-seed sequence might have an influence on targeting a different set of mRNAs (Didiano & Hobert, 2006), for instance by targeting mRNAs via the divergent 3´-terminus of miR-K12-11 (figure 40).

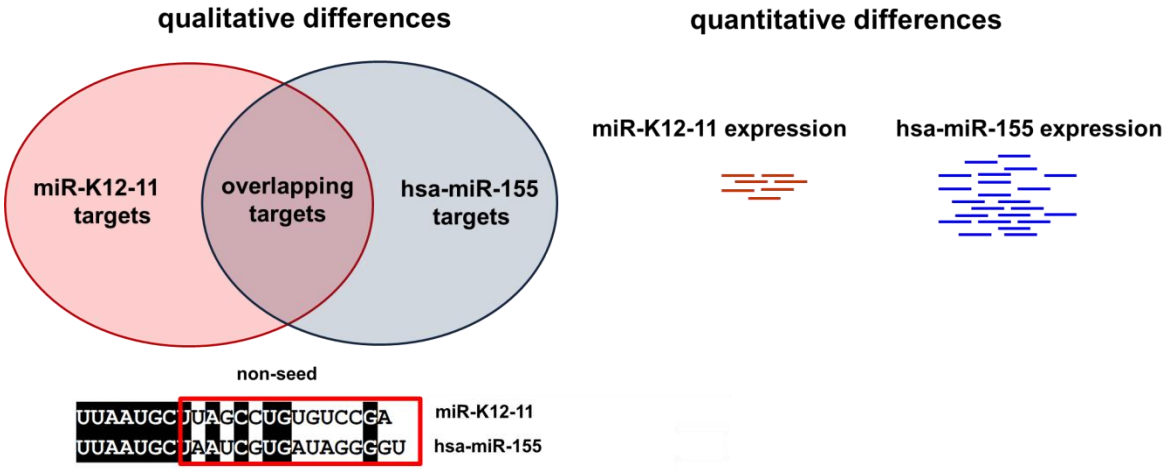

Figure 40: Qualitative or quantitative differences might lead to differently pronounced phenotypes. Phenotypes of miRNA expressing mouse cohorts were different pronounced. Potential reasons for this observation include: Left: One possibility might be qualitative differences. Even though seed sharing is expected to result in an overlapping set of targets, non-canonical targeting by non-seed sequence might lead to an additional set of targets that is distinct for each miRNA. Right: Quantitative differences might lead to different pronounced phenotypes. A different concentration of miRNAs per cell might influence the phenotypic magnitude, where low-level expression is expected to result in a less pronounced phenotype.

4.4.2 The impact of miR-K12-11 in cellular processes

The altered phenotypes in BM and spleen raised the question of underlying cellular processes. Mechanisms that facilitate robust expression of B-cell receptors, CD40 or cytokine receptors are likely contributing factors, since they promote B-cell response, B-cell differentiation as well as B-cell survival. Modulation of proliferation, pro-survival, anti-apoptosis, migration and lineage commitment pathways may also be responsible for the observed expanded B-cell fraction in BM and splenic compartment and the enhanced GC formation in both miRNA expressing mouse cohorts.

The finding that both miRNA expressing mouse cohorts displayed a decrease in the myeloid lineage, but a concomitant increase in the B-cell lineage in the BM indicates that miR-K12-11/miR-155 expression has an influence on lineage commitment. So far, several reports demonstrated that miRNAs can interfere with or regulate lineage commitment (Chen et al., 2004; Kluiver et al., 2006; Havelange & Garzon, 2010). One example is represented by miR-181, which has been demonstrated to promote the B-lineage when ectopically expressed (Chen et al., 2004). Although lineage changes in BM cells in our mouse cohorts are not statistically significant, the findings underline the notion that miR-K12-11 and hsa-miR-155 may have this potential as well. Since changes were moderate in their extent, this is probably a minor effect of miR-K12-11/hsa-miR-155 expression.

Because KSHV does not infect HPCs, mediating lineage commitment of BM cells is probably not biological relevant for KSHV.

The induction of higher proliferation rates is an obvious mechanism that potentially leads to the increased number of B-cells in both miRNA expressing mouse cohorts. A recent report by Liu et al. argues for increased proliferation since they observed an increased cell proliferation when miR-K12-11 is ectopically expressed. The authors explained this observation with attenuated TGFβ signaling via miR-K12-11 mediated SMAD5 repression (Liu et al., 2012). miRNA mediated mechanisms to induce proliferation rates is in line with data from Brian Cullen´s group, in which the authors showed that growth of LCL cells was reduced when miR-155 activity was repressed by specific miR-155 sponges (Linnstaedt et al., 2010).

The increased number of B-cells in miRNA expressing mice may also originate from enhanced pro-survival signaling imparted by miR-K12-11 expression. Beemon and colleagues demonstrated that a miR-155 mediated repression of *JARID2* mRNA level is linked to enhanced survival in B-cells (Bolisetty et al., 2009). This is an important aspect regarding our mouse model, because we observed a repressed *Jarid2* level in GFP^+ sorted BM cells (see also section 1.4.3). A selective pro-survival effect within the B-cell fraction is conceivable and represents an interesting mechanism that would benefit KSHV to achieve long-term persistence in B-cells.

Formation and persistence of GCs require enhanced anti-apoptosis to increase the survival rate of GC B-cells. This is underscored by the impact of the anti-apoptotic molecule Mcl1, which has been shown to be crucial for GC formation and persistence (Vikstrom et al., 2010). The observed increase in GC reaction and in B-cell numbers in the spleen in both miRNA mouse cohorts let assume that both miRNAs may influence anti-apoptotic signaling. In line with this, Joan Burnside and Robin Morgan demonstrated an anti-apoptotic effect by both miR-155 and the MDV-encoded miR-M4 (which, like miR-K12-11, shares its seed with hsa-miR-155) (Burnside & Morgan, 2011).

An influence on B-cell homing may represent another interesting feature for KSHV, since migration of B-cells to secondary lymphoid organs, such as spleen, is a pre-requisite for GC formation and differentiation into memory B-cells. The observed increased pre-B-cell fraction in BM and expanded B-cell population in spleen raises the question of whether the number of splenic B-cells is increased due to enhanced migration of the BM pre-B-cells to spleen. Since pre-B-cells do not migrate to the spleen under normal circumstances, they probably require strong signals for migration. However, as there is no

published data about miRNAs that favor migration so far, the above remains a speculation. Another scenario might be that miR-K12-11/hsa-miR-155 expressing cells impart lineage commitment toward immature B-cells, which then migrate to periphery, particularly to spleen. If such cells do not recirculate, they may accumulate in the spleen.

In light of the above discussion, there is much evidence to support the idea that miRNAs can function in several different cellular processes. As known for cellular miRNAs, it is likely that miR-K12-11 targets a large number of mRNAs, and consequently rather regulates numerous pathways instead of a single one**.** Indeed this possibility is underlined when combining our findings with results from other miR-155 mouse studies, because each mouse model revealed a distinct phenotype (Costinean et al., 2006; Rodriguez et al., 2007; Thai et al., 2007; O'Connell et al., 2008; Boss et al., 2011). These differences are explainable by distinct experimental set ups (each system employed different cellular backgrounds, promoters, miRNA expression levels and time-points of analyses). We therefore speculate that hsa-miR-155 and miR-K12-11 trigger unique phenotypes when expressed at different cell stages, in distinct cell types or even with different miRNA concentrations**.** It is very likely that hsa-miR-155 and miR-K12-11 are multifunctional and play a role in several pathways, at different stages during hematopoiesis and B-cell response. miR-K12-11 and hsa-miR-155 may act in diverse pathways in a fine-tuning fashion and likely orchestrate several processes, including proliferation, pro-survival, anti-apoptosis, migration or lineage commitment.

4.4.3 **Molecular mechanisms influenced by miR-K12-11**

The identification of miRNA targets is important to specify molecular mechanisms that underlie the observed increased B-cell fractions and the enhanced GC formation in the miRNA expressing mice. The genes encoding *SPI1*, *FOS*, *c-MYB* and *JARID2* attracted our interest because they (a) harbor binding sites for miR-155/miR-K12-11, (b) were already identified as targets of miR-155, and (c) play a role in B-cell development and B-cell response (Gottwein et al., 2007; Rodriguez et al., 2007; Skalsky et al., 2007; O'Connell et al., 2008; Bolisetty et al., 2009; Imig et al., 2011). These genes are promising miR-K12-11 targets that may have a biological relevance in the context of KSHV and its persistence in B-cells as well as in lymphomagenesis.

Downregulation of putative targets *in vivo*

PU.1 is a transcription factor, which plays an important role in myeloid and lymphoid cell fate (Singh et al., 1999; John et al., 2004; Nutt et al., 2005). The gene *SPI1/Sfpi1*, encoding PU.1, is conserved between mouse and humans and harbors one binding site

for miR-K12-11 and hsa-miR-155. Our data are not consistent with studies by Vigorito et al., O´Connell et al. and Muylkens et al., in which *SPI1/Sfpi1* was proposed to be a direct target of miR-155 (Vigorito et al., 2007; O'Connell et al., 2008; Muylkens et al., 2010). We detected a similar low *Sfpi1* expression level in one of our control mice compared to miRNA expressing mice.

The laboratories of Martin Turner, David Baltimore and Carlo Croce confirmed the direct binding of miR-155 to the 3´UTR of *Sfpi1* via luciferase reporter assays; luciferase activity was reduced when miR-155 was expressed and repression was alleviated when the predicted binding sites was mutated. Furthermore, Vigorito and colleagues analyzed the PU.1 protein level of B-cells from miR-155 deficient mice and compared this level to control B-cells. Whereas control cells expressed PU.1 at a detectable level, PU.1 was not detectable in B-cells from miR-155 deficient mice. These data provide strong evidence that miR-155 directly targets *Sfpi1* and that this binding results in a repressed protein level; consequently miR-155 mediated PU.1 repression is probably biological relevant.

Although our data was not consistent with these studies, it is likely that miR-K12-11 directly target *SPI1* to repress PU.1 protein levels. Our result might be caused by an outlier or a sub-optimal control sample that might exhibit different proportions of cell type fractions resulting in reduced *Sfpi1* expression level *per se* (for more detail, see section below). PU.1 seems to be an important target gene for KSHV since it has been postulated that repression of this transcription factor is an important factor for GC reaction. Whereas PU.1 is highly expressed in GC B-cells, it is downregulated in post-GC B-cells (Cattoretti et al., 2006). Moreover, Vigorito et al. observed *in vitro* that overexpression of PU.1 leads to a lower number of IgG B-cells (isotype switched B-cells), and they postulated that miR-155 mediated repression of PU.1 results in the opposite phenotype, for instance an enhanced B-cell production. This hypothesis is underscored by an immune-deficient phenotype in the generated miR-155 knockout mice (Rodriguez et al., 2007; Vigorito et al., 2007). Therefore this gene represents an important target gene candidate in the context of KSHV infection in B-cells, since it acts at different cell stages during B-cell development and differentiation and importantly at GC B-cells.

C-MYB is a cellular proto-oncogene with important functions during hematopoiesis and B-cell development as well as in G_1/S cell cycle transition (Gonda & Metcalf, 1984; Bender et al., 1987; Liebermann & Hoffman, 1994; Thomas et al., 2005). Regulation of *c-MYB* mRNA level is of particular importance during B-cell development, since *c-MYB* mRNA levels need to be repressed during the transition from pre-B to immature B-cell stages (Bender et al., 1987; Thomas et al., 2005).

In both miRNA expressing mouse cohorts, a downregulation of *c-Myb* in GFP^+ BM cells compared to the control cells was observed. This is consistent with earlier reports. For example, Gottwein et al. suggested that *c-MYB* is a shared target of miR-K12-11 and hsa-miR-155, since it was downregulated in BJAB cells that were transduced with lentiviral particles expressing miR-K12-11 or hsa-miR-155. However, the authors did not further validate this gene (Gottwein et al., 2007). *C-MYB* was recently shown to be regulated by miR-155 via two binding sites in its 3´UTR (Imig et al., 2011). Luciferase reporter assays using authentic and mutated predicted binding sites in its 3´UTR sequence confirmed a seed dependency.
Noteworthy, a second cellular miRNA besides of miR-155, namely miR-150, also targets *c-MYB* to promote the transition from early B-cells toward later B-cells. However, the precise mechanisms are not fully understood (Xiao et al., 2007; Zhou et al., 2007). The combinatorial binding by more than one miRNA species is a commonly accepted model of how miRNAs regulate cellular processes (Doench & Sharp, 2004). Therefore, it is conceivable that miR-150 and miR-K12-11/miR-155 act synergistically to repress c-MYB protein expression. This might be an important factor for KSHV to modulate pathways during B-cell development and cell cycle transition.

Like *c-Myb*, *Fos (*murine) was downregulated in GFP^+ BM cells of both miRNA expressing mouse cohorts. This data is consistent with earlier results, in which *FOS* (human) was validated as a common target of miR-K12-11 and hsa-miR-155 (Gottwein et al., 2007; Yin et al., 2008b; Gottwein et al., 2011b). *FOS* is a proto-oncogene and functions as one subunit of a group of homo- or hetero-dimeric transcription factors referred to as activating protein 1 (AP-1). It plays a role in diverse processes, including innate immune response, cell cycle progression, proliferation, differentiation, apoptosis, responses to stress and oncogenic transformation (Wagner, 2001; Eferl & Wagner, 2003; Gottwein et al., 2007). Recently, FOS repression by miR-155 was shown to stimulate dendritic cell (DC) activation (Dunand-Sauthier et al., 2011). Since FOS expression is regulated in a large number of pathways, it seems likely that its regulation is biologically relevant for KSHV to ensure its persistence in the host.

It is worth to note that there are two caveats when interpreting the results. Firstly, all analyzed samples consist of GFP^+ BM cells that are divergent in their proportion of different cell types. A bias might be generated when a sample consists predominantly of B-cells whereas another sample has a higher proportion of another cell type, for instance myeloid cells. The gene of interest may be expressed in B-cells but not in myeloid lineage cells, thereby having a lower expression in myeloid cells *per se*. Because of a too low

amount of isolated RNA of GFP^+ sorted B-cells, we cannot exclude the possibility that the miRNA expressing BM cells have a higher content on myeloid cells and therefore having a repressed mRNA level of the analyzed mRNAs *per se* that appears to be a miRNA mediated repression, which possibly is not the case.

Secondly, miRNA-mediated mRNA repression is not an explicit parameter for validating targets, because miRNAs can repress protein expression via mRNA destabilization and 'slicing', or via translational repression (Guo et al., 2010). miRNAs 'slicing' activity occurs whenever the miRNA is perfectly complementary to the mRNA (and which rarely occurs in mammals). miRNAs also deadenylate mRNAs, which results in its subsequent degradation (Eulalio et al., 2008; Fabian et al., 2010; Guo et al., 2010). The translational inhibition can occur for instance by inhibiting the ribosome 80S complex assembly (Fabian et al., 2010). Whereas deadenylation and 'slicing' are processes generally detectable using expression profiling, processes like inhibition of 80S ribosome complex assembly have little or no influence on mRNA levels (Guo et al., 2010). Although it is suggested that miRNAs combine different mechanisms for post-transcriptional repression, downregulated mRNA levels do not always have to correlate with the protein level. Since we analyzed exclusively mRNA levels of these three genes, we cannot judge whether they are either directly or indirectly targeted, if and to what extent both miRNAs act on the protein level, and lastly to what extent this has a consequence in the biological context. Hence, we cannot conclude from the results obtained for *Sfpi1* that this transcript is not targeted by hsa-miR-155 and miR-K12-11. Nevertheless, the detection of the repressed *Fos* and *c-Myb* mRNA levels are in line with the notion that both miRNAs may contribute to the repression of these genes.

Jarid2 – a novel target of miR-K12-11

JARID2 attracted our interest since it has an impact on epigenetic modifications, which in turn plays an important role during hematopoiesis and cell differentiation (Kitajima et al., 1999; Landeira et al., 2010). JARID2 is the founding member of the Jumonji C (JmjC)-domain protein family and a co-factor of PRC2 (Peng et al., 2009). PRC2 contains members of Polycomb-group proteins (PcG), and its occupancy on genes leads to tri-methylation of histone 3 at lysine 27 (H3K27-me3) (Li et al., 2007; Li et al., 2010), a mark for facultative heterochromatin. Consequently, as a co-factor of PRC2, JARID2 is therefore expected to have an important role in the regulation of transcriptional silencing.

In this work, we succeeded not only in confirming *Jarid2* as a target of hsa-miR-155, but also in identifying it as a novel target of miR-K12-11. Seed dependency was validated for both miRNAs. Additionally, for the first time, hsa-miR-155 as well as miR-K12-11 was

demonstrated to efficiently suppress protein expression from an authentic Jarid2-encoding transcript.

Four previous studies are in line with our findings, since they observed a miR-155 mediated decrease of *JARID2/Jarid2* mRNA in human and mouse cells, particularly in splenocytes, B- and leukemic cells (Rodriguez et al., 2007; O'Connell et al., 2008; Bolisetty et al., 2009; Xu et al., 2010b). One of these studies demonstrated repression of heterologous luciferase reporters bearing the *JARID2* 3'-UTR by miR-155 (Bolisetty et al., 2009). Furthermore Gottwein and colleagues detected a repressed *JARID2* mRNA level in the lymphoma cell line PEL via PAR-CLIP (Gottwein et al., 2011a). One of the target sites, which was validated in our study, was recovered, underscoring the notion that miR-K12-11 mediates *JARID2* repression, which further may have an impact in KSHV-induced lymphomas (Gottwein et al., 2011a).

The identification of *JARID2* as a target of miR-K12-11 raises the question which functions this gene has in the context of KSHV and its persistence in B-cells, or in the onset of a lymphoma. Physiological roles of JARID2 imply regulation of embryonic development and cell differentiation (Pasini et al., 2010; Landeira & Fisher, 2011; Zhang et al., 2011). Besides these roles it has been shown that it functions as a tumor suppressor in hematological disorders (Kitajima et al., 1999; O'Connell et al., 2008). Functions of JARID2 have been predominantly shown in ES and HSCs (Landeira et al., 2010; Landeira & Fisher, 2011), and little is known about its role in B-lineage cells. Since other members of PRC2, namely EED (embryonic ectoderm development), EZH2 (Enhancer of zeste homolog 2) and YY1 (Yin Yang 1) function in B-cell commitment, B-cell differentiation and B-cell apoptosis, there is indirect evidence that JARID2 may play a role in B-cell biology as well (Lessard et al., 1999; Liu et al., 2007; Velichutina et al., 2010; McCabe et al., 2012; Pan et al., 2012). Additionally, JARID2 may be one of the (likely multiple) factors that, when repressed, contributes to increased B-cell survival (Bolisetty et al., 2009).

In line with this, there is evidence that JARID2 plays a role in tumor development. Several studies observed dysregulated methylation patterns and activities of PRC2 and JARID2 in several cancers, including carcinoma, neuroblastoma, hematologic malignancies and lymphomas (Bolisetty et al., 2009; Martin-Perez et al., 2010; Portela & Esteller, 2010; Margueron & Reinberg, 2011; Richly et al., 2011; Sandoval & Esteller, 2012).

Another attractive role for miR-K12-11 dependent repression of JARID2 during KSHV infection is a potential influence on PRC2-mediated repression and H3K27 tri-methylation of the viral genome, which has been demonstrated to be an important mechanism for the repression of lytic genes during latent expression (Günther & Grundhoff, 2010). Thus,

repression of JARID2 might be a factor that contributes to the establishment of latency by fine-tuning expression of lytic and latent KSHV genes on the epigenetic level.
Besides viral gene expression, it is likely that miR-K12-11 mediated repression of JARID2 may also alter the transcription profile of the infected host cell. Fine-tuning of H3K27-me3 patterns might be crucial to balance the processes of differentiation and proliferation, which is an important mechanism during lymphopoiesis and B-cell differentiation. Because dysregulated JARID2 expression is found in several cancers, there is evidence that JARID2 plays also a role in KSHV-induced tumorigenesis.

With regard to the impact of polycomb proteins in KSHV-life cycle it is worth noting that a second PcG protein, *JARID1b*, was identified as a target of miR-K12-11/hsa-miR-155 using luciferase reporter assays (see appendix, suppl. figure 2). JARID1b (also referred to as KDM5B) was investigated during the master thesis of Philipp Schult (Master of Science, University Lübeck), which was performed under my guidance. JARID1b can selectively remove H3K4 methylation marks from histones (Secombe & Eisenman, 2007). H3K4 methylation is a *transcription*-associated histone modification (Bernstein et al., 2002; Faucher & Wellinger, 2010), and a reduced JARID1b is linked to cellular transformation (Defeo-Jones et al., 1991; Fattaey et al., 1993). The question if miRNA-mediated JARID1b repression is biological relevant for KSHV infection cannot be answered so far; but it is an interesting scenario that viral miRNAs modulate methylation patterns, and thereby may have a global effect on transcription of viral and host genes, which likely facilitates establishment and maintenance of latency.

Taken together, although *in vivo* systems allow important insights into putative pathways modulated by miR-K12-11, the nature of these processes remain unsolved. While the specific functions of miR-K12-11 have not been elucidated, there is strong evidence that miR-K12-11 fine-tunes the host response to infection by regulating a diverse range of pathways. The putative as well as established miR-K12-11 targets discussed above provides evidence that miR-K12-11 is multifunctional. This is further underlined by recent PAR-CLIP data that revealed targeting of more than 2000 cellular mRNAs by KSHV miRNAs (Gottwein et al., 2011a). Furthermore, results from laboratories of Martin Turner, Carlo Croce and David Baltimore support this hypothesis, since each of the group performed a microarray expression analysis of miR-155 expressing cells and observed regulation of minimally 50 genes (Costinean et al., 2006; Rodriguez et al., 2007; O'Connell et al., 2008). Thus, our data combined with earlier reports about genes regulated by miR-155 and miR-K12-11 support the notion that miRNAs are multifunctional and act in complex regulatory networks to orchestrate multiple pathways, thereby modulating several

cellular processes in different cell types and at different stages during lineage commitment.

4.5 THE ROLE OF MIR-K12-11 IN TUMORIGENESIS

One of the most pressing questions regarding KSHV biology is the identification of genes and mechanisms that contribute to KSHV-induced tumorigenesis. The fact that only KSHV-infected individuals with severe immunosuppression develop tumors with significant frequency supports the idea that KSHV has evolved strategies to minimize its pathogenic potential in its host. Rather than induce hyperproliferation that leads to lymphomagenesis, it is likely that KSHV latent gene products modulate B-cell development and/or differentiation in order to allow the virus to persist in the host. However, as the majority of cells in KSHV malignancies are latently infected, latent gene products clearly can also have an impact on tumorigenesis. Since the latent gene product miR-K12-11 shares the seed sequence with hsa-miR-155, which is frequently deregulated in cancers, a role of miR-K12-11 in KSHV-induced tumorigenesis is likely. Further support for this hypothesis comes from the observation that the oncogenic MDV-1, an alphaherpesvirus that induces T-cell lymphoma in birds, also encodes a miRNA with an identical seed as miR-155, and loses its oncogenic potential *in vivo* in its natural host when the miRNA is mutated (Morgan et al., 2008; Zhao et al., 2011). Therefore, it seems likely that miR-K12-11 expression continues to regulate a set of miR-155 targets that directly promotes deregulated B-cell proliferation and lymphomagenesis. However, the molecular mechanisms that underlie miR-K12-11/miR-155 mediated tumorigenesis are still unknown.

Repression of *TGFβ* and *JARID2* mRNA expression levels represent two possible mechanisms that may contribute to KHSV-associated tumorigenesis. Liu et al. has proposed that miR-K12-11 has oncogenic potential by interfering with TGFβ signaling via *SMAD5* targeting (Liu et al., 2012). TGFβ expression facilitates growth inhibition and apoptosis in various cell types, whereby its downregulation results in cell growth and proliferation. Aberrant expression of JARID2 is found in several cancers and its influence in B-cell proliferation, when JARID2 expression is repressed, represents a possible mechanism to induce or promote lymphomagenesis.

In this work, miR-K12-11 was investigated with regard to its oncogenic activity, asking if the expression of this single viral miRNA is sufficient to contribute to KSHV-induced lymphomagenesis. However, lymphomas were not detected after 3 - 4 months of reconstitution in either miRNA expressing mouse cohorts. Boss et al. explored miR-K12-11 and hsa-miR-155 expression in a humanized model and analyzed mice after 14 weeks

post-transplantation, and importantly, also did not detect lymphoma (Boss et al., 2011). In neither our study nor in Boss´ study, where the respective miRNAs were expressed at near-physiological levels, was a frank B-cell lymphoma observed, in contrast to that reported in miR-155 transgenic mice that expressed miR-155 under control of the IgG heavy chain promoter (Costinean et al., 2006).

It is likely that transformation requires more factors than the expression of this single miRNA. Additional contributing factors may be the acquisition of gene mutations or chromosomal aberrations within the host genome, aberrant high-levels of miRNA expression, or the synergestic effects that result from the simultaneous expression of multiple viral gene products in latently infected cells.

Multistep process

It has been suggested, as reviewed by Hanahan and Weinberg, that cancer is a manifestation of six alterations in cell physiology, assumed to occur in most if not all human cancers (Hanahan & Weinberg, 2000). The successive accumulation of genetic changes leads to the acquisition of these six alterations: self-sufficiency in growth signals, insensitivity to growth inhibitory signals, evasion of apoptosis, limitless replicative potential, sustained angiogenesis, tissue invasion and metastases. The multistep process is driven by genetic alterations that range from point mutations to loss of whole chromosomes, resulting in either in loss of “tumor suppressor” activity or gain of “oncogenic” function. Mutations disrupting tumor suppressor genes (TSG) have been observed in numerous cancers and, in general, must impact both alleles to be effective (Knudson, 1971). Aberrant miRNA expression has the potential to promote cancer by repressing the translation of TSG transcripts, and thus resembles the situation of loss-of-function mutations of both alleles. TSG function is to limit inappropriate cell growth and cell division and stimulate cell death. Furthermore, some genes are involved in DNA repair processes, avoiding accumulation of mutations in cancer-related genes. Thus, TSGs inhibit cells from being driven into a cancer cell.

Interestingly, Dirk Dittmer and Debasmita Roy identified recently an inactivated tumor suppressor in KS and PEL cell lines. They observed in these cells that the important tumor suppressor phosphatase and tensin homolog (PTEN) is heavily phosphorylated at serine 380, which is an inactivating modification, which therefore resembles the situation of a deletion (Roy & Dittmer, 2011). PTEN is involved in growth, survival and proliferation and a loss of function occurs in a wide spectrum of human cancers (Chalhoub & Baker, 2009). Therefore, a heavily phosphorylated PTEN together with sustained miR-K12-11 expression might induce or promote lymphomagenesis.

Co-expression with latent viral proteins

Since all KSHV miRNAs are co-expressed along with a number of viral latent proteins it is very likely that KSHV gene products act in combinatorial fashion. We therefore suggest that co-expression of miR-K12-11 with viral proteins, like LANA, vIL6 or K1, may provoke the onset of a tumor.

LANA is an interesting candidate as such a co-factor, since it is constitutively expressed in all KSHV-infected cells due to its requirement for viral episome maintenance (Ballestas et al., 1999; Garber et al., 2001). Furthermore, LANA binds to p53, thereby inhibiting transcription and apoptosis, inactivates the tumor suppressor pRb, and binds to to GSK3β (Friborg et al., 1999; Radkov et al., 2000; Fujimuro et al., 2003). GSK3 binding prevents degradation of beta-catenin in the cytoplasm, consequently beta-catenin translocates into the nucleus and binds with transcription factors to activate for instance genes including MYC, which plays a role in cell cycle regulation promoting cell growth (Boshoff, 2003; Fujimuro et al., 2003). Furthermore, LANA functions as a transcriptional activator of its own and cellular gene promoters. Therefore a role for LANA in lymphomagenesis seems very likely (Jeong et al., 2001; Renne et al., 2001). Nevertheless, transgenic mice expressing LANA under its own promoter exhibit hyperresponsive and hyperproliferative B-cells, but like miR-K12-11 expressing mice do not develop frank B-cell lymphoma (Fakhari et al., 2006). Hence, it would be very interesting to test whether co-expression of LANA and miR-K12-11 in a mouse model would result in lymphomagenesis (Fakhari et al., 2006). The finding that both gene products negatively modulate the TGFβ signaling underscores the notion of synergistic activity, given that TGFβ signaling is often modified in human cancers (Di Bartolo et al., 2008).

Another candidate thought to play an important role in KSHV-induced lymphomagenesis is vIL6, since this protein is detected in both malignancies MCD and PEL (Molden et al., 1997; Hassman et al., 2011). vIL6 signaling triggers the JAK/STAT (Janus tyrosine kinase signal transducers and activators of transcription) and MAPK pathways (Molden et al., 1997). Although vIL6 protein is highly expressed during the lytic cycle, it is also expressed in latently infected B-cells. This is of particular interest since vIL6 can influence B-cell development and promotes B-cell survival and growth (Schulz, 2001). Sanjay Chandriani and Don Ganem underscored the importance of vIL6 suggesting that vIL6 has an important impact on promoting persistence of infected B-cells *in vivo* (Chandriani & Ganem, 2010). Interestingly, another group inoculated vIL6-producing clones of NIH3T3 cells into mice and observed stimulated hematopoiesis and tumor formation (Aoki et al., 2001). Therefore, co-expression with miR-K12-11 in B-cells might promote tumorigenesis.

K1 is of considerable interest, because it is involved in activating B-cells, but also in protecting these cells from Fas-induced apoptosis (Tomlinson & Damania, 2004, 2008). K1 mimics signaling through the B-cell antigen receptor. Interestingly, a similar mechanism is also used by EBV, which expresses the latent protein LMP2, an essential factor for allowing latently infected cells to gain access to the memory B-cell pool (Lagunoff et al., 1999). Transgenic mice expressing K1 exhibit constitutive activation of NFkB and an incrase of Lyn-tyrosine kinase phosphorylation activity. Importantly, some of the mice developed lymphomas (Prakash et al., 2002). Consequently, simultaneous expression of K1 and miR-K12-11 may lead to increased B-cell growth thereby promoting tumor formation (Lee et al., 1998; Bellare & Ganem, 2009).

Taken together, it is well possible that expression of the above viral proteins contribute to stimulation of B-cell differentiation, B-cell survival and/or growth. These factors predispose the host cell to transformation and co-expression with miR-K12-11 may result in lymphoma.

4.6 SUMMARY: MIR-K12-11 AND ITS ROLE IN B-CELL BIOLOGY

Our findings support the hypothesis that miR-K12-11 has co-evolved to mimic miR-155 functions, because both miRNA mouse cohorts showed similar phenotypes, indicating that miR-K12-11 mimics hsa-miR-155 functions during hematopoiesis With regard to the physiological role of miR-K12-11 during the viral life-cycle, we hypothesize that KSHV uses miR-K12-11 to modulate host transcription in the infected cell in order to induce B-cell differentiation (figure 41). The miR-K12-11 and hsa-miR-155 mice showed an increased fraction of pre-B-cells ($CD19^+/CD43^-$) and total B-cells ($B220^+$, $CD19^+$) in BM and spleen, respectively. In addition, we detected repressed levels of *c-Myb* and *Fos*, two genes with crucial roles in B-cell biology, in miRNA expressing BM cells. *Jarid2* has been identified as a novel target of miR-K12-11; and although its role in B-cell biology is still elusive, it is thought that it influences proliferation and B-cell survival. Importantly, the observed increased GC reaction in spleen lends further credibility to the theory that KSHV infects naïve B-cells and employs miR-K12-11 expression to induce the differentiation of B-cells into memory B-cells by undergoing GC formation, and hence allowing the virus to establish persistence in this long-lived B-cell compartment.

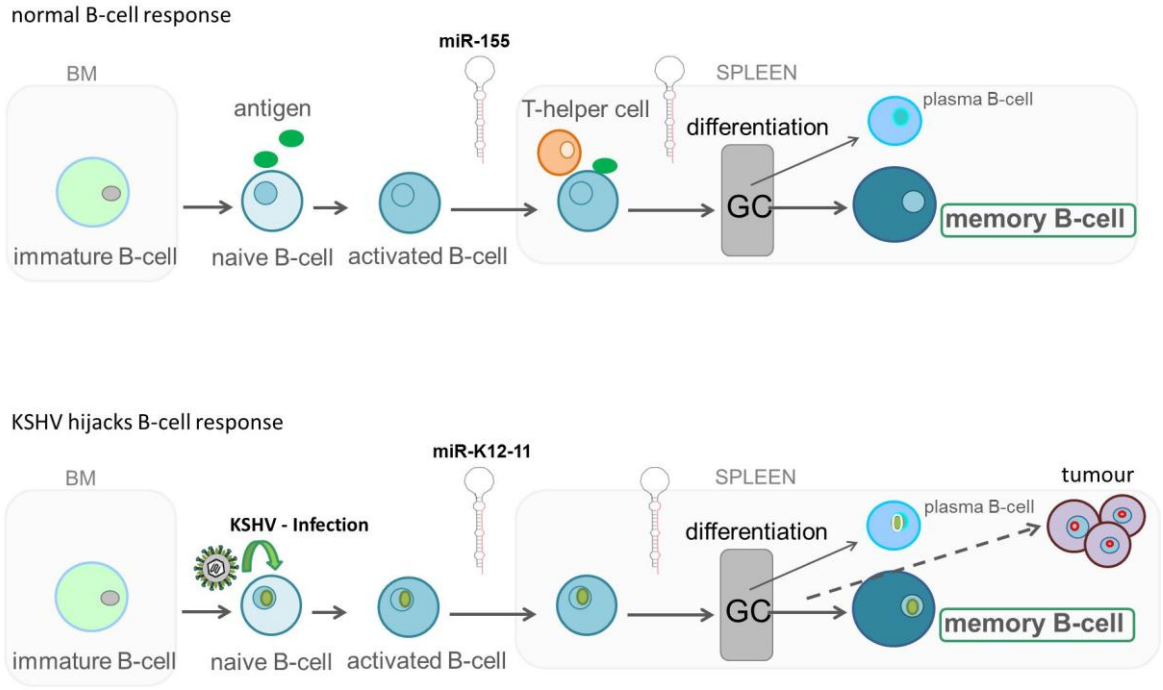

Figure 41: KSHV hijacks normal B-cell biology. B-cell development starts in BM where HSCs develop into the immature B-cell stage. Immature B-cells migrate to secondary lymphoid organs where they are activated by specific antigens. When the B-cell binds an antigen and receives T-cell help in a secondary lymphoid organ like spleen it may cause GC formation, followed by differentiation into plasma or memory B.cells. The simplified schematic drawing shows the normal B-cell development and differentiation (upper figure), whereas the lower figure represents a model of how KSHV might exploit normal B-cell biology to gain access to the memory B-cell pool by using expression of miR-K12-11. KSHV infects naïve B-cells that circulate in the periphery (green circle: KSHV episome) and expresses miR-K12-11 to mimic miR-155 expression. Sustained expression of miR-K12-11 might contribute to tumorigenesis.

4.7 FUTURE DIRECTIONS

The generation of transgenic mice represents an optimal tool to explore synergistic effects of miR-K12-11 expression and other KSHV gene products. Transgenic mice that co-express miR-K12-11 with LANA, vIL6 or K1 may recapitulate important aspects in virus-host interactions.

Additionally, extended analyses of targets using new technologies, for instance Next Generation Sequencing (NGS), will provide a better understanding of the function of this viral ortholog in B-cell expansion and oncogenesis. A subsequent functional analysis of these targets might aid in understanding important mechanisms in the context of KSHV biology; for instance how this virus establishes and/or maintains latency in the infected B-cell.

Recently, protocols were developed to establish and maintain KSHV latency in B-cells, which provide new perspectives in B-cell biology in the context of KSHV infection (Myoung & Ganem, 2011; Cho & Kang, 2012). One promising method is a protocol developed by

Kati et al. (unpublished data), in which a KSHV-negative B-cell line was latently infected with a recombinant KSHV.219 or BAC36-derived KSHV, using both cell-free virus stocks and cell-cell transmission. These generated stable BJAB/KSHV cell lines show a similar KSHV expression profile compared to PEL cell lines, which may help to unravel key aspects of lymphomagenesis.

Another interesting aspect concerns to the identification of *JARID2* as a novel target of miR-K12-11 in this work. Further studies are required to elucidate the role of miR-K12-11 mediated JARID2 repression in the context of viral latency and lymphomagenesis.

Taken together, these studies will help to better understand the molecular mechanisms that underlie the pathogenesis associated with KSHV infection.

5 LITERATURE

Abend J, Uldrick T, Ziegelbauer J. 2010. Regulation of tumor necrosis factor-like weak inducer of apoptosis receptor protein (TWEAKR) expression by Kaposi's sarcoma-associated herpesvirus microRNA prevents TWEAK-induced apoptosis and inflammatory cytokine expression. *J Virol 84*:12139-12151.

Alfieri C, Birkenbach M, Kieff E. 1991. Early events in Epstein-Barr virus infection of human B lymphocytes. *Virology 181*:595-608.

Aoki Y, Yarchoan R, Wyvill K, Okamoto S, Little R, Tosato G. 2001. Detection of viral interleukin-6 in Kaposi sarcoma-associated herpesvirus-linked disorders. *Blood 97*:2173-2176.

Ballestas M, Chatis P, Kaye K. 1999. Efficient persistence of extrachromosomal KSHV DNA mediated by latency-associated nuclear antigen. *Science 284*:641-644.

Bartel D. 2004. MicroRNAs: Genomics, Biogenesis, Mechanism, and Function. *Cell Press 116*:281–297.

Bartel D. 2009. MicroRNAs: target recognition and regulatory functions. *Cell 136*:215-233.

Behm-Ansmant I, Rehwinkel J, Doerks T, Stark A, Bork P, Izaurralde E. 2006. mRNA degradation by miRNAs and GW182 requires both CCR4:NOT deadenylase and DCP1:DCP2 decapping complexes. *Genes Dev 20*:1885-1898.

Bellare P, Ganem D. 2009. Regulation of KSHV lytic switch protein expression by a virus-encoded microRNA: an evolutionary adaptation that fine-tunes lytic reactivation. *Cell Host Microbe 6*:570-575.

Bender T, Kuehl W. 1987. Differential expression of the c-myb proto-oncogene marks the pre-B cell/B cell junction in murine B lymphoid tumors. *J Immunol 139*:3822-3827.

Bender T, Thompson C, Kuehl W. 1987. Differential expression of c-myb mRNA in murine B lymphomas by a block to transcription elongation. *Science 237*:1473-1476.

Bernstein B, Humphrey E, Erlich R, Schneider R, Bouman P, Liu J, Kouzarides T, Schreiber S. 2002. Methylation of histone H3 Lys 4 in coding regions of active genes. *Proc Natl Acad Sci 99*:8695-8700.

Bernstein E, Caudy A, Hammond S, Hannon G. 2001. Role for a bidentate ribonuclease in the initiation step of RNA interference. *Nature 409*:363-366.

Beyer T, Kolowos W, Dumitriu I, Voll R, Heyder P, Gaipl U, Kalden J, Herrmann M. 2002. Apoptosis of the teratocarcinoma cell line Tera-1 leads to the cleavage of HERV-K10gag proteins by caspases and/or granzyme B. *Scand J Immunol 56*:303-309.

Bogerd H, Karnowski H, Cai X, Shin J, Pohlers M, Cullen B. 2010. A mammalian herpesvirus uses noncanonical expression and processing mechanisms to generate viral MicroRNAs. *Mol Cell 37*:135-142.

Bolisetty M, Dy G, Tam W, Beemon K. 2009. Reticuloendotheliosis virus strain T induces miR-155, which targets JARID2 and promotes cell survival. *J Virol 83*:12009-12017.

Boshoff C. 2003. Kaposi virus scores cancer coup. *Nat Med 9*:261-262.

Boshoff C. 2011. Unraveling virus-induced lymphomagenesis. *J Clin Invest 121*:838-841.

Boss I, Nadeau P, Abbott J, Yang Y, Mergia A, Renne R. 2011. A Kaposi's sarcoma-associated herpesvirus-encoded ortholog of microRNA miR-155 induces human splenic B-cell expansion in NOD/LtSz-scid IL2Rγnull mice. *J Virol 85*:9877-9886.

Boulanger E, Gérard L, Gabarre J, Molina J, Rapp C, Abino J, Cadranel J, Chevret S, Oksenhendler E. 2005. Prognostic factors and outcome of human herpesvirus 8-associated primary effusion lymphoma in patients with AIDS. *J Clin Oncol 23*:4372-4380.

Burger R, Neipel F, Fleckenstein B, Savino R, Ciliberto G, Kalden J, Gramatzki M. 1998. Human herpesvirus type 8 interleukin-6 homologue is functionally active on human myeloma cells. *Blood 91*:1858-1863.

Burnside J, Morgan R. 2011. Emerging roles of chicken and viral microRNAs in avian disease. *BMC Proc 5*.

Cai X, Cullen BR. 2006. Transcriptional origin of Kaposi's sarcoma-associated herpesvirus microRNAs. *J Virol 80*:2234-2242.

Cai X, Lu S, Zhang Z, Gonzalez C, Damania B, Cullen B. 2004. Kaposi's sarcoma-associated herpesvirus expresses an array of viral microRNAs in latently infected cells. *PNAS 102*:5570-5575.

Cai X, Lu S, Zhang Z, Gonzalez C, Damania B, Cullen B. 2005. Kaposi's sarcoma-associated herpesvirus expresses an array of viral microRNAs in latently infected cells. *Proc Natl Acad Sci U S A 102*:5570-5575.

Cameron J, Fewell C, Yin Q, McBride J, Wang X, Lin Z, Flemington E. 2008. Epstein-Barr virus growth/latency III program alters cellular microRNA expression. *Virology 382*:257-266.

Cannon J, J N, Orenstein J, Mann R, Murray P, Browning P, DiGiuseppe J, Cesarman E, Hayward G, Ambinder R. 1999. Heterogeneity of viral IL-6 expression in HHV-8-associated diseases. *J Infect Dis 180*:824-828.

Carbone A, Cilia A, A G, Capello D, Todesco M, Quattrone S, Volpe R, Gaidano G. 1998. Establishment and characterization of EBV-positive and EBV-negative primary effusion lymphoma cell lines harbouring human herpesvirus type-8. *Br J Haematol 102*:1081-1089.

Castleman B, Iverson L, Menendez V. 1956. Localized mediastinal lymphnode hyperplasia resembling thymoma. *Cancer 9*:822-830.

Cattoretti G, Shaknovich R, Smith P, Jäck H, Murty V, Alobeid B. 2006. Stages of germinal center transit are defined by B cell transcription factor coexpression and relative abundance. *J Immunol 177*:6930-6939.

Cesarman E, Chang Y, Moore P, Said J, Knowles D. 1995. Kaposi's sarcoma-associated herpesvirus-like DNA sequences in AIDS-related body-cavity-based lymphomas. *N Engl J Med 18*:1186-1191.

Chalhoub N, Baker S. 2009. PTEN and the PI3-kinase pathway in cancer. *Annu Rev Pathol 4*:127-150.

Chandriani S, Ganem D. 2010. Array-based transcript profiling and limiting-dilution reverse transcription-PCR analysis identify additional latent genes in Kaposi's sarcoma-associated herpesvirus. *J Virol 84*:5565-5573.

Chang Y, Cesarman E, Pessin M, Lee F, Culpepper J, Knowles D, Moore P. 1994. Identification of herpesvirus-like DNA sequences in AIDS-associated Kaposi's sarcoma. *Science*:1865-1869.

Chen C, Li L, Lodish H, Bartel D. 2004. MicroRNAs modulate hematopoietic lineage differentiation. *Science 303*:83-86.

Chen C, Ridzon D, Broomer A, Zhou Z, Lee D, Nguyen J, Barbisin M, Xu N, Mahuvakar V, Andersen M, Lao K, Livak K, Guegler K. 2005. Real-time quantification of microRNAs by stem-loop RT-PCR. *Nucleic Acids Res 33*.

Chendrimada T, Gregory R, Kumaraswamy E, Norman J, Cooch N, Nishikura K, Shiekhattar R. 2005. TRBP recruits the Dicer complex to Ago2 for microRNA processing and gene silencing. *Nature 436*:740-744.

Cho H, Kang H. 2012. KSHV infection of B-cell lymphoma using a modified KSHV BAC36 and coculturing system. *J Microbiol 50*:285-292.

Chomczynski P, Sacchi N. 1987. Single-step method of RNA isolation by acid guanidinium thiocyanate-phenol-chloroform extraction. *Anal Biochem 162*:156-159.

Clurman B, Hayward W. 1989. Multiple proto-oncogene activations in avian leukosis virus-induced lymphomas: evidence for stage-specific events. *Mol Cell Biol 9*:2657-2664.

Costinean S, Zanesi N, Pekarsky Y, Tili E, Volinia S, Heerema N, Croce C. 2006. Pre-B cell proliferation and lymphoblastic leukemia/high-grade lymphoma in E(mu)-miR155 transgenic mice. *Proc Natl Acad Sci 103*:7024-7029.

Defeo-Jones D, Huang P, Jones R, Haskell K, Vuocolo G, Hanobik M, Huber H, Oliff A. 1991. Cloning of cDNAs for cellular proteins that bind to the retinoblastoma gene product. *Nature 352*:251-254.

Denli A, Tops B, Plasterk R, Ketting R, Hannon G. 2004. Processing of primary microRNAs by the Microprocessor complex. *Nature 432*:231-235.

Di Bartolo D, Cannon M, Liu Y, Renne R, Chadburn A, Boshoff C, Cesarman E. 2008. KSHV LANA inhibits TGF-beta signaling through epigenetic silencing of the TGF-beta type II receptor. *Blood 111*:4731-4740.

Didiano D, Hobert O. 2006. Perfect seed pairing is not a generally reliable predictor for miRNA-target interactions. *Nat Struct Mol Biol 13*:849-851.

Dittmer D, Lagunoff M, Renne R, Staskus K, Haase A, Ganem D. 1998. A cluster of latently expressed genes in Kaposi's sarcoma-associated herpesvirus. *J Virol 72*:8309-8315.

Djerbi M, Screpanti V, Catrina A, Bogen B, Biberfeld P, Grandien A. 1999. The inhibitor of death receptor signaling, FLICE-inhibitory protein defines a new class of tumor progression factors. *J Exp Med 190*:1025-1032.

Doench J, Sharp P. 2004. Specificity of microRNA target selection in translational repression. *2004 18*:504-511.

Dourmishev L, Dourmishev A, Palmeri D, Schwartz R, Lukac D. 2003. Molecular genetics of Kaposi's sarcoma-associated herpesvirus (human herpesvirus-8) epidemiology and pathogenesis. *Microbiol Mol Bio Rev 67*:175-212.

Du M, Diss T, Liu H, Ye H, Hamoudi R, Cabeçadas J, Dong H, Harris N, Chan J, Rees J, Dogan A, Isaacson P. 2002. KSHV- and EBV-associated germinotropic lymphoproliferative disorder. *Blood 100*:3415-3418.

Dunand-Sauthier I, Santiago-Raber M, Capponi L, Vejnar C, Schaad O, Irla M, Seguín-Estévez Q, Descombes P, Zdobnov E, Acha-Orbea H, Reith W. 2011. Silencing of c-Fos expression by microRNA-155 is critical for dendritic cell maturation and function. *Blood 117*:4490-4500.

Dupin N, Diss T, Kellam P, Tulliez M, Du M, Sicard D, Weiss R, Isaacson P, Boshoff C. 2000. HHV-8 is associated with a plasmablastic variant of Castleman disease that is linked to HHV-8-positive plasmablastic lymphoma. *Blood 95*:1406-1412.

Duro D, Schulze A, Vogt B, Bartek J, Mittnacht S, Jansen-Dürr P. 1999. Activation of cyclin A gene expression by the cyclin encoded by human herpesvirus-8. *J Gen Virol 80*:549-555.

Eferl R, Wagner E. 2003. AP-1: a double-edged sword in tumorigenesis. *3*:859-868.

Eis P, Tam W, Sun L, Chadburn A, Li Z, Gomez M, Lund E, Dahlberg J. 2005. Accumulation of miR-155 and BIC RNA in human B cell lymphomas. *Proc Natl Acad Sci 102*:3627-3632.

Elbashir S, Lendeckel W, Tuschl T. 2001. RNA interference is mediated by 21- and 22-nucleotide RNAs. *Genes Dev 15*:188-200.

Eulalio A, Huntzinger E, Izaurralde E. 2008. Getting to the root of miRNA-mediated gene silencing. *Cell 132*:9-14.

Fabian M, Sonenberg N, Filipowicz W. 2010. Regulation of mRNA translation and stability by microRNAs. *Annu Rev Biochem 79*:351-379.

Fadeel B. 2005. Raji revisited: cytogenetics of the original Burkitt's lymphoma cell line. *Leukemia 19*:159-161.

Fais F, Gaidano G, Capello D, Gloghini A, Ghiotto F, Roncella S, Carbone A, Chiorazzi N, Ferrarini M. 1999. Immunoglobulin V region gene use and structure suggest antigen selection in AIDS-related primary effusion lymphomas. *Leukemia 13*:1093-1099.

Fakhari F, Jeong J, Kanan Y, Dittmer D. 2006. The latency-associated nuclear antigen of Kaposi sarcoma-associated herpesvirus induces B cell hyperplasia and lymphoma. *J Clin Invest 116*:735-742.

Fattaey A, Helin K, Dembski M, Dyson N, Harlow E, Vuocolo G, Hanobik M, Haskell K, Oliff A, Defeo-Jones D, al. e. 1993. Characterization of the retinoblastoma binding proteins RBP1 and RBP2. *Oncogene 8*:3149-3156.

Faucher D, Wellinger R. 2010. Methylated H3K4, a transcription-associated histone modification, is involved in the DNA damage response pathway. *Plos Genet 6*.

Fernando T, Rodriguez-Malave N, Rao D. 2012. MicroRNAs in B cell development and malignancy. *J Hematol Oncol 2012*.

Flint S, Enquist L, Racaniello V. 2004. Principles of Virology: Molecular Biology, Pathogenesis, and Control of Animal Viruses. *American Society for Microbiology*.

Friborg JJ, Kong W, Hottiger M, Nabel G. 1999. p53 inhibition by the LANA protein of KSHV protects against cell death. *Nature 402*:889-894.

Friedman J, Jones P. 2009. MicroRNAs: critical mediators of differentiation, development and disease. *Swiss Med Wkly 139*:466-472.

Fujimuro M, Wu F, ApRhys C, Kajumbula H, Young D, Hayward G, Hayward S. 2003. A novel viral mechanism for dysregulation of beta-catenin in Kaposi's sarcoma-associated herpesvirus latency. *Nat Med 9*:300-306.

Gaidano G, Gloghini A, Gattei V, Rossi M, Cilia A, Godeas C, Degan M, Perin T, Canzonieri V, Aldinucci D, Saglio G, Carbone A, Pinto A. 1997. Association of Kaposi's sarcoma-associated herpesvirus-positive primary effusion lymphoma with expression of the CD138/syndecan-1 antigen. *Blood 90*:4894-4900.

Garber A, Shu M, Hu J, Renne R. 2001. DNA binding and modulation of gene expression by the latency-associated nuclear antigen of Kaposi's sarcoma-associated herpesvirus. *J Virol* 7882-7892.

Gatto G, Rossi A, Rossi D, Kroening S, Bonatti S, Mallardo M. 2008. Epstein-Barr virus latent membrane protein 1 trans-activates miR-155 transcription through the NF-kappaB pathway. *Nucleic Acids Res 36*:6608-6619.

Gibcus J, Tan L, Harms G, Schakel R, de Jong D, Blokzijl T, Möller P, Poppema S, Kroesen B, van den Berg A. 2009. Hodgkin lymphoma cell lines are characterized by a specific miRNA expression profile. *Neoplasia 11*:167-176.

Gibson U, Heid C, Williams P. 1996. A novel method for real time quantitative RT-PCR. *Genome Res 6*:995-1001.

Gonda TJ, Metcalf D. 1984. Expression of myb, myc and fos proto-oncogenes during the differentiation of a murine myeloid leukaemia. *Nature 310*:249-251.

Gottwein E. 2012. Kaposi's Sarcoma-Associated Herpesvirus microRNAs. *Front Microbiol 165*.

Gottwein E, Corcoran D, Mukherjee N, Skalsky R, Hafner M, Nusbaum J, Shamulailatpam P, Love C, Dave S, Tuschl T, Ohler U, Cullen B. 2011a. Viral microRNA

targetome of KSHV-infected primary effusion lymphoma cell lines. *Cell Host Microbe 10*:515-526.

Gottwein E, Corcoran DL, Mukherjee N, Skalsky RL, Hafner M, Nusbaum JD, Shamulailatpam P, Love CL, Dave SS, Tuschl T, Ohler U, Cullen BR. 2011b. Viral microRNA targetome of KSHV-infected primary effusion lymphoma cell lines. *Cell Host Microbe 10*:515-526.

Gottwein E, Cullen B. 2010. A human herpesvirus microRNA inhibits p21 expression and attenuates p21-mediated cell cycle arrest. *J Virol 84*:5229-5237.

Gottwein E, Mukherjee N, Sachse C, Frenzel C, Majoros W, Chi J, Braich R, Manoharan M, Soutschek J, Ohler U, Cullen B. 2007. A viral microRNA functions as an ortholog of cellular miR-155. *Nature 450*:1096-1099.

Graham F, Smiley J, Russell W, Nairn R. 1977. Characteristics of a human cell line transformed by DNA from human adenovirus type 5. *J Gen Virol 36*:59-74.

Grandadam M, Dupin N, Calvez V, Gorin I, Blum L, Kernbaum S, Sicard D, Buisson Y, Agut H, Escande J, Huraux J. 1997. Exacerbations of clinical symptoms in human immunodeficiency virus type 1-infected patients with multicentric Castleman's disease are associated with a high increase in Kaposi's sarcoma herpesvirus DNA load in peripheral blood mononuclear cells. *J Infect Dis 175*:1198-1201.

Grundhoff A, Ganem D. 2003. The latency-associated nuclear antigen of Kaposi's sarcoma-associated herpesvirus permits replication of terminal repeat-containing plasmids. *J Virol 77*:2779-2783.

Grundhoff A, Ganem D. 2004. Inefficient establishment of KSHV latency suggests an additional role for continued lytic replication in Kaposi sarcoma pathogenesis. *J Clin Invest 113*:124-136.

Grundhoff A, Sullivan C. 2011. Virus-encoded microRNAs. *Virology 411*:325-343.

Grundhoff A, Sullivan C, Ganem D. 2006a. A combined computational and microarray-based approach identifies novel microRNAs encoded by human gamma-herpesviruses. *RNA 12*:733-750.

Grundhoff A, Sullivan CS, Ganem D. 2006b. A combined computational and microarray-based approach identifies novel microRNAs encoded by human gamma-herpesviruses. *Rna 12*:733-750.

Günther T, Grundhoff A. 2010. The epigenetic landscape of latent Kaposi sarcoma-associated herpesvirus genomes. *PLoS Pathog 6*.

Guo H, Ingolia N, Weissman J, Bartel D. 2010. Mammalian microRNAs predominantly act to decrease target mRNA levels. *Nature 466*:835-840.

Hammond S. 2005. Dicing and slicing: The core machinery of the RNA interference pathway. *FEBS Letters 579*:5822-5829.

Hanahan D, Weinberg R. 2000. The hallmarks of cancer. *Cell 100*:57-70.

Hardy R, Kincade P, Dorshkind K. 2007. The Protean Nature of Cells in the B Lymphocyte Lineage. *Cell Press 26*:703-714.

Hassman L, Ellison T, Kedes D. 2011. KSHV infects a subset of human tonsillar B cells, driving proliferation and plasmablast differentiation. *J Clin Invest 121*:752-768.

Havelange V, Garzon R. 2010. MicroRNAs: emerging key regulators of hematopoiesis. *Am J Hematol 85*:935-942.

Hutvágner G, McLachlan J, Pasquinelli A, Bálint E, Tuschl T, Zamore P. 2001. A cellular function for the RNA-interference enzyme Dicer in the maturation of the let-7 small temporal RNA. *Science 293*:834-838.

Imig J, Motsch N, Zhu J, Barth S, Okoniewski M, Reineke T, Tinguely M, Faggioni A, Trivedi P, Meister G, Renner C, Grässer F. 2011. microRNA profiling in Epstein-Barr virus-associated B-cell lymphoma. *Nucleic Acids Res 39*:1880-1893.

Islam A, Richter W, Lopez-Bigas N, Benevolenskaya E. 2011. Selective targeting of histone methylation. *Cell Cycle 10*:413-424.

Jainchill J, Aaronson S, Todaro G. 1969. Murine Sarcoma and Leukemia Viruses: Assay Using Clonal Lines of Contact-Inhibited Mouse Cells. *J Virol 4*:549-553.

Jenner R, Mar Alba M, Boshoff C, Kellam P. 2001. The full repertoire of viral gene expression occurs only during lytic replication, when virus progeny are produced and the host cell is destroyed. *J Virol 75*:891-902.

Jeong J, Papin J, Dittmer D. 2001. Differential regulation of the overlapping Kaposi's sarcoma-associated herpesvirus vGCR (orf74) and LANA (orf73) promoters. *J Virol 75*:1798-1807.

John B, Enright A, Aravin A, Tuschl T, Sander C, Marks D. 2004. Human MicroRNA targets. *PloS Biol 2*:363.

Jones K, Aoki Y, Chang Y, Moore P, Yarchoan R, Tosato G. 1999. Involvement of interleukin-10 (IL-10) and viral IL-6 in the spontaneous growth of Kaposi's sarcoma herpesvirus-associated infected primary effusion lymphoma cells. *Blood 94*:2871-2879.

Kim V. 2005. Small RNAs: classification, biogenesis, and function. *Mol Cells 19*:1-15.

Kitajima K, Kojima M, Nakajima K, Kondo S, Hara T, Miyajima A, Takeuchi T. 1999. Definitive but not primitive hematopoiesis is impaired in jumonji mutant mice. *Blood 93*:87-95.

Kluiver J, Kroesen B, Poppema S, van den Berg A. 2006. The role of microRNAs in normal hematopoiesis and hematopoietic malignancies. *Leukemia 20*:1931-1936.

Knudson A. 1971. Mutation and Cancer: Statistical Study of Retinoblastoma. *Proc Natl Acad Sci 68*:820-823.

Lagunoff M, Majeti R, Weiss A, Ganem D. 1999. Deregulated signal transduction by the K1 gene product of Kaposi's sarcoma-associated herpesvirus. *Proc Natl Acad Sci 96*:5704-5709.

Laichalk L, Hochberg D, Babcock G, Freeman R, Thorley-Lawson D. 2002. The dispersal of mucosal memory B cells: evidence from persistent EBV infection. *immunity 16*:745-754.

Laichalk L, Thorley-Lawson D. 2005. Terminal differentiation into plasma cells initiates the replicative cycle of Epstein-Barr virus in vivo. *J Virol 79*:1296-1307.

Landeira D, Fisher A. 2011. Inactive yet indispensable: the tale of Jarid2. *Trends Cell Biol 21*:74-80.

Landeira D, Sauer S, Poot R, Dvorkina M, Mazzarella L, Jørgensen H, Pereira C, Leleu M, Piccolo F, Spivakov M, Brookes E, Pombo A, Fisher C, Skarnes W, Snoek T, Bezstarosti K, Demmers J, Klose R, Casanova M, Tavares L, Brockdorff N, Merkenschlager M, Fisher A. 2010. Jarid2 is a PRC2 component in embryonic stem cells required for multi-lineage differentiation and recruitment of PRC1 and RNA Polymerase II to developmental regulators. *Nat Cell Biol 12*:618-624.

Lawrie C, Gal S, Dunlop H, Pushkaran B, Liggins A, Pulford K, Banham A, Pezzella F, Boultwood J, Wainscoat J, Hatton C, Harris A. 2008. Detection of elevated levels of tumour-associated microRNAs in serum of patients with diffuse large B-cell lymphoma. *Br J Haematol 141*:672-675.

Lee H, Veazey R, Williams K, Li M, Guo J, Neipel F, Fleckenstein B, Lackner A, Desrosiers R, Jung J. 1998. Deregulation of cell growth by the K1 gene of Kaposi's sarcoma-associated herpesvirus. *Nat Med 4*:435-440.

Lee Y, Jeon K, Lee J, Kim S, Kim V. 2002. MicroRNA maturation: stepwise processing and subcellular localization. *EMBO J 21*:4663-4670.

Lee Y, Kim M, Han J, Yeom K, Lee S, Baek S, Kim V. 2004. MicroRNA genes are transcribed by RNA polymerase II. *EMBO J 23*:4051-4060.

Lessard J, Schumacher A, Thorsteinsdottir U, van Lohuizen M, Magnuson T, Sauvageau G. 1999. Functional antagonism of the Polycomb-Group genes eed and Bmi1 in hemopoietic cell proliferation. *Genes Dev 13*:2691-2703.

Lewis B, Shih I, Jones-Rhoades M, Bartel D, Burge C. 2003. Prediction of mammalian microRNA targets. *Cell 115*:787-798.

Li B, Zhou J, Liu P, Hu J, Jin H, Shimono Y, Takahashi M, G X. 2007. Polycomb protein Cbx4 promotes SUMO modification of de novo DNA methyltransferase Dnmt3a. *Biochem J 405*:369-378.

Li G, Margueron R, Ku M, Chambon P, Bernstein B, Reinberg D. 2010. Jarid2 and PRC2, partners in regulating gene expression. *Genes Dev*:368-380.

Li M, MacKey J, Czajak S, Desrosiers R, Lackner A, Jung J. 1999. Identification and Characterization of Kaposi's Sarcoma-Associated Herpesvirus K8.1 Virion Glycoprotein. *J Virol 73*:1341-1349.

Liebermann DA, Hoffman B. 1994. Differentiation primary response genes and proto-oncogenes as positive and negative regulators of terminal hematopoietic cell differentiation. *Stem Cells 12*:352-369.

Lim C, Sohn H, Lee D, Gwack Y, Choe J. 2002. Functional dissection of latency-associated nuclear antigen 1 of Kaposi's sarcoma-associated herpesvirus involved in latent DNA replication and transcription of terminal repeats of the viral genome. *J Virol 76*:10320-10331.

Lin Y, Sullivan C. 2011. Expanding the role of Drosha to the regulation of viral gene expression. *Proc Natl Acad Sci 108*:11229-11234.

Linnstaedt S, Gottwein E, Skalsky R, Luftig M, Cullen B. 2010. Virally Induced Cellular MicroRNA miR-155 Plays a Key Role in B-Cell Immortalization by Epstein-Barr Virus. *J Virol 84* 11670-11678

Liu H, Schmidt-Supprian M, Shi Y, Hobeika E, Barteneva N, Jumaa H, Pelanda R, Reth M, Skok J, Rajewsky K, Shi Y. 2007. Yin Yang 1 is a critical regulator of B-cell development. *Genes Dev 21*:1179-1189.

Liu J, Carmell M, Rivas F, Marsden C, Thomson J, Song J, Hammond S, Joshua-Tor L, Hannon G. 2004. Argonaute2 is the catalytic engine of mammalian RNAi. *2004 305*:1437-1441.

Liu Y, Sun R, Lin X, Liang D, Deng Q, Lan K. 2012. Kaposi's sarcoma-associated herpesvirus-encoded microRNA miR-K12-11 attenuates transforming growth factor beta signaling through suppression of SMAD5. *JVirol 86*:1372-1381.

Livak KS, TD. 2001. Analysis of relative gene expression data using real-time quantitative PCR and the 2(-Delta Delta C(T)) Method. *Methods 25*:402-408.

Lu F, Stedman W, Yousef M, Renne R, Lieberman P. 2010. Epigenetic regulation of Kaposi's sarcoma-associated herpesvirus latency by virus-encoded microRNAs that target Rta and the cellular Rbl2-DNMT pathway. *J Virol 84*:2697-2706.

Lubyova B, Pitha P. 2000. Characterization of a novel human herpesvirus 8-encoded protein, vIRF-3, that shows homology to viral and cellular interferon regulatory factors. *J Virol 74*:8194-8201.

Majewski I, Blewitt M, de Graaf C, McManus E, Bahlo M, Hilton A, Hyland C, Smyth G, Corbin J, Metcalf D, Alexander W, Hilton D. 2008. Polycomb repressive complex 2 (PRC2) restricts hematopoietic stem cell activity. *PloS Biol 6*.

Margueron R, Reinberg D. 2011. The Polycomb complex PRC2 and its mark in life. *Nature 469*:343-349.

Martin-Perez D, Piris MA, Sanchez-Beato M. 2010. Polycomb proteins in hematologic malignancies. *Blood 116*:5465-5475.

Matthias P, Rolink A. 2005. Transcriptional networks in developing and mature B cells. *Nat Rev Immunol 5*:497-508.

McCabe M, Graves A, Ganji G, Diaz E, Halsey W, Jiang Y, Smitheman K, Ott H, Pappalardi M, Allen K, Chen S, Della PAr, Dul E, Hughes A, Gilbert S, Thrall S, Tummino P, Kruger R, Brandt M, Schwartz B, Creasy C. 2012. Mutation of A677 in histone methyltransferase EZH2 in human B-cell lymphoma promotes hypertrimethylation of histone H3 on lysine 27 (H3K27). *Proc Natl Acad Sci 109*:2989-2994.

McCormick C, Ganem D. 2005. The kaposin B protein of KSHV activates the p38/MK2 pathway and stabilizes cytokine mRNAs. *Science 307*:739-741.

McGeoch D, Davison A. 1999. The descent of human herpesvirus 8. *Semin Cancer Biol 9*:201-209.

Meister G, Landthaler M, Patkaniowska A, Dorsett Y, Teng G, Tuschl T. 2004. Human Argonaute2 mediates RNA cleavage targeted by miRNAs and siRNAs. *Mol Cell 15*:185-197.

Mesri E, Cesarman E, Arvanitakis L, Rafii S, Moore M, Posnett D, Knowles D, Asch A. 1996. Human herpesvirus-8/Kaposi's sarcoma-associated herpesvirus is a new transmissible virus that infects B cells. *J Exp Med 183*:2385-2390.

Molden J, Chang Y, You Y, Moore P, Goldsmith M. 1997. A Kaposi's sarcoma-associated herpesvirus-encoded cytokine homolog (vIL-6) activates signaling through the shared gp130 receptor subunit. *J Biol Chem 272*:19625-19631.

Moore M, Boshoff C, Weiss R, Chang Y. 1996a. Molecular mimicry of human cytokine and cytokine response pathway genes by KSHV. *Science*:1739-1744.

Moore P, Gao S, Dominguez G, Cesarman E, Lungu O, Knowles D, Garber R, Pellett P, McGeoch D, Chang Y. 1996b. Primary characterization of a herpesvirus agent associated with Kaposi's sarcomae. *J Virol 70*:549-558.

Morgan R, Anderson A, Bernberg E, Kamboj S, Huang E, Lagasse G, Isaacs G, Parcells M, Meyers BC, Green PJ, Burnside J. 2008. Sequence conservation and differential expression of Marek's disease virus microRNAs. *J Virol 82*:12213-12220.

Morita S, Kojima T, Kitamura T. 2000. Plat-E: an efficient and stable system for transient packaging of retroviruses. *Gene Ther 12*:1063-1066.

Morrison S, Wright D, Cheshier S, Weissman I. 1997. Hematopoietic stem cells: challenges to expectations. *Curr Opin Immunol 9*:216-221.

Muylkens B, Coupeau D, Dambrine G, Trapp S, Rasschaert D. 2010. Marek’s disease virus microRNA designated Mdv1-pre-miR-M4 targets both cellular and viral genes *Arch Virology 11*:1823-1837.

Myoung J, Ganem D. 2011. Infection of lymphoblastoid cell lines by Kaposi's sarcoma-associated herpesvirus: critical role of cell-associated virus. *J Virol 85*:9767-9777.

Nachmani D, Stern-Ginossar N, Sarid R, Mandelboim O. 2009. Diverse herpesvirus microRNAs target the stress-induced immune ligand MICB to escape recognition by natural killer cells. *Cell Host Microbe 5*:376-385.

Naranatt P, Krishnan H, Svojanovsky S, Bloomer C, Mathur S, Chandran B. 2004. Host gene induction and transcriptional reprogramming in Kaposi's sarcoma-associated herpesvirus (KSHV/HHV-8)-infected endothelial, fibroblast, and B cells: insights into modulation events early during infection. *Cancer Res 64*:72-84.

Neipel F, Albrecht J, Fleckenstein B. 1997. Cell-homologous genes in the Kaposi's sarcoma-associated rhadinovirus human herpesvirus 8: determinants of its pathogenicity? *J Virol 71*:4187-4192.

Nutt S, Kee B. 2007. The transcriptional regulation of B cell lineage commitment. *Immunity 26*:715-725.

Nutt S, Metcalf D, D'Amico A, Polli M, Wu L. 2005. Dynamic regulation of PU.1 expression in multipotent hematopoietic progenitors. *J Exp Med 201*:221-231.

O'Connell R, Chaudhuri A, Rao D, Gibson W, Balazs A, Baltimore D. 2010. MicroRNAs enriched in hematopoietic stem cells differentially regulate long-term hematopoietic output. *Proc Natl Acad Sci 107*:14235-14240.

O'Connell R, Rao D, Chaudhuri A, Boldin M, Taganov K, Nicoll J, Paquette R, Baltimore D. 2008. Sustained expression of microRNA-155 in hematopoietic stem cells causes a myeloproliferative disorder. *J Exp Med 205*:585-594.

Oksenhendler E, Carcelain G, Aoki Y, Boulanger E, Maillard A, Clauvel J, Agbalika F. 2000. High levels of human herpesvirus 8 viral load, human interleukin-6, interleukin-10, and C reactive protein correlate with exacerbation of multicentric castleman disease in HIV-infected patients. *Blood 96*:2069-2073.

Pan X, Jones M, J J, Zaprazna K, Yu D, Pear W, Maillard I, Atchison M. 2012. Increased expression of PcG protein YY1 negatively regulates B cell development while allowing accumulation of myeloid cells and LT-HSC cells. *Plos One 7*.

Parkin D. 2006. The global health burden of infection-associated cancers in the year 2002. *Int J Cancer 118*:3030-3044.

Parravicini C, Chandran B, Corbellino M, Berti E, Paulli M, Moore P, Chang Y. 2000. Differential viral protein expression in Kaposi's sarcoma-associated herpesvirus-infected diseases: Kaposi's sarcoma, primary effusion lymphoma, and multicentric Castleman's disease. *Am J Pathol 156*:743-749.

Pasini D, Cloos P, Walfridsson J, Olsson L, Bukowski J, Johansen J, Bak M, Tommerup N, Rappsilber J, Helin K. 2010. JARID2 regulates binding of the Polycomb repressive complex 2 to target genes in ES cells. *Nature*:306-310.

Payne K, Crooks G. 2007. Immune-cell lineage commitment: translation from mice to humans. *Immunity 26*:674-677.

Pegtel D, Cosmopoulos K, Thorley-Lawson D, van Eijndhoven M, Hopmans E, Lindenberg J, de Gruijl T, Würdinger T, Middeldorp J. 2010. Functional delivery of viral miRNAs via exosomes. *Proc Natl Acad Sci 107*:6328-6333.

Peng J, Valouev A, Swigut T, Zhang J, Zhao Y, Sidow A, Wysocka J. 2009. Jarid2/Jumonji coordinates control of PRC2 enzymatic activity and target gene occupancy in pluripotent cells. *Cell 139*:1290-1302.

Pfaffl M. 2001. A new mathematical model for relative quantification in real-time RT–PCR. *Nucleic Acids Res*.

Pfeffer S, Sewer A, Lagos-Quintana M, Sheridan R, Sander C, Grässer F, van Dyk L, Ho C, Shuman S, Chien M, Russo J, Ju J, Randall G, Lindenbach B, Rice C, Simon V, Ho D, Zavolan M, Tuschl T. 2005. Identification of microRNAs of the herpesvirus family. *Nat Methods 2*:269-276.

Portela A, Esteller M. 2010. Epigenetic modifications and human disease. *Nat Biotechnol 28*:1057-1068.

Prakash O, Tang Z, Peng X, Coleman R, Gill J, Farr G, Samaniego F. 2002. Tumorigenesis and aberrant signaling in transgenic mice expressing the human herpesvirus-8 K1 gene. *J Natl Cancer Inst 94*:926-935.

Puda A, Milosevic J, Berg T, Klampfl T, Harutyunyan A, Gisslinger B, Rumi E, Pietra D, Malcovati L, Elena C, Doubek M, Steurer M, Tosic N, Pavlovic S, Guglielmelli P, Pieri L, Vannucchi A, Gisslinger H, Cazzola M, Kralovics R. 2012. Frequent deletions of JARID2 in leukemic transformation of chronic myeloid malignancies. *Am J Hematol 87*:245-250.

Radkov S, Kellam P, Boshoff C. 2000. The latent nuclear antigen of Kaposi sarcoma-associated herpesvirus targets the retinoblastoma-E2F pathway and with the oncogene Hras transforms primary rat cells. *Nat Med 6*:1121-1127.

Rainbow L, Platt G, Simpson G, Sarid R, Gao S, Stoiber H, Herrington C, Moore P, Schulz T. 1997. The 222- to 234-kilodalton latent nuclear protein (LNA) of Kaposi's

sarcoma-associated herpesvirus (human herpesvirus 8) is encoded by orf73 and is a component of the latency-associated nuclear antigen. *J Virol 71*:5915-5921.

Rappocciolo G, Jenkins F, Hensler H, Piazza P, Jais M, Borowski L, Watkins S, Rinaldo C. 2006. DC-SIGN is a receptor for human herpesvirus 8 on dendritic cells and macrophages. *J Immunol 176*:1741-1749.

Renne R, Barry C, Dittmer D, Compitello N, Brown P, Ganem D. 2001. Modulation of cellular and viral gene expression by the latency-associated nuclear antigen of Kaposi's sarcoma-associated herpesvirus. *J Virol 75*:458-468.

Renne R, Zhong W, Herndier B, McGrath M, Abbey N, Kedes D, D G. 1996. Lytic growth of Kaposi's sarcoma-associated herpesvirus (human herpesvirus 8) in culture. *Nat Med 2*:342-346.

Richly H, Aloia L, Di Croce L. 2011. Roles of the Polycomb group proteins in stem cells and cancer. *Cell Death Dis 2*:e204.

Rivas C, Thlick A, Parravicini C, Moore P, Chang Y. 2001. Kaposi's sarcoma-associated herpesvirus LANA2 is a B-cell-specific latent viral protein that inhibits p53. *J Virol 75*:429-438.

Rodriguez A, Vigorito E, Clare S, Warren M, Couttet P, Soond D, van Dongen S, Grocock R, Das P, Miska E, Vetrie D, Okkenhaug K, Enright A, Dougan G, Turner M, Bradley A. 2007. Requirement of bic/microRNA-155 for normal immune function. *Science 316*:608-611.

Roughan J, Thorley-Lawson D. 2009. The Intersection of Epstein-Barr Virus with the Germinal Center. *J Virol 83*:3968-3976.

Roy D, Dittmer D. 2011. Phosphatase and tensin homolog on chromosome 10 is phosphorylated in primary effusion lymphoma and Kaposi's sarcoma. *Am J Pathol 174*:2108-2119.

Russo J, Bohenzky R, Chien M, Chen J, Yan M, Maddalena D, Parry J, Peruzzi D, Edelman I, Chang Y, Moore P. 1996. Nucleotide sequence of the Kaposi sarcoma-associated herpesvirus (HHV8). *Proc Natl Acad Sci 93*:14862-14867.

Sakakibara S, Tosato G. 2011. Viral interleukin-6: role in Kaposi's sarcoma-associated herpesvirus: associated malignancies. *J Interferon Cytokine Res 31*:791-801.

Samols M, Hu J, Skalsky R, Renne R. 2005. Cloning and identification of a microRNA cluster within the latency-associated region of Kaposi's sarcoma-associated herpesvirus. *J Virol 79*:9301-9305.

Sandoval J, Esteller M. 2012. Cancer epigenomics: beyond genomics. *Curr Opin Genet Dev 22*:50-55.

Schambach A, Mueller D, Galla M, Verstegen M, Wagemaker G, Loew R, Baum C, Bohne J. 2006. Overcoming promoter competition in packaging cells improves production of self-inactivating retroviral vectors. *Gene Ther 13*:1524-1533.

Schulz T. 2000a. Kaposi's sarcoma-associated herpesvirus (human herpesvirus 8): epidemiology and pathogenesis. *J Antimicrob Chemother 45*:15-27.

Schulz T. 2000b. KSHV (HHV8) infection. *J Infect 41*:125-129.

Schulz T. 2001. KSHV/HHV8-associated lymphoproliferations in the AIDS setting. *Eur J Cancer 37*:1217-1226.

Schulz T. 2006. The pleiotropic effects of Kaposi's sarcoma herpesvirus. *J Pathol 208*:187-198.

Schulz T, Moore P. 1999. Kaposi's sarcoma-associated herpesvirus: a new human tumor virus, but how?

Schulz TF, Moore PS. *Trends Microbiol 7*:196-200.

Schwieger M, Löhler J, Friel J, Scheller M, Horak I, Stocking C. 2002. AML1-ETO inhibits maturation of multiple lymphohematopoietic lineages and induces

myeloblast transformation in synergy with ICSBP deficiency. *J Exp Med 196*:1227-1240.

Secombe J, Eisenman R. 2007. The function and regulation of the JARID1 family of histone H3 lysine 4 demethylases: the Myc connection. *Cell Cycle 6*:1324-1328.

Shen X, Kim W, Fujiwara Y, Simon M, Liu Y, Mysliwiec M, Yuan G, Lee Y, Orkin S. 2009. Jumonji modulates polycomb activity and self-renewal versus differentiation of stem cells. *Cell 139*:1303-1314.

Shin C, Nam J, Farh K, Chiang H, Shkumatava A, Bartel D. 2010. Expanding the microRNA targeting code: functional sites with centered pairing. *Mol Cell 38*:789-802.

Sin S, Fakhari F, Dittmer D. 2010. The viral latency-associated nuclear antigen augments the B-cell response to antigen in vivo. *J Virol 84*:10653-10660.

Singh H, DeKoter R, Walsh J. 1999. PU.1, a shared transcriptional regulator of lymphoid and myeloid cell fates. *Cold Spring Harb Symp Quant Biol 64*:13-20.

Skalsky R, Samols M, Plaisance K, Boss I, Riva A, Lopez M, Baker H, Renne R. 2007. Kaposi's sarcoma-associated herpesvirus encodes an ortholog of miR-155. *J Virol 81*:12836-12845.

Snodgrass R, Keller P. 1990. Life span of multipotential hematopoietic stem cells in vivo. *J Exp Med 171*:1407-1418.

Soulier J, Grollet L, Oksenhendler E, Cacoub P, Cazals-Hatem D, Babinet P, d'Agay M, Clauvel J, Raphael M, Degos L. 1995. Kaposi's sarcoma-associated herpesvirus-like DNA sequences in multicentric Castleman's disease. *Blood 86*:1276-1280.

Souza TA, Stollar BD, Sullivan JL, Luzuriaga K, Thorley-Lawson DA. 2005. Peripheral B cells latently infected with Epstein–Barr virus display molecular hallmarks of classical antigen-selected memory B cells. . *PNAS 102*:18093-18098.

Spangrude G, Heimfeld S, Weissman I. 1988. Purification and characterization of mouse hematopoietic stem cells. *Science 241*:58-62.

Spangrude G, Smith L, Uchida N, Ikuta K, Heimfeld S, Friedman J, Weissman I. 1991. Mouse hematopoietic stem cells. *Blood 78*:1395-1402.

Stedman W, Deng Z, Lu F, Lieberman P. 2004. ORC, MCM, and histone hyperacetylation at the Kaposi's sarcoma-associated herpesvirus latent replication origin. *J Virol 78*:12566-12575.

Steinitz M, Klein G. 1975. Comparison between growth characteristics of an Epstein--Barr virus (EBV)-genome-negative lymphoma line and its EBV-converted subline in vitro. *Proc Natl Acad Sci U S A 72*:3518-3520.

Tam W, Ben-Yehuda D, Hayward W. 1997. bic, a novel gene activated by proviral insertions in avian leukosis virus-induced lymphomas, is likely to function through its noncoding RNA. *Mol Cell Biol 17*:1490-1502.

Thai T, Calado D, Casola S, Ansel K, Xiao C, Xue Y, Murphy A, Frendewey D, Valenzuela D, Kutok J, Schmidt-Supprian M, Rajewsky N, Yancopulos G, Rao A, Rajewsky K. 2007. Regulation of the germinal center response by microRNA-155. *Science 316*:604-608.

Thomas MD, Kremer CS, Ravichandran KS, Rajewsky K, Bender TP. 2005. c-Myb is critical for B cell development and maintenance of follicular B cells. *Immunity 23*:275-286.

Thorley-Lawson D. 2005. EBV the prototypical human tumor virus--just how bad is it? *J Allergy Clin Immunol 116*:251-261.

Tomlinson C, Damania B. 2004. The K1 protein of Kaposi's sarcoma-associated herpesvirus activates the Akt signaling pathway. *J Virol 78*:1918-1927.

Tomlinson C, Damania B. 2008. Critical role for endocytosis in the regulation of signaling by the Kaposi's sarcoma-associated herpesvirus K1 protein. *J Virol 82*:6514-6523.

Varkonyi-Gasic E, Wu R, Wood M, Walton E, Hellens R. 2007. Protocol: a highly sensitive RT-PCR method for detection and quantification of microRNAs. *Plant Methods*:1746-1748.

Velichutina I, Shaknovich R, Geng H, Johnson N, Gascoyne R, Melnick A, Elemento O. 2010. EZH2-mediated epigenetic silencing in germinal center B cells contributes to proliferation and lymphomagenesis. *Blood 116*:5247-5255.

Verma S, Lan K, Robertson E. 2007. Structure and function of latency-associated nuclear antigen. *Curr Top Microbiol Immunol 312*:101-136.

Vigorito E, Perks K, Abreu-Goodger C, Bunting S, Xiang Z, Kohlhaas S, Das P, Miska E, Rodriguez A, Bradley A, Smith K, Rada C, Enright A, Toellner K, Maclennan I, Turner M. 2007. microRNA-155 regulates the generation of immunoglobulin class-switched plasma cells. *Immunity 27*.

Vikstrom I, Carotta S, Lüthje K, Peperzak V, Jost P, Glaser S, Busslinger M, Bouillet P, Strasser A, Nutt S, Tarlinton D. 2010. Mcl-1 is essential for germinal center formation and B cell memory. *Science 330*:1095-1099.

Volinia S, Calin G, Liu C, Ambs S, Cimmino A, Petrocca F, Visone R, Iorio M, Roldo C, Ferracin M, Prueitt R, Yanaihara N, Lanza G, Scarpa A, Vecchione A, Negrini M, Harris C, Croce C. 2006. A microRNA expression signature of human solid tumors defines cancer gene targets. *Proc Natl Acad Sci 103*:2257-2261.

Wagner E. 2001. AP-1--Introductory remarks. *Oncogene 20*:2334-2335.

Watanabe T, Sugaya M, Atkins A, Aquilino E, Yang A, Borris D, Brady J, Blauvelt A. 2003. Kaposi's sarcoma-associated herpesvirus latency-associated nuclear antigen prolongs the life span of primary human umbilical vein endothelial cells. *J Virol 77*.

Wen K, Damania B. 2010. Kaposi sarcoma-associated herpesvirus (KSHV): molecular biology and oncogenesis. *Cancer Lett 289*:140-150.

Whitby D, Howard M, Tenant-Flowers M, Brink N, Copas A, Boshoff C, Hatzioannou T, Suggett F, Aldam D, Denton A, al. e. 1995. Detection of Kaposi sarcoma associated herpesvirus in peripheral blood of HIV-infected individuals and progression to Kaposi's sarcoma. *Lancet 346*:799-802.

Wies E, Hahn A, Schmidt K, Viebahn C, Rohland N, Lux A, Schellhorn T, Holzer A, Jung J, Neipel F. 2009. The Kaposi's Sarcoma-associated Herpesvirus-encoded vIRF-3 Inhibits Cellular IRF-5. *J Biol Chem 284*:8525-8538.

Wilson S, Tsao E, Webb B, Ye H, Dalton-Griffin L, Tsantoulas C, Gale C, Du M, Whitehouse A, Kellam P. 2007. X box binding protein XBP-1s transactivates the Kaposi's sarcoma-associated herpesvirus (KSHV) ORF50 promoter, linking plasma cell differentiation to KSHV reactivation from latency. *J Virol 81*:13578-13586.

Xiao C, Calado D, Galler G, Thai T, Patterson H, Wang J, Rajewsky N, Bender T, Rajewsky K. 2007. MiR-150 controls B cell differentiation by targeting the transcription factor c-Myb. *Cell 131*:146-159.

Xu G, Fewell C, Taylor C, Deng N, Hedges D, Wang X, Zhang K, Lacey M, Zhang H, Yin Q, Cameron J, Lin Z, Zhu D, Flemington E. 2010a. Transcriptome and targetome analysis in MIR155 expressing cells using RNA-seq. *RNA 16*:1610-1622.

Xu G, Fewell C, Taylor C, Deng N, Hedges D, Wang X, Zhang K, Lacey M, Zhang H, Yin Q, Cameron J, Lin Z, Zhu D, Flemington EK. 2010b. Transcriptome and targetome analysis in MIR155 expressing cells using RNA-seq. *RNA 16*:1610-1622.

Yi R, Qin Y, Macara I, Cullen B. 2003. Exportin-5 mediates the nuclear export of pre-microRNAs and short hairpin RNAs. *Genes Dev 17*:3011-3016.

Yin Q, McBride J, Fewell C, Lacey M, Wang X, Lin Z, Cameron J, Flemington E. 2008a. MicroRNA-155 is an Epstein-Barr virus-induced gene that modulates Epstein-Barr virus-regulated gene expression pathways. *J Virol 82*:5295-5306.

Yin Q, Wang X, McBride J, Fewell C, Flemington E. 2008b. B-cell receptor activation induces BIC/miR-155 expression through a conserved AP-1 element. *J Biol Chem 283*:2654-2662.

Yu F, Feng J, Harada J, Chanda S, Kenney S, Sun R. 2007. B cell terminal differentiation factor XBP-1 induces reactivation of Kaposi's sarcoma-associated herpesvirus. *FEBS Letters 581*:3485-3488.

Zeng Y, Cullen B. 2004. Structural requirements for pre-microRNA binding and nuclear export by Exportin 5. *Nucleic Acids Res 32*:4776-4785.

Zhang Z, Jones A, Sun C, Li C, Chang C, Joo H, Dai Q, Mysliwiec M, Wu L, Guo Y, Yang W, Liu K, Pawlik K, Erdjument-Bromage H, Tempst P, Lee Y, Min J, Townes T, Wang H. 2011. PRC2 complexes with JARID2, MTF2, and esPRC2p48 in ES cells to modulate ES cell pluripotency and somatic cell reprogramming. *Stem Cells 29*:229-240.

Zhao Y, Xu H, Yao Y, Smith L, Kgosana L, Green J, Petherbridge L, Baigent S, Nair V. 2011. Critical role of the virus-encoded microRNA-155 ortholog in the induction of Marek's disease lymphomas. *PLoS Pathog 7*.

Zhou B, Wang S, Mayr C, Bartel D, Lodish H. 2007. miR-150, a microRNA expressed in mature B and T cells, blocks early B cell development when expressed prematurely. *2007 104*:7080-7085.

6 ABBREVIATIONS AND NOMENCLATURE

5-FU	5-fluorouracil
A	
Ago	argonaute
AIDS	acquired immunodeficiency syndrome
AML	acute myelogenous leukemia
ATP	adenosine triphosphate
B	
BCBL	body cavity-based lymphoma
BCL2	B-cell lymphoma 2
BCLAF	Bcl2-Associated Transcription Factor
BCR	B-cell receptor
BIC	B-cell integration cluster
BM	bone marrow
bp	base-pairs
BS	binding site
ß-gal	beta-galactosidase
C	
CBC	complete blood count
cDNA	complementary DNA
CIP	calf intestine phosphatase
C. elegans	*Caenorhabditis elegans*
CLL	chronic lymphocytic leukemia
CLP	common lymphoid progenitors
CMP	common myeloid progenitors
C_T	cycle threshold
D	
d	day
DC	dendritic cell
DGCR	DiGeorge syndrome critical region
dH_2O	distilled H_2O
DLBCL	diffuse large B-cell lymphoma
DMEM	Dulbecco's modified Eagle medium
ds	double-stranded
DMSO	dimethylsulfoxid

DNA	desoxyribonucleic acid
dNTP	deoxyribonukleotid-Mix
E	
E	early gene
EBNA	EBV nuclear antigen
EBV	Epstein-Barr virus
E. coli	*Escherichia coli*
EDTA	ethylenediaminetetra acetic acid
Eed	embryonic ectoderm development
enhanced GFP	eGFP
ER stress	endoplasmic reticulum stress
et al.	*et alteri*
EtOH	ethanol
Exp5	exportin 5
Ezh2	enhancer of zeste homolog 2
F	
FACS	fluorescence activated cell sorting
FCS	foetal calf serum
FITC	fluoresceinisothiocyanat
fl	fulllength
FLICE	Fas-associated death domain-like interferon converting enzyme
Fsc	forward scatter
G	
g	gram
GAPDH	glyceraldehyde 3-phosphate dehydrogenase
GC	germinal center
GFP	green fluorescent protein
GMP	granulo/monocytic progenitor
GSK-3β	glycogen synthase kinase-3β
H	
h	hour(s)
HAART	highly active antiretroviral treatment
Hb	hemoglobin
HCMV	human cytomegalovirus
HCT	hematocrit
HDFa	*human dermal fibroblasts* (Humane dermale Fibroblasten)

hFLT3	human Flt3-ligand
HHV	human herpesvirus
hIL-11	human interleukin 11
HIV	human immunodeficiency virus
HPC	hematopoietic progenitor
hsa	homo sapiens
HSC	hematopoietic stem cell
HSV	herpesvirus simplex
HVS	herpesvirus samirii
I	
IE	immediate early gene
IF	immunofluorescence
IFN	interferon
Ig	immunoglobulin
IHC	immunohistochemistry
IPTG	isopropyl-ß-D-thio-galactopyranoside
IRES	internal ribosome entry sites
i.v.	intravenous
J	
K	
kbp	kilobase-pairs
kDa	kilo Dalton
KS	Kaposi´s sarcoma
KSHV	Kaposi´s sarcoma-associated herpesvirus
L	
L	late gene
LANA	latency associated nuclear antigen
LAR	latency-associated region
LB	lysogeny broth
LCL	lymphoblastoid cell lines
LT-HSC	long-term hematopoietic stem cell
LMP	latent membrane protein
LPS	lipopolysaccharide
LT_C	latency cluster
LTR	long terminal repeat
LUR	long unique coding region
M	

mA	milliampere
MAF	musculoaponeurotic fibrosarcoma
MCD	multicentric Castleman´s disease
MCM	minichromosome maintenance complex
MDV	Marek´s disease virus
MEP	megacaryotic/erythroid progenitors
MHV	murine gamma-herpesvirus
MICB	MHC class I polypeptide-related sequence B
mIL-11	murine interleukin 11
miRNA	microRNA
mmu	mus musculus
MOPS	4-Morpholinepropanesulfonic acid
MPP	multipotent progenitors
mRNA	messenger ribonucleic acid
mSCF	murine stem cell factor
N	
NFkB	nuclear factor kappa B
NK cells	natural killer cells
nt	nucleotide
O	
OD	optical density
ONPG	2-Nitrophenyl β-D-galactopyranoside
ORC	origin of replication
ORF	open reading frame
P	
PAR-CLIP	photoactivatable-Ribonucleoside-Enhanced Crosslinking and Immunoprecipitation
PBS	phosphate buffered saline
PCR	poly-chain reaction
PEI	polyethylenimine
PEL	primary effusion lymphoma
Pen/Strep	penicillin-Streptomycin
PNA	peanut agglutinin
pol	polymerase
PRC2	polycomb repressive complex 2
pre-miRNA	precursor miRNA
pri-miRNA	primary microRNA

PTEN	phosphatase and tensin homolog
R	
Rb1	retinoblastoma 1
RBC	red blood cell
$RbCL_2$	rubidium chloride
Rbl2	retinoblastoma-like protein 2
RDA	representational difference analysis
RISC	RNA-induced silencing complex
RLB	Renilla Lysis Buffer
RNA	ribonucleic acid
rpm	rounds per minute
RPMI	Roswell Park Memorial Institute
RRV	rhesus monkey rhadinovirus
RT	reverse transcriptase
RTA	replication and transcription activator
S	
SFEM	serum-free expansion medium
SL	stemloop
Ssc	side scatter
ST-HSC	short-term hematopoietic stem cell
T	
TFB	transformation buffer
TGFβ	transforming-growth factor β
TR	terminal repeat
TSG	tumor suppressor gene
U	
UTR	untranslated region
V	
vFLIP	viral FLICE-inhibitory protein
vIL6	viral interleukin 6
vIRF3	viral interferon 3
VZV	Varizella Zoster virus
W	
WBC	white blood cell
X	
XBP-1	X-box binding protein 1
XGal	ß-D-galactopyranosid

Y

YY1	Yin Yang 1

Nomenclature:

Human gene symbols are designated by upper-case Latin letters and Arabic numerals. Italics were used.

Mouse gene symbols are designated by first upper-case Latin letter and then lower-case Latin letters. Arabic numerals and Italics were used.

Protein symbols: murine and human proteins were designated by upper-case Latin letters and Arabic numerals.

Species designation: Mus musculus is abbreviated with mmu. Homo sapiens is designated as hsa.

7 APPENDIX

7.1 SUPPLEMENTARY FIGURES

Supplementary figure 1.

Transient expression of KSHV-encoded miRNAs during KSHV *de novo* infection

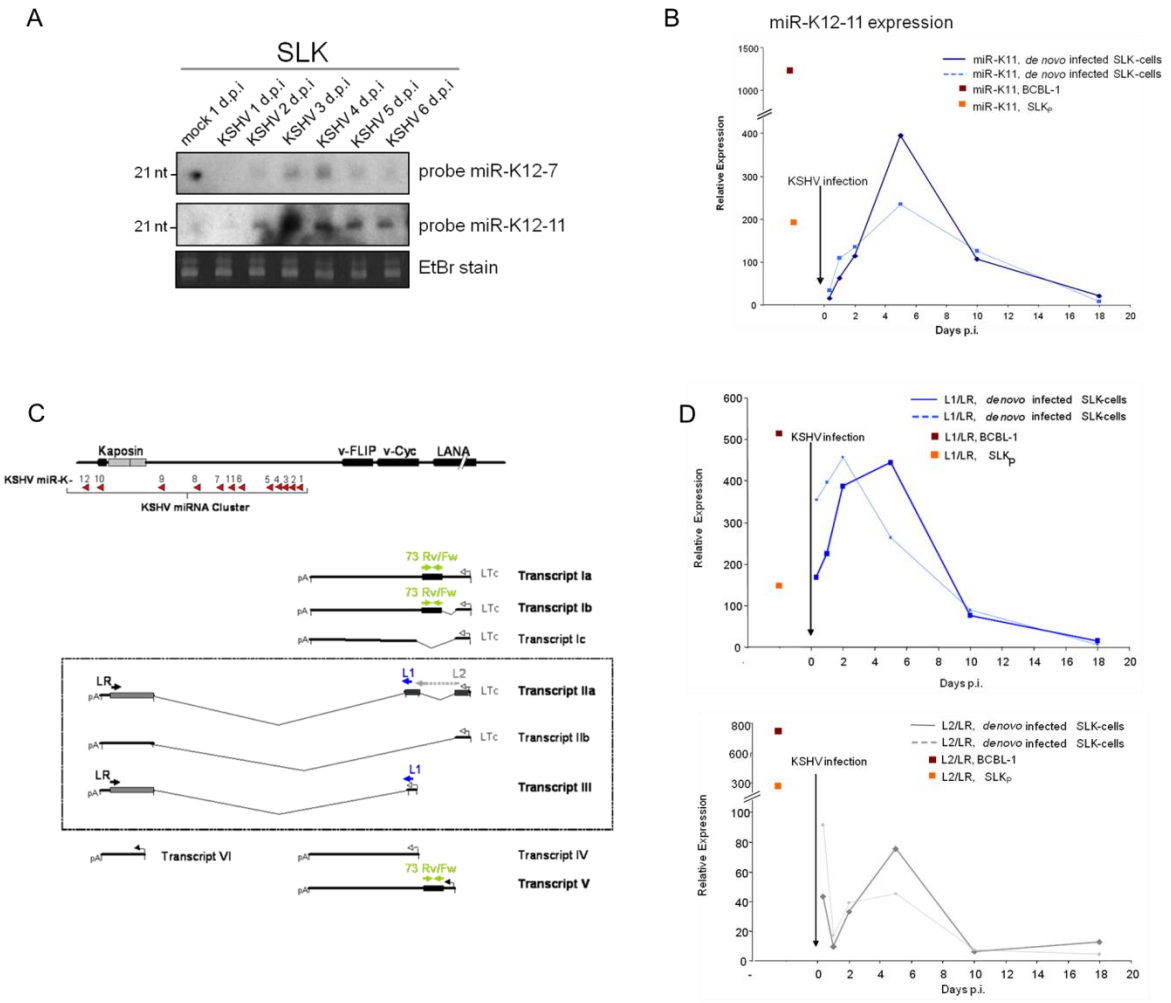

Figure S1: Transient miRNA expression. A) KSHV *de novo* infection of SLK cells. miRNAs were detected by northern blotting. B) TaqMan miR-K12-11 assay of *de novo* infected SLK cells. Steady state miR-K12-11 levels in BCBL-1 and SLK_P cells (stable KSHV positive cells) are indicated by colored rectangles. Data were normalized to GAPDH transcripts (dotted lines), or to GAPDH levels and additionally episome content (solid lines). C) Schematic depiction of the genomic KSHV miRNA locus. Transcripts IIa and III, which also serve as pri-miRNAs, were monitored by primers L2/LR and L1/LR. D) RT-qPCR analysis of *de novo* infected SLK cells was performed using primers L1/LR (upper graph) and L2/LR (lower graph). Steady state expression levels of transcripts IIa and III in BCBL-1 and SLK_p cells are indicated by colored rectangles. Data were normalized to GAPDH transcript levels (dotted lines), or GAPDH levels and episome copy numbers (solid lines).

Supplementary figure 3

Luciferase Reporter Assays were performed to verify Jarid1b as a target of miR-K12-11 and hsa-miR-155.

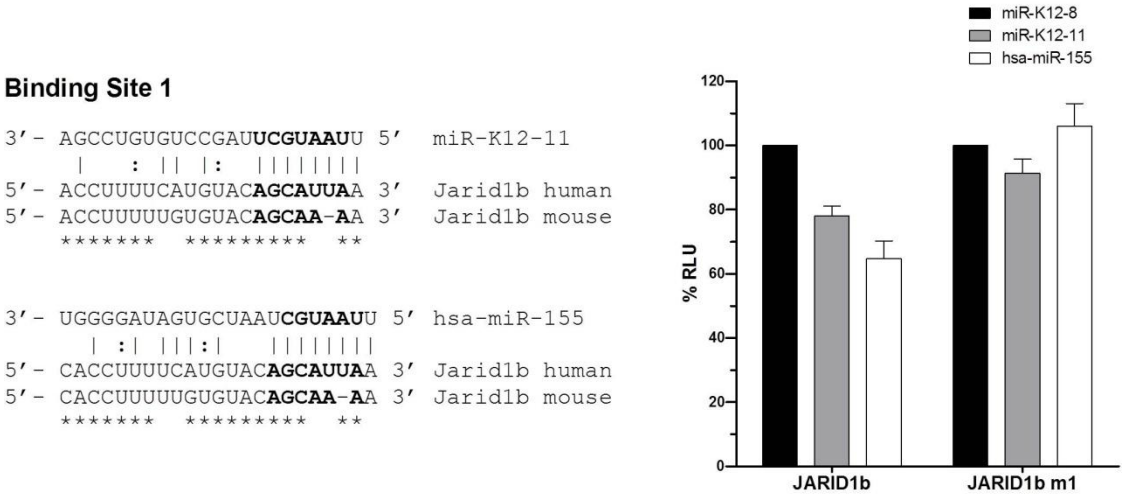

Figure S3: miR-K12-11 and hsa-miR-155 can directly repress Jarid1b mRNA. The 3´UTR of Jarid1b harbors one binding site for each miR-K12-11 and hsa-miR-155. Left: The alignment depicts the two mature miRNAs and the binding site within the 3´UTR of Jarid1b (Jarid1b homo sapiens: NM006618, mus musculus: NM152895). The mutation vector Jarid1b m1 contains a mutation of three nucleotides in the seed binding site. Right: miR-K12-11 and hsa-miR-155 targets Jarid1b. Luciferase reporter assay revealed a reduction in luciferase activity when the appropriate miRNAs were overexpressed. 293T cells were co-transfected with pMIR-Jarid1b or the mutated pMIR-Jarid1b vector together with one of the miRNA expression vector. The co-expression with the mutated Jarid1b-vector revert the reduced luciferase activity.

Supplementary figure 2

$CD19^+/CD43^+$ expression in GFP^+ BM cells

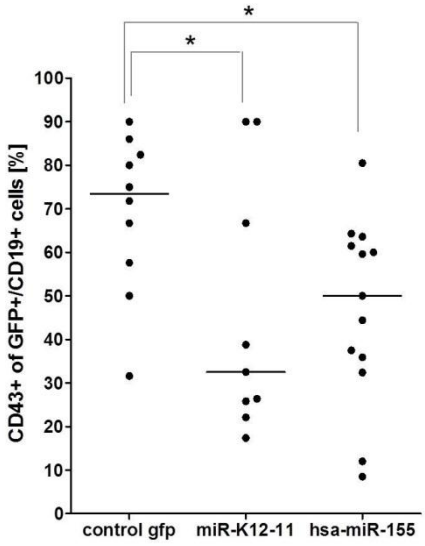

Figure S2: Decreased number of early B-cells. CD43 expression evaluated by flow cytometry on $GFP^+/CD19^+$ gated BM cells revealed a significant decrease of the early B-cell population ($CD19^+/CD43^+$) in the BM of miRNA expressing mice, indicating a shift toward the later B-cells if the miRNA is expressed.

7.2 ENZYMES, REAGENTS AND CYTOKINES

7.2.1 Restriction enzymes

Restriction enzymes were purchased from New England Biolabs (NEB) and Fermentas. They were used for restriction analysis and cloning.

Table: Enzymes.

Name	*Restriction sites*	*Company*
BamHI	G↓GATCC	NEB, Fermentas
EcoRI	G↓AATTC	NEB, Fermentas
EcoRV	GAT↓ATC	NEB
HindIII	A↓AGCTT	NEB, Fermentas
HpaI	GTT↓AAC	NEB
KpnI	GGTAC↓C	NEB
NotI	GC↓GGCCGC	NEB, Fermentas
SmaI	CCC↓GGG	NEB
SpeI	A↓CTAGT	NEB, Fermentas
XbaI	T↓CTAGA	NEB, Fermentas
XhoI	C↓TCGAG	NEB, Fermentas

7.2.2 Media, solutions and additives for eukaryotic cell culture

Media, solutions and additives used for diverse cell culture experiments with cell lines, primary cells or mouse experiments are listed in the following table.

Table..: Media, Solution and Additives that were used in this work.

Media, Solution, Additives	*Type of Experiment*	*Company*
Dulbecco´s Modified Eagle Medium (DMEM)	Adherent cell lines, cultivation	PAA
Fetal Calf Serum (FCS)	Cell lines and primary cells, cultivation	PAA
Penicillin/Streptomycin (Pen/Strep)	Cell lines, cultivation	PAA
Trypsin/EDTA	Adherent cell lines	PAA
Roswell Park Memorial Institute 1640 (RPMI 1640)	Suspension cell lines, cultivation	Gibco
Sodium Pyruvate	Cell lines, cultivation	Gibco
Iscove´s Modified Dulbecco's Media (IMDM)	Primary murine BM cells	Invitrogen
5-fluorouracil (5-FU)	Enrichment of progenitor cells	GRY-Pharma
Hank's Balanced Salt Solution (HBSS)	Primary murine BM cells	Invitrogen
Polybrene	Transduction	Sigma-Aldrich
Polyethyleneimine (PEI)	Transfection	
StemSpan Serum-free expansion medium (SFEM)	Primary murine BM cells	StemCell Technologies
Glutamine	Cell Culture	Gibco
RetroNectin®	Plate coating for retroviral transduction	TaKaRa Bio INC.

7.2.3 **Cytokines**

Following cytokines were used in this work for cultivation of primary bone marrow cells.

Table: Cytokines.

Cytokine	*Concentration*	*Company*
murine stem cell factor (mSCF)	100 ng/ml	Peprotech
human Flt3-ligand (hFlt3-L)	100 ng/ml	Peprotech
human interleukin 11 (hIL-11)	100 ng/ml	Peprotech
murine interleukin 3 (mIL-3)	10 ng/ml	Peprotech

7.3 SAFETY-RELATED DATA

Table 7-1 R and S clauses for chemicals

Substance	Danger Symbol	R-Clause	S-Clause
2-Mercaptoethanol	T, N	R 20/22-24-34-51/53	S 26-36/37/39-45-61
2-Propanol	F,xi	R 10-36/38-67	S 7-16-24/25-26-36/37
p-Coumaric acid	Xi	R 36/37/38	S 26-36
Acetone	F,xi	R 11-36-66-67	S 9-16-26
Acetonitrile	F,xn	R 11-20/21/22-36	S 16-36/37
Acrylamid	T	R 45-46-20/21-25-36/38-43-48/23/24/25-62	S 53-26-36/37-45
Ampicillin	Xn	R 36/37/38-42/43	S 22-26-36/37
Ammonium persulfate (APS)	Q,xn	8-22-36/37/38-42/43	S 22-24-26-37
Bisacrylamid	Xn	R 22-20/21/22	S 24/25-36/37
Boric acid	T	R 60-61	S 53-45
Bromophenol Blue			S 22-24/25
Calcium chloride ($CaCl_2$)	Xi	R 36	S 22-24
Chloroform	F,xn	R 11-22-36/38-40-48/20/22-66-67	S 9-16-26-36
Diethyl pyrocarbonate (DEPC)	Xn	R 22-36/37/38	S 26-36
N.N-Dimethylformamide	T	R 61-20/21-36	S 53-45
DL-Dithiothreitol (DTT)	Xn	R 22-36/37/38	S 26-36
Ethylendiaminetetraacetic acid (EDTA)	Xi	R 36-52/53	S 26-61
Glacial acetic acid	C	R 10-35	S 23-26-45
Ethanol	F	R 11	S 7-16
Ethidium bromide solution 10 mg/ml	T	R 23-68	S 36/37-45
Formaldehyde	T	R 23/24/25-34-39/23/24/25-40-43	S 26-36/37/39-45-51
Formamide	T	R 61	S 53-45
Glycin			S 22-24/25
Hydrochloric acid 37%	C	R 34-37	S 26-36/37/39-45
Hydrogen peroxide solution 30%	Xn	R 22-41	S 26-39
Isoamyl alcohol	Xn	R 10-20-37-66	S 46
Isopropyl-ß-D-thio-galactopyranoside (IPTG)			S 22-24/25
Kanamycinsulfate	T	R 61	S 45-36/37/39
Luminol	Xi	R 36/37/38	S 26-36/37
Methanol	F, T	R 11-23/24/25-39/23-24/25	S 7-16-36/37-45
Magnesium chloride ($MgCl_2$)			S 22-24/25
$MgSO_4$			S 22-24/25
MOPS	Xi	R 36/37/38	S 26-36
N,N,N',N'-Tetramethylethylene-diamine	F, C	R 11-20/22-34	S 16-26-36/37/39-45
Neomycin sulfate (G418)	T,xi	R 63-42/43-36 37/38	S 45-26-36/37/39
Neomycin sulfate	Xn	R 42/43	S 22-36/37-45

Substance	Danger Symbol	R-Clause	S-Clause
Nonidet™ P 40 Substitute	Xi	R 37-41	S 26-39
2-Nitrophenyl β-D-galactopyranoside (ONPG)			S22-24/25
Penicillin	Xn	R 42/43	S 22-36/37-45
Phenol	T, C	R 23/24/25-34-48/20/21/22-68	S 24/25-26-28-36/37/39-45
Polyethylenimine (PEI)	Xi	R 36/37/38	S 26-36
Potassium cloride			S 22-24/25
Proteinase K	Xn	R 36/37/38-42	S 22-24-26-36/37
Rubidium chloride ($RbCl_2$)			S 22-24/25
Sodium azide	T+, N	R 28-32-50/53	S 28-45-60-61
Sodium acetate			S 22-24/25
Sodium carbonate	Xi	R 36	S 22-26
Sodium dodecyl sulfate	F,xn	R 11-21/22-36/37/38	S 26-36/37
Sodium hydroxide	C	R 35	S 26-37/39-45
Streptomycin	Xn	R 22	
Trichloroacetic acid	C, N	R 35-50/53	S 26-36/37/39-45-60-61
Triton®X-100	Xi; N	R 22-41-51/53	S 26-36/39-61
TRIS base	Xi	R 36	S 26
Trypan blue	T	R 45	S 53-45
Trypsin	Xn	R 36/37/38-42	S 22-24-26-36/37
Xylene cyanol	Xi	R 36/37/38	S 26-36

8 ACKNOWLEDGMENT

First and foremost I would like to express my gratitude to **Dr. Adam Grundhoff** for the opportunity to perform and complete this doctoral thesis in his lab. Furthermore, I would like to thank him for his ideas and our fruitful discussions. Thank you for sharing your knowledge on miRNAs and KSHV. And thank you for your patience and support.

Second, I would like to thank **Prof. Dr. Thomas Dobner** for the supervision of this thesis. Furthermore, I want to thank **PD Hartwig Lüthen** for evaluating/administrating the oral thesis defense as well as the involved questionnaires.

In addition, I would like to thank my co-supervisor **Dr. Nicole Fischer** for all our discussions, your interest and valuable advice.

I would also like to express my gratitude to **Dr. Carol Stocking**. Thank you for your skilful guidance and your kindness and for always finding time for discussions. And, of course, thank you for correcting my English grammar.

Additionally, I would like to thank the **Heinrich-Pette-Institut** for supporting my PhD with the Ferdinand-Bergen-funding.

'**Zelluläre Virusabwehr'** group – It was a pleasure working with you. **Uwe Tessmer**, thank you so much for all our discussions, your help, support and our non-laboratory talks. My lovely lab-pal and friend **Thomas Christalla**: Thank you for being so funny and friendly and for all your music we had to listen to during work. **Nicole Walz**, you are a very caring and unselfish person. Thank you for all your help in every possible way. And I appreciate all your hard work on establishing luciferase reporter assays; the most important point to remember when doing these assays: never do them on a Friday!! Thank you, **Thomas Günther,** for all our fruitful discussions and supporting the Real-Time-PCR-stuff. And finally, **Juliane Theis**, thank you for reading parts of my thesis. You are a really kind and humble person and I wish you all the best for your PhD.

I would like to thank **Philipp Schult** for being a great Master student. Thank you for assisting in establishing the luciferase reporter assays.

Furthermore I would like to thank the group of Carol Stocking (Molekular Pathologie); **Katrin Maul, Maike Täger, Birte Niebuhr, Kira Behrens, Ulla Bergholz, Ulla Müller, Susanne Roscher, Marion Ziegler.** Thank you all for always being so kind to me. Although I am not a 'member' of the group, I never felt like a 'stranger'. I especially want to thank **Ulla Müller** for the early-bird-mouse-sessions and **Maike, Katrin and Birte** for their technical assistance with mouse transplantations and 5-FU and lineage depletion experiments. And my special thanks go to **Katrin** for always helping me in every possible way and having such a warm personality.

Gundula Pilnitz-Stolze, thank you for your support and technical assistance in the IHC and for almost always smiling.

I want to thank **Dr. Jürgen Löhler** for sharing his knowledge about splenic structures and germinal centers. Thank you so much for our fruitful discussions and your advice.

I would like to express my gratitude to **Nicole W., Sophie Borchert, Juliane, Thomas G.**, **Daniela Müller** and **Katrin** for reading and correcting parts of my manuscript.

I would like to thank **Nicole W., Thomas C., Thomas G, Carina Banning, Katrin** and **Sophie** for sharing all the ups and downs of PhD-life.

Stefan, my funny Real-Time brother, thanks a lot for long-time discussions regarding Real-Time problems!

Thank you **Braslav**; you were my first lab-pal in my life and introduced me into the weird lab-world. I would like to work with you again at some point.

I would like to thank my friends, especially **Carina**, **Grazyna**, **Julia**, **Dagmar, Sophie, Semrah** and the **Pickelnesen-Girls**. Thank you for listening to all my problems, believing in me and your friendships.

I thank **Lars,** my love, for being Lars. You are simply wonderful. Ich würde dir immer helfen, eine Leiche zu verscharren, wenn's nicht meine ist, versprochen.

Piet and **Franka**, thank you for being crazy, funny and lovely persons.

Last but not least, I would like to thank my **parents**. I am so greatful for your support no matter what I decide to do in life, for your belief in me and for your love. Especially to my mum, who supported me a lot in caring for Piet and Franka and cooking soups for me. This work is dedicated to them.

.

9 PUBLICATION, FUNDING AND PRESENTATION

Funding

02.2009	PhD Funding: • Ferdinand-Bergen-Funding
08.2011	Travel Funding; University Hamburg • KSHV-Meeting, Finnland

Poster presentations at scientific meetings

C. Dahlke, K. Maul, T. Christalla, N. Walz, P. Schult, C. Stocking and A. Grundhoff; A microRNA encoded by KSHV promotes B-cell expansion *in vivo;* 14th Annual International Workshop, Helsinki, Finnland; 12-15 August 2011.

T. Christalla, C. Henning, U. Tessmer, A. Grundhoff; Transient expression of KSHV miRNAs suggests an important role during early stages of latency establishment; 19. Gesellschaft für Virologie (GfV)-Tagung, Leipzig, 18-21.03.2009.

Oral presentations at scientific meetings

C. Henning, K. Maul, T. Christalla, N. Walz, P. Schult, C. Stocking and A. Grundhoff; A microRNA encoded by Kaposi's sarcoma-associated herpesvirus promotes B-cell expansion *in vivo;* 21. GfV-Tagung, Freiburg, 23-26.03.2011.

C. Henning, K. Maul, T. Christalla, N. Walz, P. Schult, C. Stocking and A. Grundhoff; *In vivo* analysis of a microRNA encoded by a tumorigenic Herpesvirus; Annunal Retreat Virus-Host Interaction,Heinrich-Pette-Institut, Hamburg, Deutschland, 01.11.2010

Publication

C. Dahlke, K. Maul, T. Christalla, N. Walz, P. Schult, C. Stocking and A. Grundhoff; A microRNA encoded by Kaposi Sarcoma-associated herpesvirus promotes B-cell expansion *in vivo.* [in press, PLOS One].